$$(\mathbf{v})_{XYZ} \equiv (\mathbf{v} + \boldsymbol{\omega} \times \mathbf{r})_{123} \tag{186}$$

and conversely

$$(\mathbf{v})_{123} \equiv (\mathbf{v} - \boldsymbol{\omega} \times \mathbf{r})_{XYZ} \tag{187}$$

These identities show that the linear center of mass velocity, $\mathbf{v}$ in frame (X, Y, Z) is rigorously equivalent to the sum $\mathbf{v} + \boldsymbol{\omega} \times \mathbf{r}$ in the rotating frame $(1, 2, 3)$. Carrying out this procedure for each molecule of the ensemble, we note that the axes of the frame $(1, 2, 3)$ are each parallel to those of (x, y, z), but the origin of one frame is displaced with respect to the other. For the purposes of constructing ensemble averages the two frames are interchangeable. We can therefore continue the development with subscripts (x, y, z) substituted for $(1, 2, 3)$.

The noninertial accelerations are generated in both frames (X, Y, Z) and (x, y, z) by the equivalences

$$(\dot{\mathbf{v}})_{XYZ} \equiv (\dot{\mathbf{v}} + 2\boldsymbol{\omega} \times \mathbf{v} + \dot{\boldsymbol{\omega}} \times \mathbf{r} + \boldsymbol{\omega} \times (\boldsymbol{\omega} \times \mathbf{r}))_{xyz} \tag{188}$$

and conversely

$$(\dot{\mathbf{v}})_{xyz} \equiv (\dot{\mathbf{v}} - 2\boldsymbol{\omega} \times \mathbf{v} - \dot{\boldsymbol{\omega}} \times \mathbf{r} + \boldsymbol{\omega} \times (\boldsymbol{\omega} \times \mathbf{r}))_{XYZ} \tag{189}$$

which may be written more transparently as[246]

$$\hat{D}_f^2 \mathbf{r} \equiv \hat{D}_f(\hat{D}_f \mathbf{r}) \equiv (\hat{D}_m + \boldsymbol{\omega} \times)(\hat{D}_m + \boldsymbol{\omega} \times \mathbf{r}) \tag{190}$$

and conversely

$$\hat{D}_M^2 \mathbf{r} \equiv \hat{D}_m(\hat{D}_m \mathbf{r}) \equiv (\hat{D}_f - \boldsymbol{\omega} \times)(\hat{D}_f - \boldsymbol{\omega} \times \mathbf{r}) \tag{191}$$

These equivalences define the noninertial linear acccl erations, which are real in both frames of reference. They are known as the molecular Coriolis acceleration $-2\boldsymbol{\omega} \times \mathbf{v}$, the molecular Eulerian acceleration $-\dot{\boldsymbol{\omega}} \times \mathbf{r}$, and molecular centripetal acceleration $\boldsymbol{\omega} \times (\boldsymbol{\omega} \times \mathbf{r})$.

It follows that acf and ccf may be constructed involving these accelerations, and also the non inertial linear velocity

$$\mathbf{v}_{\text{noninertial}} \equiv -\boldsymbol{\omega} \times \mathbf{r}$$

which involves the position vector in both frames. The theory of Section I contains no specific mention of correlations such as these, which clearly

contain both rotational and translational molecular dynamical quantities. Some of these correlations were described earlier in this section using simulation and symmetry.

The process leading to Eqs. (188) and (189) may be extended to the complete set of time derivatives of noninertial linear accelerations by operating repeatedly in each frame

$$\hat{D}_f^3 \mathbf{r} \equiv (\hat{D}_m + \boldsymbol{\omega} \times)(\hat{D}_m + \boldsymbol{\omega} \times)(\hat{D}_m + \boldsymbol{\omega} \times \mathbf{r}) \tag{192}$$

and conversely

$$\hat{D}_m^3 \mathbf{r} \equiv (\hat{D}_f - \boldsymbol{\omega} \times)(\hat{D}_f - \boldsymbol{\omega} \times)(\hat{D}_f - \boldsymbol{\omega} \times \mathbf{r}) \tag{193}$$

The number of terms increases rapidly and there is an infinite number of ccf's describing simultaneous rotation and translation in molecular ensembles. The majority of these vanish by symmetry, but this still leaves an infinite number which does not. All of these, in both frames of reference, contribute to spectra in some way, but clearly, no spectral observation can determine them unequivocally. Computer simulation is able to generate the first few members of the infinite sets in frames (X, Y,Z) and (x, y, z).

N. Consequences for the Theory of Diffusion

The major consequence for the theory of rotational diffusion is to make the appropriate Langevin equations intractable. This is easily demonstrated by considering the diffusion of the asymmetric top in three dimensions. To consider the simultaneous rotational and translational diffusion means supplementing the Euler–Langevin structure Eqs. (68)–(70) with the translational Langevin equation written in frame (x, y, z). It becomes the highly nonlinear stochastic differential equation

$$(\dot{\mathbf{v}} + 2\boldsymbol{\omega} \times \mathbf{v} + \dot{\boldsymbol{\omega}} \times \mathbf{r} + \boldsymbol{\omega} \times (\boldsymbol{\omega} \times \mathbf{r}) + \beta(\mathbf{v} + \boldsymbol{\omega} \times \mathbf{r}))_{xyz} = (\mathbf{F}/m)_{xyz} \tag{194}$$

There is no known analytical solution of this equation, even if did not have to be solved simultaneously with the intractable Euler–Langevin equations (68)–(70).

This is a simple illustration of the limits of usefulness of the analytical diffusion theory.[1,247–255] In this situation, limited progress is possible only by relying on computer simulation and symmetry, and by attempting to put the rigorous analytical theory in a form suitable for approximate solution. An example of what is possible is given next.

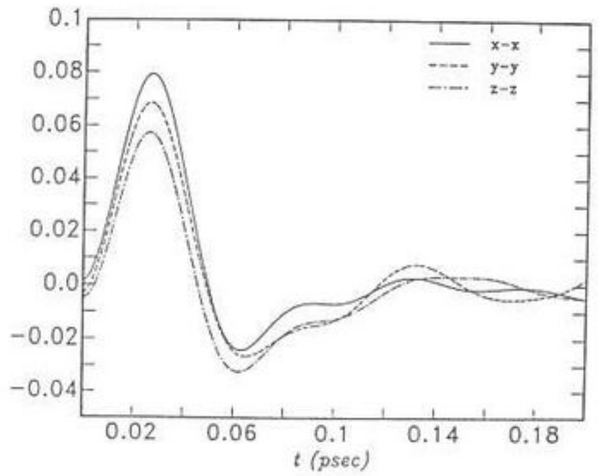

Figure 30. Diagonal elements of the laboratory frame ccf $\langle \dot{\mu}(t)\mathbf{v}^T(0)\rangle_{XYZ}$ from a recent computer simulation of liquid water.

O. A Simple Langevin Theory[256] of ccf's in Frame (X, Y, Z)

The c.c.f. between $\mathbf{v}$ and $\boldsymbol{\omega}$ vanishes for all t in frame (X, Y, Z). It is therefore incorrect to write two Langevin equations in this frame directly linked by cross friction coefficients because this would produce a non-zero value for thc ccf. Cross friction coefficients such as those of eqns (175) and (176) must vanish with the applied electric field. (For finite $\mathbf{E}$ however, the ccf exists.)

We have seen from elementary dynamical considerations that the ccf between linear and rotational velocity, $\langle \mathbf{v}(t)\dot{\boldsymbol{\mu}}(0)\rangle$, exists in frame (X, Y, Z) directly, (Eq. (49) to (52)). This is supported by the symmetry rules of this section bccause the complete D symmetry of this ccf contains the totally symmetric representation of $R_h(3)$. This represents the trace of the ccf, the sum of the diagonal elements. These are illustrated in Fig. 30 from a recent computer simulation.[256] The off-diagonal elements vanish for all t.

Simulation and symmetry lead to a simple Langevin structure

$$\dot{\mathbf{v}} + \beta_T \mathbf{v} + \beta_{Tr}\dot{\boldsymbol{\mu}} = \mathbf{W}_1 \tag{195}$$

$$\ddot{\boldsymbol{\mu}} + \beta_\mu \dot{\boldsymbol{\mu}} + \beta_{rT}\mathbf{v} = \mathbf{W}_2 \tag{196}$$

where the β's are friction coefficients. The physical meaning of these equations becomes clear by addition, giving

$$\frac{d}{dt}(\mathbf{v} + \dot{\boldsymbol{\mu}}) + \beta_T\,\mathbf{v} + \beta_{\dot{\mu}}\dot{\boldsymbol{\mu}} + \beta_{Tr}\dot{\boldsymbol{\mu}} + \beta_{rT}\mathbf{v} = \mathbf{W}_1 + \mathbf{W}_2 \tag{197}$$

which is a Langevin equation written for the linear diffusional velocity in three dimensions of an atom of the molecule, displaced from the latter's center of mass by the vector $\boldsymbol{\mu}$. The simultaneous equations (195) and (196) can be solved[1-4] for acf's and ccf's of interest, for example,

$$\langle \mathbf{v}(t)\cdot\dot{\boldsymbol{\mu}}(0)\rangle = \frac{\langle v^2\rangle}{(c-b^2)^{1/2}}\beta_{Tr}e^{-bt}\sin((c-b^2)^{1/2}t); \qquad (c > b^2) \tag{198}$$

or

$$\langle \mathbf{v}(t)\cdot\dot{\boldsymbol{\mu}}(0)\rangle = \frac{\langle v^2\rangle}{(b^2-c)^{1/2}}\beta_{Tr}e^{-bt}\sinh(b^2-c)^{1/2}t); \qquad (c < b^2) \tag{199}$$

where $b = 2(\beta_T + \beta_{\dot{\mu}})$ and $c = \beta_T\beta_{\dot{\mu}} - \beta_{Tr}\beta_{rT}$. Furthermore, the friction coefficients β_T and $\beta_{\dot{\mu}}$ can be found from the velocity and rotational velocity acf's individually. Therefore, the new ccf's can be found approximately in terms of the coupling parameter β_{rT}. An optimum fit to the computer simulation data at 1 bar and 296 K was found[256] to be with the three friction coefficients $\beta_T = 1.0$ THz, $\beta_{\dot{\mu}} = 25.0$ THz, and $B_{Tr} = 50.0$ THz. This very simple theory can therefore provide analytical representations of the velocity, rotational velocity, and cross correlation functions in terms of the three friction coefficients. For example, the translational velocity acf becomes negative at 0.04 ps, as found in the molecular dynamics simulation of water, and the ccf rises to a maximum of about 0.3 at 0.02 ps, as illustrated in Fig. 31. However, the theoretical curves have the usual severe limitation of an essentially Markovian treatment[13] which can only be remedied with memory functions at the cost of introducing empiricism when truncating the continued fractions. The linked Langevin equations do produce a negative overshoot, however, in both acf's, as observed experimentally and numerically. This is not possible with decoupled Langevin equations, which produce simple exponential decays.

P. The Role of the Intermolecular Potential

The linked Langevin equations (195) and (196) can be modified[257] to include an effective potential $V(\mathbf{r} - \boldsymbol{\mu})$, which is the barrier height to translation caused by the simultaneous rotational velocity of the diffusing molecule. The linked Langevin equations then take the form

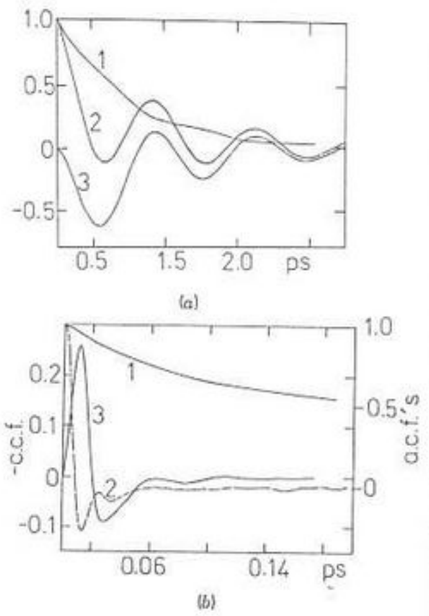

Figure 31. Comparison of theoretical (*a*) and computer-simulated (*b*) ccf's.

$$\ddot{\mathbf{r}} + \beta\mathbf{r} + V'(\mathbf{r} - \boldsymbol{\mu}) = \boldsymbol{\lambda}_1(t) \tag{200}$$

$$\ddot{\boldsymbol{\mu}} + \beta\dot{\boldsymbol{\mu}} - V'(\mathbf{r} - \boldsymbol{\mu}) = \boldsymbol{\lambda}_2(t) \tag{201}$$

$$\ddot{\mathbf{r}} + \ddot{\boldsymbol{\mu}} + \beta(\dot{\mathbf{r}} + \dot{\boldsymbol{\mu}}) = \boldsymbol{\lambda}_1(t) + \boldsymbol{\lambda}_2(t) \tag{202}$$

where $\mathbf{r}$ is the position vector in frame (X, Y, Z) of the molecular center of mass, and $\mathbf{v}$ is defined by $\mathbf{v} = \dot{\mathbf{r}}$. In order to solve these Langevin equations simultaneously it is necessary to assume [41–43] that the friction coefficient appearing in Eq. (200) is the same as that in Eq. (201). In this context V is a potential energy generated by the mutual constraints in frame (X, Y, Z) of the molecular rotational velocity on its own center-of-mass velocity. Equations (200) and (201) are then linked pendulum equations with the extra friction and stochastic terms of the Langevin approach. The stochastic terms $\boldsymbol{\lambda}_1$ and $\boldsymbol{\lambda}_2$ are Wiener processes.[1] The use of an equal friction model implies that the rotational velocity acf and the linear center of mass velocity acf must have the same analytical time dependence when both are normalized at $t = 0$. This is implies that Eqs. (200) and (201) are not applicable in the limit of free rotation, a general restriction on all Langevin equations. In general the dependence of V on its argument is intricately non linear, and obtainable from ab initio computation. However, it can be simply assumed that the argument can be expanded in a Taylor series. The harmonic approximation in this context is then

$$V'(\mathbf{r} - \boldsymbol{\mu}) \simeq 2V_0(\mathbf{r} - \boldsymbol{\mu}) \tag{203}$$

The use of a nonlinear potential would introduce into consideration barrier crossing processes superimposed on the overall diffusion process, making the equations insoluble without transformation to the Kramers form.[41–43] If the nonlinear potential is mimicked with a simple cosine, its derivative would be a sine, which can be approximated by the angular displacement itself, the harmonic approximation. This restricts the physical meaning of the theory to torsional oscillation at the bottom of a steep and deep potential well.

In the harmonic approximation the equations do have an analytical solution which is a complicated expression in terms of the friction coefficient and the parameter

$$\omega_1 = (4V_0 - \beta^2/4)^{1/2} \tag{204}$$

The solution gives a variety of results for acf's and ccf's known to exist from simulation and symmetry.[257] Some of these were compared with simulation data in Ref. 257, using simulation data for liquid water over the complete range of its thermodynamic existence.

The overall behavior of the system of Eqs. (200) and (201) is similar to that of the correlation functions from computer simulation, but we must temper this conclusion with what we know to be the shortcomings of the Langevin equations themselves. As a rough guide to understanding, however, these equations are reasonably satisfactory facsimiles of the numerical data, but become intractable if we attempt a frame transformation from (X, Y, Z) to (z, y, z). In the laboratory frame (X, Y, Z) in which solutions are available[257] the analytical rotational and linear velocity acf's become more oscillatory with increasing V, and the ccf that links them in frame (X, Y, Z) becomes stronger (Fig. 32). The barrier height V seems to be directly responsibly in this approximation for the strength of the cross correlation. The latter is therefore directly dependent on intermolecular forces and torques as well as on overall considerations of symmetry. The harmonic approximation (203) is a very simple description of the information available from symmetry and simulation. However, the theory is severely limited in several ways, because otherwise the solutions, if obtainable at all, would be overparameterized and difficult to use.

1. The friction coefficient is assumed to be a scalar, whereas it is more accurately a tensor.
2. It is assumed to be the same in both equations. More generally the friction coefficents in Eqs. (200) and (201) can take different values.

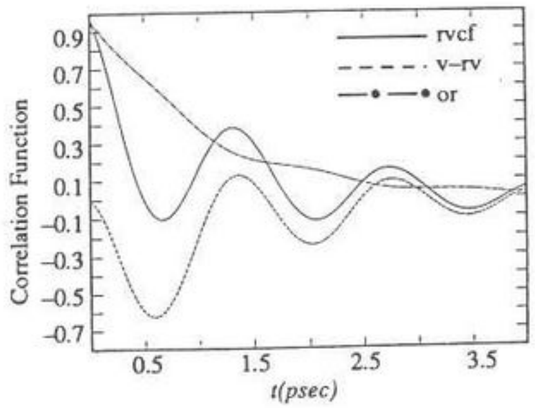

Figure 32. (*a*).

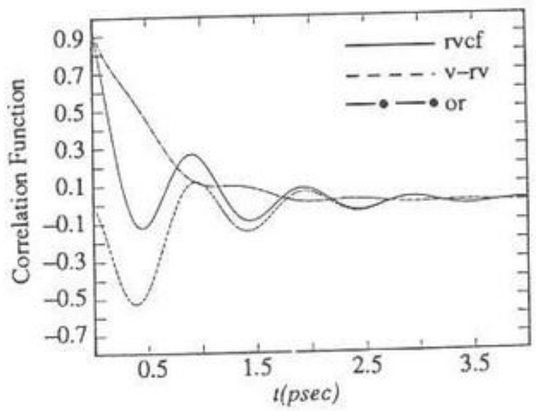

Figure 32. (*b*).

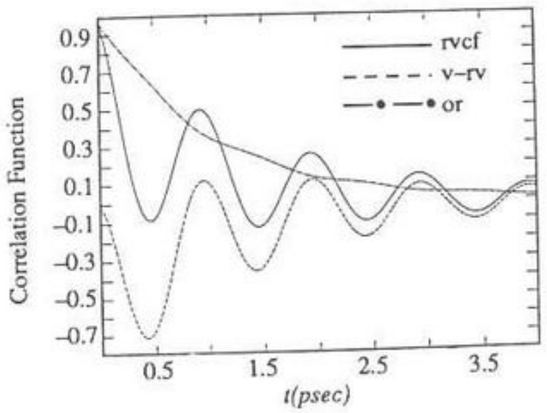

Figure 32. (*c*).

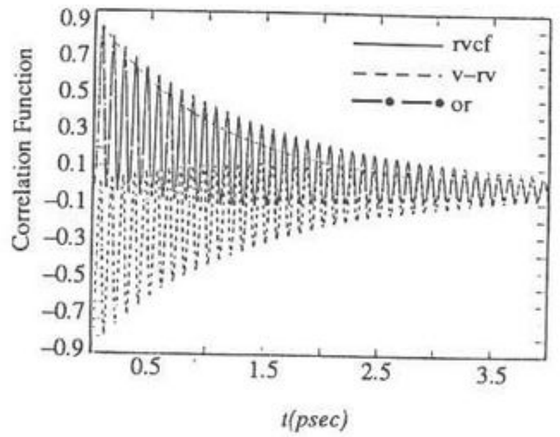

Figure 32. Analytical correlation functions as the barrier height V_0 is varied, (*a*)–(*d*).

3. The intrinsic nonlinearities of the Euler equations operate in frame (x, y, z) and in the (X, Y, Z) representation of Eqs. (200) and (201) are assumed to be contained in the potential term. This assumes that Eq. (203) describes the diffusion of a point in the molecule at the end of the axis $\mathbf{r} = 1$ in the laboratory frame.
4. There are general limitations on the use of Langevin equations, described already.

Given these limitations, Eqs. (200) and (201) represent an approach to diffusional dynamics which attempts to retain mathematical tractability and to reduce complexity.

Q. Patterns of Cross Correlations in Frame (X, Y, Z) and (x, y, z)

The set of nonvanishing ccf's obtainable from these fundamental dynamical considerations can be divided for classification into subsets, or patterns, which serve as a guide to the nature of the ccf's themselves. These patterns can be obtained from the operator equations

$$(\mathbf{v})^{(n+2)}_{XYZ} \equiv (\hat{D}_m + \boldsymbol{\omega}\times)_{(1)}(\hat{D}_m + \boldsymbol{\omega}\times)_{(2)} \ldots (\hat{D}_m + \boldsymbol{\omega})_{(n+1)} \times (\hat{D}_m + \boldsymbol{\omega}\times\mathbf{r}) \tag{205}$$

and

$$(\mathbf{v})^{(n+2)}_{xyz} \equiv (\hat{D}_f - \boldsymbol{\omega}\times)_{(1)}(\hat{D}_f - \boldsymbol{\omega}\times)_{(2)} \ldots (\hat{D}_f - \boldsymbol{\omega}\times)_{(n+1)} \times (\hat{D}_f - \boldsymbol{\omega}\times\mathbf{r}) \tag{206}$$

R. The Omega Pattern in Frame (x, y, z)

By inspection of the terms in the laboratory frame and by application of the standard rotation operation into frame (x, y, z) for any dynamical vector ccf's of the following types exist for $t < 0$ in frame (x, y, z)

$$\langle \boldsymbol{\omega}(t) \times \mathbf{A}(t)\mathbf{A}^T(0)\rangle_{xyz}$$

This is confirmed by point-group theory for all molecular symmetries and for polar vectors **A** such as velocity or inertial and noninertial linear accelerations such as the Coriolis, or centripetal terms in frame (x, y, z). This conclusion is confirmed by the available computer simulations of these ccf's.

A subset of the omega pattern is $\langle \boldsymbol{\omega}(t) \times \hat{D}_f \mathbf{A}(t)\boldsymbol{\omega}^T(0)\rangle$, all members of which exist in frame (x, y, z) from inspection of the general operator equation (206). There also exist patterns of ccf's in frame (x,y,z) made up of cross terms of the operator products in Eq. (206). None of these seems to have been explorcd yet by computer simulation, but are allowed by point group theory in frame (x, y, z) for all molecular symmetries, including that of the spherical top.

S. The $\hat{D}_f$ Pattern in Frame (X, Y, Z)

These results are generated from the subset

$$\langle \dot{\mathbf{A}}(t) \cdot \mathbf{A}(0)\rangle > 0, \qquad t > 0 \tag{207}$$

for all acfs. In Eq. (20) the ccf has been constructed between a dynamical quantity and its time derivative. By applying this result to linear but noninertial velocities and accelerations or to noninertial angular accelerations and higher time derivatives it is possible to see the emergence of many individual ccf's which may exist in frame (X, Y, Z) for all molecular symmetries, including the spherical top. None of these can be described by the theory of Section I, but can be followed approximately by linked Langevin equations of the type used in this chapter. These patterns may be summarized as follows, and emerge from the operator equation (Eq. 205).

The $\hat{D}_f$ pattern is simply

$$\mathbf{C}(t) = \langle \hat{D}_f \mathbf{B}(t)\mathbf{B}^T(0)\rangle_{XYZ} \tag{208}$$

where in general the vector quantity **B** is a linear noninertial variable such as velocity or acceleration. One of the simplest examples of this type is

$$\langle \hat{D}_f(\mathbf{v}(t) - \boldsymbol{\omega}(t) \times \mathbf{r}(t))(\mathbf{v}(0) - \boldsymbol{\omega}(0) \times \mathbf{r}(0))^T\rangle$$

which shows the possible existence in frame (X, Y, Z) of six component ccf's for $t > 0$. Each of these must be individually tested with parity and time-reversal symmetry before its exact time dependence is simulated from a model of the pair potential. For ccf's of this nature, time-reversal symmetry must be applied with care because it reverses the sign of each ccf component as it passes through $t = 0$.

Parity inversion, however, allows the existence of each member of the set of six in frame (X, Y, Z), irrespective of molecular symmetry. The first of the group, $\langle \dot{\mathbf{v}}(t) \cdot \mathbf{v}(0)\rangle$, is the inertial, or Newtonian, ccf. The other five all contain rotational variables, such as the molecular angular velocity, and are noninertial in nature. They vanish only when $\boldsymbol{\omega}$ vanishes and therefore distinguish molecular from atomic ensembles.

Repeated application of the above for more complicated vectors **B**, with more components, produces many more ccf's in frame (X, Y, Z), even for spherical top symmetry. An example is the system

$$\langle \hat{D}_f(\boldsymbol{\omega}(t) \times (\mathbf{v}(t) - \boldsymbol{\omega}(t) \times \mathbf{r}(t)))(\boldsymbol{\omega}(0) \times (\mathbf{v}(0) - \boldsymbol{\omega}(0) \times \mathbf{r}(0)))^T\rangle$$

T. Other Patterns in Frame (X, Y, Z)

The $\hat{D}_f$ pattern just described can be extended to selected cross terms from Eq. (206) provided that the general symmetry rules apply, and the overall symmetry of the ccf's remains that of Eq. (207). These terms can be obtained easily from Eq. (206) by inspection.

U. Symmetry of Some Ccf's

Although the set of diffusion equations represented by the Euler–Langevin components Eqs.(68) to (70) and Eq. (194) is insoluble, its structure may be used by inspection to predict the possible existence in frame (x, y, z) of many ccf's that are among the clearest signatures of the interrelation of the fundamental dynamical variables of molecular diffusion. These ccf's in frame (x, y, z) can be constructed[52,53] by correlating a particular term on the left-hand side of, say, Eq. (194) with counterparts on the left-hand sides of Eqs. (68)–(70), which together comprise the simplest diffusional representation of combined rotation and translation in three dimensions of the asymmetric top molecule.

The rules of parity inversion and time reversal then test the existence of the resulting ccf's in frame (X, Y, Z). These are followed both in frame (X, Y, Z) and (x, y, z) by the rules of point-group theory (Sections VII and VIII). A uniaxial electric field applied to the molecular ensemble may

produce new ccf's which may be investigated in turn with symmetry and computer simulation according to the third principle of group theoretical statistical mechanics of Section VII.

The nature of these ccf's, both in the presence and absence of an electric field, is described in more detail in the source papers.[52,53] One of the effects of the electric field can be summarized as follows:

$$\mathbf{C}_{\mathbf{v}\boldsymbol{\omega}} = \langle \mathbf{v}(t)\boldsymbol{\omega}(0)\rangle_{XYZ} \equiv \begin{bmatrix} 0 & 0 & 0 \\ 0 & 0 & 0 \\ 0 & 0 & 0 \end{bmatrix} \underset{E_Z}{\rightarrow} \begin{bmatrix} 0 & + & 0 \\ + & 0 & 0 \\ 0 & 0 & 0 \end{bmatrix} \tag{209}$$

whose off-diagonal elements exist in the presence of an electric field. In frame (x, y, z) the same effect is as follows

$$\langle \mathbf{v}(t)\boldsymbol{\omega}(0)\rangle_{xyz} \equiv \begin{bmatrix} 0 & + & 0 \\ + & 0 & 0 \\ 0 & 0 & 0 \end{bmatrix} \underset{E_Z}{\rightarrow} \begin{bmatrix} 0 & + & 0 \\ + & 0 & 0 \\ 0 & 0 & 0 \end{bmatrix} \tag{210}$$

The symmetry effect of different types of field, for example a circularly polarized field, is described in the next chapter. Different types of ccf have been simulated recently[52,53] for liquid dichloromethane and water. A complete diffusion theory of the molecular liquid state of matter would provide the time dependence of noninertial ccf's such as this consistently with those of simple acf's. In this context, computer simulation now plays a leading role in linking what we know experimentally to what we can predict on the grounds of symmetry.

In order to illustrate the limits of the analytical theory in the description of field effects on the dynamics of diffusing molecules this section ends with a short description of Mori theory applied to this problem.

V. Analytical Theory[141,142] of Field-Induced ccf's

The following analytical theory is a simple first approximation to the results available from computer simulation but is capable of anticipating an experimental method for the indirect determination of laboratory frame ccf's in the presence of an electric field. The method uses the Kerr effect and its contemporary technology for the measurement of ccf's in liquid, liquid crystals, and other states of matter such as compressed dipolar gases. Another suggested method is the measurement of electric-field

induced phenomena in liquid crystals parallel and perpendicular to an applied Z-axis electric field.

The theory is based on the Mori equation

$$\dot{\mathbf{C}}(t) = \boldsymbol{\lambda}(t)\mathbf{C}(t) - \int_0^t \boldsymbol{\phi}(t-\tau)\mathbf{C}(\tau)\, d\tau \tag{211}$$

for the correlation matrix $\mathbf{C}$ in terms of the Mori resonance operator $\boldsymbol{\lambda}$ and memory function matrix $\boldsymbol{\phi}$. It is convenient to write

$$\mathbf{C}(t) = \begin{bmatrix} \langle \mathbf{v}(t)\mathbf{v}^T(0)\rangle & \langle \mathbf{v}(t)\boldsymbol{\omega}^T(0)\rangle \\ \langle \boldsymbol{\omega}(t)\mathbf{v}^T(0)\rangle & \langle \boldsymbol{\omega}(t)\boldsymbol{\omega}^T(0)\rangle \end{bmatrix} \tag{212}$$

so that the elements of $\mathbf{C}$ are themselves matrices, whose elements in turn are correlation functions. The time evolution of the complete "supermatrix" $\mathbf{C}$ is governed by the Mori equation (Eq. 211), which is the Liouville equation put into a form more suitable for solution.

In order to reduce the problem to the simplest possible form consistent with describing the appearance of the elements of the ccf between linear and angular velocity directly in frame (X, Y, Z), the following assumptions are made:

1. The three molecular moments of inertia of the asymmetric top are approximated by the trace, a scalar average I.

2. It is assumed that the molecule carries a net dipole moment $\boldsymbol{\mu}$ which generates the torque $-\boldsymbol{\mu} \times \mathbf{E}$ described by the Mori resonance operator

$$\boldsymbol{\lambda} = i\omega_1 \begin{bmatrix} 0 & 0 \\ 0 & 1 \end{bmatrix} \tag{213}$$

The scalar frequency in this equation is

$$\omega_1 = \left(\frac{\mu E_Z}{I}\right)^{1/2} \tag{214}$$

With these assumptions we have the definitions

$$C_{vv} = \langle \mathbf{v}(t)\mathbf{v}^T(0)\rangle \tag{215}$$

$$C_{\omega\omega} = \langle \boldsymbol{\omega}(t)\boldsymbol{\omega}^T(0)\rangle \tag{216}$$

$$C_{\nu\omega} = \langle \mathbf{v}(t)\boldsymbol{\omega}^T(0)\rangle$$

$$\equiv \begin{bmatrix} 0 & \langle \nu_X(t)\omega_Y(0)\rangle & \langle \nu_X(t)\omega_Z(0)\rangle \\ \langle \nu_Y(t)\omega_X(0)\rangle & 0 & \langle \nu_Y(t)\omega_Z(0)\rangle \\ \langle \nu_Z(t)\omega_X(0)\rangle & \langle \nu_Z(t)\omega_Y(0)\rangle & 0 \end{bmatrix} \tag{217}$$

The matrix of memory functions is a supermatrix of the form

$$\boldsymbol{\phi}(t) = \begin{bmatrix} \boldsymbol{\phi}_{\nu\nu}(t) & \boldsymbol{\phi}_{\nu\omega}(t) \\ \boldsymbol{\phi}_{\omega\nu}(\mathbf{t}) & \boldsymbol{\phi}_{\omega\omega}(t) \end{bmatrix} \tag{218}$$

Using the computer simulation result that the electric field produces the elements (X, Y) and (Y, X) of $\mathbf{C}_{\nu\omega}$ for an electric field, E_Z gives the simplification

$$\mathbf{C}_{\nu\omega}(t) = \mathbf{C}_{\omega\nu}(t) = C^{xy}_{\nu\omega}(t) \begin{bmatrix} 0 & -1 & 0 \\ 1 & 0 & 0 \\ 0 & 0 & 0 \end{bmatrix} \tag{219}$$

The electric field has the dual role of promoting the existence of $\mathbf{C}_{\nu\omega}$ in frame (X,Y,Z) and of making the sample anisotropic and birefringent, that is,

$$\langle \nu_X^2\rangle = \langle \nu_Y^2\rangle \neq \langle \nu_Z^2\rangle \tag{220}$$

$$\langle \omega_X^2\rangle = \langle \omega_Y^2\rangle \neq \langle \omega_Z^2\rangle \tag{221}$$

Laplace transformation of the Mori equation gives the linear equation

$$(p\mathbf{1} + \boldsymbol{\phi}(p) - i\omega_1\mathbf{1})\mathbf{C}(p) = \mathbf{C}(0) \tag{222}$$

whose supermatrices are

$$\mathbf{C}(0) = \begin{bmatrix} \mathbf{C}_{\nu\nu}(0) & 0 \\ 0 & \mathbf{C}_{\omega\omega}(0) \end{bmatrix} \tag{223}$$

where

$$\mathbf{C}_{\nu\nu}(0) = \begin{bmatrix} \langle \nu_X^2\rangle & 0 & 0 \\ 0 & \langle \nu_Y^2\rangle & 0 \\ 0 & 0 & \langle \nu_Z^2\rangle \end{bmatrix} \tag{224}$$

and

$$\mathbf{C}(p) = \begin{bmatrix} \mathbf{C}_{\nu\nu}(p) & \mathbf{C}_{\nu\omega}(p) \\ \mathbf{C}_{\omega\nu}(p) & \mathbf{C}_{\omega\omega}(p) \end{bmatrix} \tag{225}$$

where

$$(p - i\omega_1)\mathbf{1} + \boldsymbol{\phi}(p) = \begin{bmatrix} (p - i\omega_1)\mathbf{1} + \boldsymbol{\phi}_{\nu\nu}(p) & \boldsymbol{\phi}_{\nu\omega}(p) \\ \boldsymbol{\phi}_{\omega\nu}(p) & (p - i\omega_1)\mathbf{1} + \boldsymbol{\phi}_{\omega\omega}(p) \end{bmatrix} \tag{226}$$

Using the symmetry of the computer simulation result, the elements of the memory matrix are themselves matrices defined by

$$\boldsymbol{\phi}_{\nu\omega} = \boldsymbol{\phi}_{\omega\nu} = \phi^{XY}_{\nu\omega} \begin{bmatrix} 0 & -1 & 0 \\ 1 & 0 & 0 \\ 0 & 0 & 0 \end{bmatrix} \tag{227}$$

$$\boldsymbol{\phi}_{\nu\nu} = \begin{bmatrix} \phi^{XX}_{\nu\nu} & 0 & 0 \\ 0 & \phi^{YY}_{\nu\nu} & 0 \\ 0 & o & \phi^{ZZ}_{\nu\nu} \end{bmatrix} \tag{228}$$

and so on.

For an electric field in the Z axis,

$$\phi^{XX}_{\nu\nu}(p) = \phi^{YY}_{\nu\nu}(p) \neq \phi^{ZZ}_{\nu\nu}(p) \tag{229}$$

$$\phi^{XX}_{\omega\omega}(p) = \phi^{YY}_{\omega\omega}(p) \neq \phi^{ZZ}_{\omega\omega}(p) \tag{230}$$

and similarly for $\mathbf{C}_{\nu\nu}$ and $\mathbf{C}_{\omega\omega}$ and the linear and angular velocity matrices.

Comparing scalar elements in Eq. (222) provides the following set of scalar equations in Laplace space, in terms of the Laplace variable p:

$$C_{\nu\nu}^{XX}(p) = \frac{\langle \nu_X^2 \rangle + \phi_{\nu\omega}^{XY}(p) C_{\nu\omega}^{XY}(p)}{p + \phi_{\nu\nu}^{XX}(p)} \tag{231}$$

$$C_{\nu\nu}^{YY}(p) = \frac{\langle \nu_Y^2 \rangle + \phi_{\nu\omega}^{XY}(p) C_{\nu\omega}^{XY}(p)}{p + \phi_{\nu\nu}^{YY}(p)} \tag{232}$$

$$C_{\nu\nu}^{Z}(p) = \frac{\langle \nu_Z^2 \rangle}{p + \phi_{\nu\nu}^{ZZ}(p)} \tag{233}$$

$$C_{\omega\omega}^{XX} = \frac{\langle \omega_X^2 \rangle + \phi_{\nu\omega}^{XY}(p) C_{\nu\omega}^{XY}(p)}{p - i\omega_1 + \phi_{\omega\omega}^{XX}(p)} \tag{234}$$

$$C_{\omega\omega}^{YY}(p) = \frac{\langle \omega_Y^2 \rangle + \phi_{\nu\omega}^{XY}(p) C_{\nu\omega}^{YY}(p)}{p - i\omega_1 + \phi_{\omega\omega}^{YY}(p)} \tag{235}$$

$$C_{\omega\omega}^{ZZ}(p) = \frac{\langle \omega_Z^2 \rangle}{p - i\omega_1 + \phi_{\omega\omega}^{ZZ}(p)} \tag{236}$$

The ratios of Eqs. (231)–(233) and of (234)–(236) provide the following approximate but transparent results:

$$\phi_{\nu\omega}^{XY}(p) C_{\nu\omega}^{XY}(p) \simeq \langle \nu_Z^2 \rangle \frac{C_{\nu\nu}^{XX}(p)}{C_{\nu\nu}^{ZZ}(p)} - \langle \nu_X^2 \rangle \tag{237}$$

$$\simeq \langle \omega_Z^2 \rangle \frac{C_{\omega\omega}^{XX}(p)}{C_{\omega\omega}^{ZZ}(p)} - \langle \omega_X^2 \rangle \tag{238}$$

and if, in the Markov approximation, we regard the memory function as a constant, that is,

$$\phi_{\nu\omega}^{XY}(p) \simeq \phi_{\nu\omega}^{XY} \tag{239}$$

we obtain the following results, which have a simple physical interpretation:

$$C_{\nu\omega}^{XY}(p) \simeq \frac{\langle \nu_Z^2 \rangle}{\phi_{\nu\omega}^{XY}} \frac{C_{\nu\nu}^{XX}(p)}{C_{\nu\nu}^{ZZ}(p)} - \frac{\langle \nu_X^2 \rangle}{\phi_{\nu\omega}^{XY}} \tag{240}$$

$$\simeq \frac{\langle \omega_X^2 \rangle}{\phi_{\nu\omega}^{XY}} \frac{C_{\omega\omega}^{XX}(p)}{C_{\omega\omega}^{ZZ}(p)} - \frac{\langle \omega_X^2 \rangle}{\phi_{\nu\omega}^{XY}} \tag{241}$$

Equations (240) and (241) show that it is possible to obtain an indication of the time dependence of the (X, Y) and (Y, X) elements of the ccf by

applying an electric field to a molecular liquid sample and observing the anisotropy in the angular velocity acf (and also in the linear velocity acf) with Kerr effect apparatus. Eliminating $C_{\nu\nu}^{XX}$ between Eqs. (231)–(236) and the further four relations

$$C_{\nu\omega}^{XY}(p)(p + \phi_{\nu\nu}^{XX}(p)) + \phi_{\nu\omega}^{XY}(p) C_{\omega\omega}^{XX}(p) = 0 \tag{242}$$

$$C_{\nu\omega}^{XY}(p)(p + \phi_{\nu\nu}^{XY}(p)) + \phi_{\nu\omega}^{XY}(p) C_{\omega\omega}^{YY}(0) = 0 \tag{243}$$

$$C_{\nu\omega}^{XY}(p)(1 - i\omega_1 + \phi_{\omega\omega}^{XX}(p)) + \phi_{\nu\omega}^{XY}(p) C_{\nu\nu}^{XX}(p) = 0 \tag{244}$$

$$C_{\nu\omega}^{XY}(p)(p - i\omega_1 + \phi_{\omega\omega}^{YY}(p)) + \phi_{\nu\omega}^{XY} C_{\omega\omega}^{YY}(p) = 0 \tag{245}$$

and eliminating $C_{\nu\nu}^{XX}$ between Eqs. (231) and (243) and between Eqs. (234) and (242) provides the results

$$\langle \nu_X^2 \rangle = \langle \omega_X^2 \rangle \tag{246}$$

$$\langle \nu_Y^2 \rangle = \langle \omega_Y^2 \rangle \tag{247}$$

$$\langle \nu_Z^2 \rangle \neq \langle \omega_z^2 \rangle \tag{248}$$

Solving simultaneously Eqs. (231), (234), (242), and (243) finally gives the results

$$C_{\nu\omega}^{XY} = -\frac{\langle \omega_X^2 \rangle \phi_{\nu\omega}^{XY} e^{-at/2}}{(b - a^2/4)^{1/2}} \sin((b - a^2/4)^{1/2} t) \tag{249}$$

$$C_{\nu\nu}^{XX}(t) = \langle \nu_X^2 \rangle e^{-at/2} \times \left\{ \cos(b - a^2/4)^{1/2} t) + \frac{(\phi_{\nu\nu}^{XX} - a/2)}{(b - a^2/4)^{1/2}} \sin((b - a^2/4)^{1/2} t) \right\} \tag{250}$$

$$C_{\omega\omega}^{XX}(t) = \langle \omega_X^2 \rangle e^{-at/2} \cos((b - a^2/4)^{1/2} t) + \langle \omega_X^2 \rangle \frac{(\phi_{\omega\omega}^{XX} - i\omega_1 - a/2)}{(b - a^2/4)^{1/2}} \sin((b - a^2/4)^{1/2} t) \tag{251}$$

for the angular, linear, and cross correlations as a function of the electric field strength E_z in terms of the parameters

$$a = \phi_{\nu\nu}^{XX} + \phi_{\omega\omega}^{XX} - i\omega_1 \tag{252}$$

$$b = \phi_{\nu\omega}^{XY2} + \phi_{\nu\nu}^{XX} \phi_{\omega\omega}^{XX} - i\omega_1 \phi_{\nu\nu}^{XX} \tag{253}$$

With the test parameters

$$\phi_{\nu\nu}^{XX} = \phi_{\omega\omega}^{XX} = 10^{12}\ \text{Hz}$$

the following analytical results emerge:[141,142]

1. The envelope of the oscillations remains constant for constant $\omega_1/\phi_{\nu\omega}^{XY}$ in the ccf $C_{\nu\omega}^{XY}$. By parity inversion symmetry $\phi_{\nu\omega}^{XY}$ must disappear for $\omega_1 = 0$ and, therefore, there should be some link between $\phi_{\nu\omega}^{XY}$ and ω_1.
2. It is possible to observe the function $C_{\nu\omega}^{XY}$ even for values of $\phi_{\nu\omega}^{XY}$ much smaller than $\phi_{\nu\nu}^{XX}$ and $\phi_{\omega\omega}^{XX}$.
3. The ccf vanishes as $t \to 0$ and $t \to \infty$. This is also the result obtained from computer simulation.

The simple theory of Eqs. (249)–(251) produces both the linear and angular velocity acf's observed by computer simulation consistently with a ccf, in terms of a small number of parameters. This is a small analytical step towards explaining the set of nonvanishing ccf's between rotational and translational diffusion produced by numerical simulation and allowed by symmetry. The next section provides examples of such ccf's from recent supercomputer simulations.

VI. TIME-CROSS CORRELATION FUNCTIONS—A MAJOR CHALLENGE TO DIFFUSION THEORY

The first ccf to link statistically the rotational and translational diffusion of a molecule was computed in the early eighties.[47] Prior to that the theory of diffusion had not been able to supply the time dependence of any simple but fundamental ccf. In the few years since then the number of known ccf's has increased dramatically. The symmetry laws controlling their existence (Sections VII and VIII) have been identified for all known molecules. This is clearly a major challenge to the approach of (Section I) posed at a fundamental level within the overall framework of classical statistical mechanics. Theories of rotational or translational diffusion cannot by definition describe the time dependence of the simplest type of ccf involving both motions simultaneously. Contemporary attempts at extending or adapting the fundamental theory (Section V) are first approximations which can describe a small fraction of the data available from computer simulation. A more rigorous approach developed from the principles of traditional diffusion theory[1–4] leads to great complexity and empiricism. Thc basic dynamical properties of molecular liquids can now be described more successfully and in greater detail by computer simulation. In this context classical dynamics is being applied to the motion

of molecules and through the intermediacy of powerful contemporary computers produces a range of results and depth of insight unobtainable with traditional diffusion theory. It has become clear that in comparison with simulation, diffusion theory is restricted severely by its own axioms to a few model approximations, such as the Debye theory of rotational diffusion, which are essentially mathematical approximations of the N-body problem. There are a very few of these that have a closed analytical solution for acf's and these are successful in describing only a very limited amount of spectral data, over a limited frequency range. The use of data from spectral moments soon exposes the limitations of the most elaborate analytical theory. The most accurate computer simulation is capable of describing only the first few moments of, for example, combined dielectric and far infrared spectroscopy.

The weaknesses inherent in the original axioms of diffusion theory are now exposed in several ways, for example, experimentally through the use of several different data sources under consistent conditions[1–4] of investigation, theoretically through the use of projection operators[3] applied to the Liouville equation and memory functions, and most starkly, through the set of fundamental cross-correlation functions now available from many computer simulations. The latter show, for example, that hitherto unknown ccf's exist[55–57] in a liquid of spherical top molecules, both in the laboratory frame (X, Y, Z) and in the molecule fixed frame (x, y, z). These show unequivocally and in many different ways that the rotational diffusion of a spherical top is correlated statistically to its own center-of-mass translation. Thc fundamental assumption that these motions are statistically uncorrelatcd is erroneous. Analytical attempts to remedy this error have so far run into difficulties, particularly in modelling realistically the effective pair potential. These appear even under conditions most favorable to the Debye theory, that is, for spherical tops in two or three dimensions.

In considering the diffusion through three dimensions of the most commonplace of molecules, the asymmetric top, the theory of diffusion has never been successful without the use of crude approximation. Even within the restricted confines of rotational diffusion, the Euler–Langevin equations (58)–(60) have no closed solution, and its approximation involves three unknowns, introduced 50 years ago but never determined experimentally. Their independent determination involves the use of three data sources which can be considered as mutually independent. These shortcomings are compounded greatly when account is taken of the new results briefly introduced in Section V. Modern off-shoots of the Debye theory, such as the various itinerant oscillators, have appeared[1–4] throughout the last twenty five years, but carry the same inherent flaws as the original

model. There is no itinerant oscillator theory that can describe the set of nonvanishing ccf's in frames (X, Y, Z) and (x, y, z) without excessive complexity and empiricism. There is no itinerant oscillator which is tractable and rigorous in three dimensions. These theories have achieved very little compared with computer simulation, and are empirically descriptive in nature. Even the rotational versions do not address the nonlinearities of Euler's equations, for example, and even were this to be possible the model representation of the effective pair potential is less realistic by far than those used routinely in computer simulation, sometimes taken directly from ab initio quantum mechanics. When the analytical theory of diffusion appears in the contemporary literature as a description, for example, of spectral data, that description must be tempered with the realization that the comparison of data with theory is inevitably limited to that particular context. For example, the traditional range of data from dielectric relaxation does not extend into the far infrared. The fitting of low-frequency data with a simple rotational Debye theory produces a number, the Debye relaxation time, which is no more than the result of a physically flawed curve-fitting technique.

One of the most convincing illustrations of the extent to which computer simulation has out-paced the analytical methods can be derived from a consideration of intramolecular vibration[156] in a rotating and simultaneously translating diffuser, such as a water molecule. It is now possible to construct an effectivc pair potential for the water molecule that takes into account the internal vibrations of the H_2O framework, and this is adapted for use in a molecular dynamics computer simulation.

A. Ccf's Involving Molecular Vibration

The potential energy between two flexible water molecu!es can be written as the sum of two contributions arising from inter- and intramolecular motions

$$V(\mathbf{r}_{\alpha\beta}, \mathbf{q}_i) = V_{\text{inter}} + V_{\text{intra}} \tag{254}$$

where $\mathbf{r}_{\alpha\beta}$ are the intermolecular atomic distances, and $\mathbf{q}_i$ the internal coordinates. The potential is built up[258] from a consideration of thc rigid MCY ab initio potential,[151] which is itself built up from first principles. The flexibility of the water molecule is modelled with a further ab initio term for the intramolecular motions taken from a high-quality computation by Bartlett, Shavitt, and Purvis.[259] The original rigid MCY potential[151] contains a negative charge which does not coincide with any atom of the molecule, and its extension to flexible geometry assumes that the charge always resides on the line bisecting the H–O–H angle within the molecular framework. This reduces to the rigid MCY potential when there is no framework distortion. The new flexible potential is known as the MCYL potential, which can be used[156] in a computer simulation.

B. Computer Simulation of Flexible Water

The system used for the computation[156] of ccf's in flexible water consisted of 343 water molecules subject to periodic boundary conditions (Chapter 3) and a cut-off radius of 10.87 A. Coded into the algorithm was a numerical method for the evaluation of reaction fields, using a method developed by van Gunsteren et al.[260] The forces due to the complete inter- and intramolecular potential energies and the reaction energy were then evaluated using a sixth-order Gear algorithm. To start the run, the atoms of the ensemble were given random velocities with a Maxwell–Boltzmann distribution, the initial spatial configuration being taken from a previous Monte Carlo simulation. The time step was 0.15 fs for all data evaluation and collection. This allowed the simulation of vibrational features such as infrared and Raman fundamentals with frequencies of up to 100 THz. With this time-step the energy was conserved to 0.0033% in 1000 steps. Trajectories were saved every 10 time steps and the total number of configurations collected was 7600, corresponding to a total simulation time of 11.4 ps.

This method is independent of the simulation of rigid water[202–204] carried out by the present author with a 5×5 site-site model potential. This used no reaction fields, and integrated the equations of motion with an entirely different method. The simulation of flexible water, on the other hand, takes each atom as a separate diffuser, the translational motion of which is constrained by potential bond terms linking it to other atoms of the molecule. This method uses no rotational equations of motion. In order to build up correlation functions of molecular dynamical quantities such as angular velocity, and in order to define orientational and rotational velocity acf's, the data must be refined, allowing direct comparison with the simulation of rigid water[202] and with experimental data. Comparison of results from the two algorithms also allows the estimation of the effect of flexibility on the overall molecular dynamics.

C. The Effect of Internal Vibrations on Correlation Functions

The two methods are capable of producing a set of acf's and ccf's whose individual members contain information on the diffusion in three dimensions of a rigid and flexible model of water. Comparison of the rotational velocity acf from both sources (i.e., the Fourier transform of the far infrared spectrum) exposes the effect of vibration on an essentially rotational and translational motion. In this context the minimum in the

rotational velocity acf from the MCYL flexible potential is s
and more structured up to 0.1 ps, but otherwise there is lit
from the results of the rigid model potential developed b
author. Vibration does not significantly affect the far infra
The results for the rigid water molecule were obtained with
saved configurations and 108 molecules. The results fron
model were computed for 343 molecules over 3400 configura
the numerous approximations in both algorithms, and des
different models used for the water–water pair potential, th
both algorithms are very similar.

The same is true, essentially speaking, for other acf's fro
tions, with the exception of the center-of-mass linear velocit
significantly more oscillatory in the model of flexible water d
displacements of the water center of mass with respect to the
ing atoms. It is significant that the angular velocity acf's fr
rithms are similar in time dependence and also nearly ide
frames (X, Y, Z) and (x, y, z) with the rotational velocity ac
rigid and flexible models of water. The orientational acf's d
slowly in both models. In other words, the far infrared libra
is a far faster process than the low-frequency dielectric adju
frequency of the dielectric loss is about 50 times lower tha
far infrared power absorption coefficient. This is close to what
experimentally, and the results from the flexible water model
agree with those from the rigid model in producing an an
angular and linear acf's in frame (x, y, z), anisotropies that a
experimentally in both cases with, for example, NMR rela
tracer diffusion analysis. The similarities between rigid and fle
acf's extends to the noninertial linear velocities and accelera
duced in Section V. However, a major difference emerges, a
in the acf's of atomic linear velocities in frames (X, Y, Z) a
The acf of the velocity of the diffusing hydrogen atom in particu
oscillatory over a short time scale in the femtosecond rang
frequencies). The rigid model does not produce these oscillati
the H atom does not vibrate with respect to the O atom in t
molecule. The rigid model cannot therefore produce the f
vibrational frequencies of the infrared spectrum.

D. Cross-Correlation Functions

Due to the flexible nature of the MCYL pair potential thc
provides information on the statistical cross correlations betwe
translation and intramolecular bond vibration in the diffusing

tle difference
y the present
red spectrum.
as few as 500
n the flexible
tions. Despite
spite the very
e results from

m the simula-
y acf which is
ue to internal
three vibrat-
m both algo-
ntical in both
f both for the
ecay far more
tional motion
nct. The peak
n that of the
at is observed
el also closely
anisotropy of
are verifiable
laxation and
lexible model
rations intro-
as expected,
and (x, y, z).
ular is highly
e (infrared
ons because
he diffusing
undamental

simulation
en rotation,
water mol-

lightly deeper

available.

E. Vibration–Translation

The ccf between vibration and center-of-mass translation in the water molecule can be defined as follows. The vibration is described through the linear velocity $\mathbf{v}_H$ in frame (x, y, z) of the hydrogen atom, and translation as the linear velocity of the complete molecule, defined as that of the center of mass $(\mathbf{v})$ in the same frame (x, y, z). The latter is fixed by the axes of the molecular principal moments of inertia, which are vibration dependent. The nine elements of the tensor

$$\mathbf{C}_{vt} = \left\{ \frac{\langle \mathbf{v}_H(t)\mathbf{v}(0)\rangle}{\langle v_H\rangle^{1/2}\langle v^2\rangle^{1/2}} \right\}_{xyz} \tag{255}$$

provide the details of this cross correlation. The overall symmetry of this tensor was found to be

$$\mathbf{C}_{vt} = \begin{bmatrix} + & + & 0 \\ + & + & 0 \\ 0 & 0 & + \end{bmatrix}_{xyz} \tag{256}$$

and the time dependence of the nonvanishing elements is illustrated in Figs. 33 and 34. Both the diagonal and off-diagonal elements are very anisotropic, and it is clear that the translational diffusion of the molecular center of mass is correlated statistically to the individual H-atom translation in several different ways. Thc coupling in the (yy) component (Fig. 33*b*) is oscillatory at the frequency of the H-atom vibration, because the y axis is the one that approximately bisects the molecule through thc oxygen atom and the centre of mass. The xx component (Fig. 34*a*) shows the fast oscillations superimposed on slower oscillations of the O-atom vibration. The zz component (Fig. 33*c*) is free of vibrational oscillations because the z axis is perpendicular to the plane of the molecule. This element is nearly identical with the off-diagonal xz element of the ccf. $\mathbf{C}_{v\omega}$ between the center-of-mass linear velocity and the molecular angular velocity ω in frame (x, y, z). Only the off-diagonal elements (Figs. 34*a* and *b*) of $\mathbf{C}_{vt}$ not involving the z axis exist. There is no correlation of the atomic and center-of-mass linear velocity components parallel and perpendicular to the plane of the molecule, but only for those vector components that are both either in or normal to the plane of the molecule.

ecule. This is wholly outside the scope of the diffusion theories now

(Y, Z) and (Z, Y) elements appear in response to a static electric field in the X axis.

The complete set of results summarized briefly in this section must be used in general to characterize the effect of the external circularly polarized field on the molecular dynamics of water.

N. Chiral Liquids

The equivalent effect of the external laser field on the acf's and ccf's of a chiral liquid such as bromochlorofluoromethane introduces an extra element of symmetry. There are two enantiomorphs (mirror-image pairs) which are physically distinct liquids. These are composed of the R and S enantiomer molecules. If these liquids are mixed in equal proportion, the racemic mixture is formed. The physical properties of each enantiomorph, such as melting point, boiling point, density, refractive index, infrared spectrum, and so on are identical in frame (X, Y, Z). However, the two enantiomers rotate the plane of polarized light in equal but opposite directions, and the well-known phenomenon of circular dichroism results from the interaction of circularly polarized radiation with optically active liquids.

These are all well-known properties of optically active liquids (Section IX) but the use of computer simulation has produced a new and fundamental property of thc optically active molecular liquid state discovered by the present author[48] in 1983. This involves the nature of statistical cross correlation in frame (x, y, z) between $\mathbf{v}$ and $\boldsymbol{\omega}$ in the enantiomorphs and racemic mixture of an optically active (chiral) liquid. It was shown that the ccf in frame (x, y, z) was *different* in the enantiomorphs. In general all nine elements of the ccf exist (Sections VII and VIII) and all change sign from one enantiomorph to the mirror image

$$\begin{bmatrix} + & + & + \\ + & + & + \\ + & + & + \end{bmatrix} \rightarrow \begin{bmatrix} - & - & - \\ - & - & - \\ - & - & - \end{bmatrix}_{(x,y,z)} \tag{274}$$

The time dependencies of the elements are equal and opposite in general, and the ccf's cancel in the racemic mixture. The signs of the elements can change from positive to negative or vice versa. In optically active liquids with molecules containing more than one optically active center, it is likely that permutations and combinations of sign changes will become possible. In the simplest type of chiral molecule there is only one optically active center and the switching properties in general depend on

the molecular symmetry. In the lowest chiral molecular point group (C_1), the ccf symmetries are in general

$$\begin{bmatrix} + & + & + \\ + & + & + \\ + & + & + \end{bmatrix} \rightarrow \begin{bmatrix} 0 & 0 & 0 \\ 0 & 0 & 0 \\ 0 & 0 & 0 \end{bmatrix} \leftarrow \begin{bmatrix} - & - & - \\ - & - & - \\ - & - & - \end{bmatrix}_{(x,y,z)} \tag{275}$$

This is a fundamental physical property of all chiral liquids and occurs only in frame (x, y, z). It is another substantial challenge to the approach of Section I.

Dichroism (Section IX) can be computer simulated by applying an external circularly polarized laser field to both the R and S enantiomers of, for example, bromochlorofluoromethane. The results[240] in frames (X, Y, Z) and (x, y, z) can be measured through the appropriate set of acf's and ccf's as for water. In this case, however, additional information is provided by the fact that there are three types of liquid available, denoted by (R), (S), and (RS). In the orientational ccf tensor the off-diagonal structure induced by the field in frame (X, Y, Z) is dominated for all three liquids by the (Z, Y), and (Y, Z) elements for a circularly polarized laser applied in the X axis. There is no discernible symmetry change between enantiomers and mixtures and the result can be summarized as

$$\begin{bmatrix} + & 0 & 0 \\ 0 & + & 0 \\ 0 & 0 & + \end{bmatrix}_R \rightarrow \begin{bmatrix} + & 0 & 0 \\ 0 & + & + \\ 0 & - & + \end{bmatrix}_{R(X,Y,Z)} \tag{276}$$

and similarly for the S enantiomorph and the racemic mixture. However, for the rotational velocity correlation tensor a difference develops between the off-diagonal elements of the enantiomers and racemic mixture, a laboratory frame difference between the response of the enantiomers and the racemic mixture. Part of the explanation for the dynamics of circular dichroism lies in this observation, which can be summarized as

$$\begin{bmatrix} + & 0 & 0 \\ 0 & + & 0 \\ 0 & 0 & + \end{bmatrix}_R \rightarrow \begin{bmatrix} + & - & + \\ - & + & + \\ - & - & + \end{bmatrix}_{R(X,Y,Z)} \tag{277}$$

and

$$\begin{bmatrix} + & 0 & 0 \\ 0 & + & 0 \\ 0 & 0 & + \end{bmatrix}_{RS} \rightarrow \begin{bmatrix} + & + & + \\ - & + & + \\ + & - & + \end{bmatrix}_{RS(X,Y,Z)} \tag{278}$$

There is a different symmetry in the field-on ccf's for the enantiomer and the racemic mixture attributable to the different response of the liquids to the circularly polarized laser field. The symmetry pattern reverses in a left and right circularly polarized field and signals a dichroism in the far infrared and lower frequency adjuncts of the zero to THz range. The birefringence associated with the dichroism manifests itself in the anisotropy of the diagonal element of the rotational velocity and orientational correlation tensors. There is also an interesting indirect effect on the elements of the linear velocity correlation tensor in frame (X, Y, Z). The pattern of field induced cross correlation is further exemplified in the molecular angular velocity correlation tensor in frame (X, Y, Z), but in this case the effect is opposite in the off-diagonals:

$$\begin{bmatrix} + & 0 & 0 \\ 0 & + & 0 \\ 0 & 0 & + \end{bmatrix}_R \rightarrow \begin{bmatrix} + & + & - \\ + & + & + \\ + & - & + \end{bmatrix}_{R(X,Y,Z)} \tag{279}$$

and on the racemic mixture

$$\begin{bmatrix} + & 0 & 0 \\ 0 & + & 0 \\ 0 & 0 & + \end{bmatrix}_{RS} \rightarrow \begin{bmatrix} + & 0 & 0 \\ 0 & + & + \\ 0 & - & + \end{bmatrix}_{RS(X,Y,Z)} \tag{280}$$

There is a direct laboratory frame difference in the off-diagonal elements for enantiomers and racemic mixture related to the fundamental dynamics of linear and nonlinear circular dichroism.

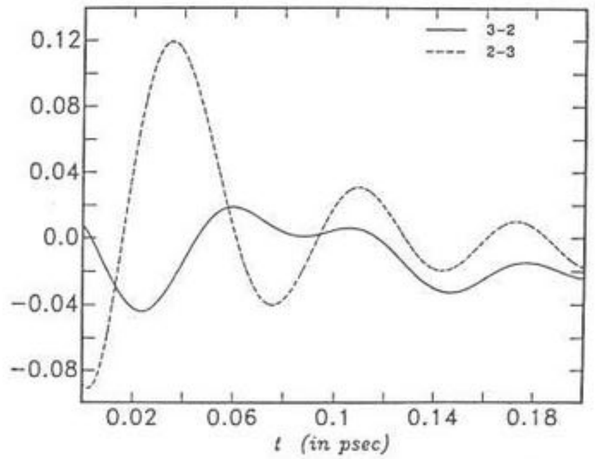

Figure 44. Simple ccf under the influence of a circularly polarized electromagnetic field applied to liquid water, zx and xz elements.

There appears to be no such change, however, in the symmetry of the center of mass linear velocity correlation tensors in frame (X, Y, Z)

$$\begin{bmatrix} + & 0 & 0 \\ 0 & + & 0 \\ 0 & 0 & + \end{bmatrix} \rightarrow \begin{bmatrix} + & 0 & 0 \\ 0 & + & - \\ 0 & + & + \end{bmatrix}_{(X,Y,Z)} \tag{281}$$

both for the enantiomers and the racemic mixture. It is noteworthy that the field induces no new elements of $\langle \mathbf{v}(t)\boldsymbol{\omega}(0) \rangle$ either in the enantiomers or the racemic mixture. The reason for this is that the rotating electric field component of the circularly polarized laser has gerade symmetry, and the ccf has ungerade symmetry to parity inversion.

In the frame (x, y, z) the following symmetry changes were observed when the three liquids are treated in turn with a circularly polarized laser field. The simple ccf just described for frame (X, Y, Z) exists for $t > 0$ and is different in time dependence in frame (x, y, z) for enantiomer and racemic mixture. In the presence of a right circularly polarized field the zy and yz elements in each case are not symmetric in time dependence, but are otherwise similar both for the enantiomer and mixture. Substantial differences begin to appear in the xz and zx elements, the former attaining twice its normalized maximum value for the enantiomer compared with the mixture. The main overall effect of the field on these (x, y, z) frame elements is to remove symmetry difference at field off equilibrium between enantiomer and racemic mixture. These effects are illustrated in Fig. 44.

The circularly polarized field has no effect on thc overall symmetry of

the ccf's in frame (x, y, z), and this is again a consequence of point group theory described in (Sections VII and VIII). It is an advantage to work directly in the laboratory frame (X, Y, Z) when simulating the effect of external fields, allowing direct comparisons to be made with the available experimental data.

O. Circular Flow in Liquid Water

The conditions for simulating circular flow in liquid water were defined in Section IV, where mention was made of birefringence induced by this effect in frame (X, Y, Z). In this section we examine the effect of the flow on correlation matrices of type $\langle \mathbf{A}(t)\mathbf{B}(0)\rangle$ where $\mathbf{A}$ and $\mathbf{B}$ are dynamical quantities in either frame. Circular now effects on the molecular level can be studied through the symmetry changes induced in matrices of this type, which is a key to detecting cross mode couplings in macroscopic flows such as vortices and eddies. There is an infinite number of molecular ccf matrices which may be utilized to explore flow effects, utilizing noninertial and inertial molecular dynamical quantities. Symmetry tests exist to predetermine which members of the set of nonvanishing ccf's may exist for $t > 0$.

In the laboratory frame (X, Y, Z) ccf's of the general type $\langle \mathbf{A}(t)\dot{\mathbf{A}}(0)\rangle$ are affected by the applied flow field. An example is

$$\frac{d}{dt}\langle \mathbf{v}(t) \times \boldsymbol{\omega}(t)\mathbf{v}(0) \times \boldsymbol{\omega}(0)\rangle$$

$$= \langle \dot{\mathbf{v}}(t) \times \boldsymbol{\omega}(t)\mathbf{v}(0) \times \boldsymbol{\omega}(0)\rangle + \langle \mathbf{v}(t) \times \dot{\boldsymbol{\omega}}(t)\mathbf{v}(0) \times \boldsymbol{\omega}(0)\rangle \quad (282)$$

Both the components on the right-hand side exist in frame (X, Y, Z) and the effect of the flow field is to induce off-diagonal elements with $D_g^{(2)}$ symmetry (Sections VII and VIII)

$$\begin{bmatrix} + & 0 & 0 \\ 0 & + & 0 \\ 0 & 0 & + \end{bmatrix} \rightarrow \begin{bmatrix} + & + & 0 \\ + & + & 0 \\ 0 & 0 & + \end{bmatrix}_{(X,Y,Z)} \quad (283)$$

The rotational flow changes considerably the time dependence of the diagonal elements, inducing a nonzero value at $t = 0$ for each. In the absence of flow each element vanishes at $t = 0$, and the properties of this ccf alone give ample scope for linking rotational flow to molecular dynamics.

In frame (x, y, z) rotational flow also has an effect on the overall symmetry of the simple ccf between molecular linear and angular velocities, thc yz element, for example, is amplified to twice its field-free maximum, and the zy element reaches a minimum of -0.12. In contrast, the effect on

$$\mathbf{C}_{r\omega} = \left[\frac{\langle \mathbf{r}(t) \times \boldsymbol{\omega}(t)\mathbf{r}(0)\rangle}{\langle (\mathbf{r} \times \boldsymbol{\omega})^2\rangle^{1/2}\langle r^2\rangle^{1/2}} \right]_{(x,y,z)} \quad (284)$$

is to decrease the amplitude of the diagonal elements, and different again is the behavior of the matrix

$$\mathbf{C}_{r\omega\omega} = \left[\frac{\langle \boldsymbol{\omega}(t) \times (\boldsymbol{\omega}(t) \times \mathbf{r}(t)\boldsymbol{\omega}(0) \times \mathbf{r}(0))\rangle}{\langle (\boldsymbol{\omega} \times (\boldsymbol{\omega} \times \mathbf{r}))^2\rangle^{1/2}\langle (\boldsymbol{\omega} \times \mathbf{r})^2\rangle^{1/2}} \right]_{(x,y,z)} \quad (285)$$

where there is little change in amplitude or time dependence as a result of applying the field.

Another pattern of symmetry changes is produced in the ccf matrix

$$\mathbf{C}_{\omega v} = \left[\frac{\langle \boldsymbol{\omega}(t) \times \mathbf{v}(t)\mathbf{v}(0)\rangle}{\langle (\boldsymbol{\omega} \times \mathbf{v})^2\rangle^{1/2}\langle v^2\rangle^{1/2}} \right]_{(x,y,z)} \quad (286)$$

between the molecular Coriolis acceleration and linear velocity in frame (x, y, z). The overall symmetry effect appears to be

$$\begin{bmatrix} + & 0 & 0 \\ 0 & + & 0 \\ 0 & 0 & + \end{bmatrix} \rightarrow \begin{bmatrix} + & 0 & + \\ 0 & + & + \\ + & + & + \end{bmatrix}_{(x,y,z)} \quad (287)$$

The amplitude of the diagonal elements is increased to about twice the value in the field-free sample, and there appear to be extra off-diagonal elements, which however may be noise, because they are symmetry-disallowed.

Off-diagonal elements are produced by the field of acf's in the laboratory frame (X, Y, Z), whose symmetry is $D_g^{(2)}$. These off-diagonal elements vanish in the field-free isotropic liquid and in consequence there is scope for analysing external flow in terms of field-induced ccf's of this type, using the laboratory frame directly.

P. Other Types of Applied External Field

The examples so far have shown how the application of external, symmetry-breaking, force fields produces new ccf's in frame (X, Y, Z). The discussion has been restricted to a few examples, and in general there are many types of field which can be considered:

1. A magnetic field has the symmetry breaking properties of an applied axial vector, such as the circularly polarized electromagnetic field, rotating electric field, or rotational flow, and would be expected to induce similar dynamical effects in both frames of reference. In this case there is an interaction via the magnetic field–dipole torque and the Lorentz force on each dipole charge. Linear and nonlinear magnetic field effects can be investigated by molecular dynamics computer simulation of a liquid subjected to a magnetic field.

2. Nonlinear effects may be coded by considering the torque generated by an induced dipole moment and terms to higher order in the electric field strength **E** and magnetic field strength **B** of the electromagnetic field. The same equations may be used within the context of classical physics to investigate the effect of neutron radiation, provided that account is taken of the greater transfer of momentum between neutron and molecule. These considerations would, however, involve tensor traces such as that of the molecular polarizability, hyperpolarizability, and so forth, which arc usually unknown experimentally to any precision, except for some limited number of small molecules. The anisotropy of the molecular polarizability appears in the conventional theory of the Kerr effect, and this can also be investigated by computer simulation provided some way is found of mimicking the anisotropy with pair potentials. This is not, however, a straightforward procedure because polarizability is not pairwise additive.

3. Gravitational fields are already used successfully in computer simulations of flow past a disk in two dimensions or a cylinder in three. These produce all the characteristics of macroscopic flow phenomena as derived from continuum hydrodynamics, effects which are always accompanied by new symmetries in ccf tensors at the fundamental molecular level. Two major branches of physics are related in this way, hydrodynamics and classical molecular dynamics.

4. There is a large and growing area of physics devoted to the molecular dynamics simulation of transport phenomena using new types of algorithm.

5. In chiral media the effects discussed above are supplemented by the possibility of investigating the three symmetries represented by (R), (S), and (RS).

Q. Removal of H-Bonding, the Computer Simulation[270] of Hydrogen Selenide

The dynamics of hydrogen selenide can be investigated in the liquid state using ccf tensors. The dynamics of hydrogen bonding can be described in liquid water in this way, using an approach which is intrinsically much simpler than conventional theories of hydrogen bonding. A complete picture of an H-bonded entity such as water can be built up using a few members of the complete set of ccf's, each one of which is an individual signature of the complete dynamical process. The available analytical theory can be made to attempt to follow the wealth of data from a single computer simulation, but at the price of over-parameterization and overwhelming mathematical complexity. The greatest single drawback of the analytical theory is that it is not predictive, whereas the computer simulation can produce the time dependence of correlation functions from a model of the pair potential that is much more realistic than its equivalent in diffusion theory. As an illustration of the use of computer simulation to investigate the effective removal of H-bonding from the dynamical environment of a water-like asymmetric top, we describe results from the recent computer simulation[270] of hydrogen selenide, a C_{2v} asymmetric top, H_2Se.

Hydrogen selenide has one moment of inertia much smaller than the other two, and the subsequent anisotropy of the molecular diffusion is greater than that in water. Diffusion theory therefore requires the solution of the Euler–Langevin equations and three rotational friction coefficients, together with the translational Langevin equations in frame (x, y, z). This is mathematically intractable and no further progress can be made without approximation. From basic considerations, however, we know that the selenium atom is almost two orders of magnitude more massive than the two hydrogen atoms, causing pronounced anisotropy of both rotational and translational dynamics. Computer simulation can be used to investigate this in great detail, and also to follow the diffusional dynamics from liquid to compressed gas. This can be achieved by use of the atom–atom Lennard–Jones potential,[270] from which several ccf's are obtainable using good-quality runs over 6000 time steps. The molecular dynamics were simulated in Ref. 270 at several state points and Fig. 45 illustrates a direct laboratory frame ccf, $\langle \mathbf{v}(t)\dot{\boldsymbol{\mu}}(0)\rangle$, as a function of molar volume. As this is decreased from 180 cm^3/mole in the compressed gas to 40 cm^3/mole in the liquid, the amplitude increases by a factor of about 10. The amplitude is plotted against molar volume in Fig. 46, and it is clear that at high

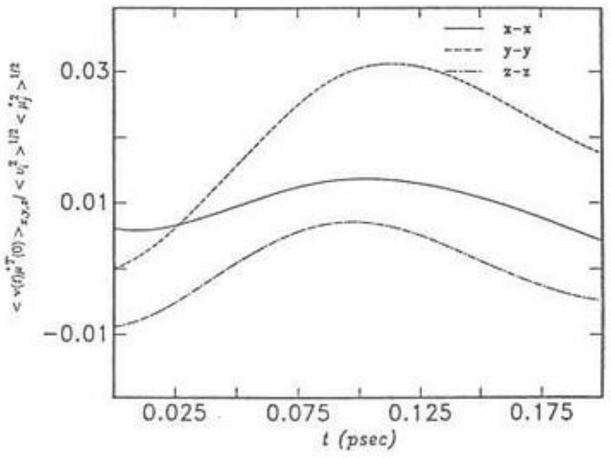

(a)

Figure 45. (*a*).

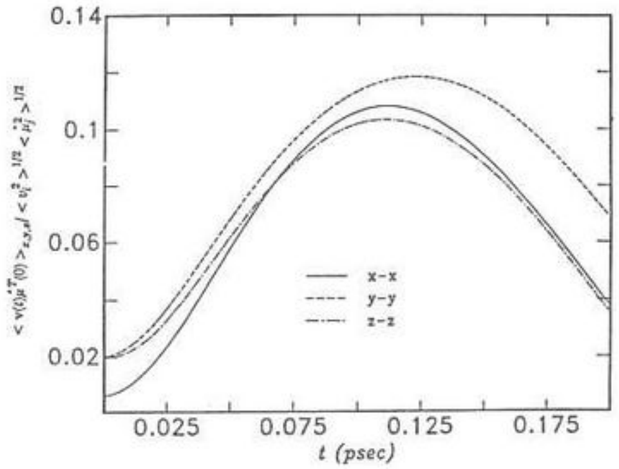

(b)

Figure 45. (*b*).

number densities there is considerable cross correlation. Figure 46 is a plot of the height of the first peak against molar volume and the transition from compressed gas to liquid is marked with a dashed line. As the line is crossed there is a discontinuity in the dependence of the height of the first peak on the molar volume, that is, there is a pronounced change of slope. The phase transition is measurable through the fact that the total energy of the system changes from positive (compressed gas) to negative (liquid). At constant temperature the change of slope becomes apparent at a molar volume of 150 cm^3/mole, which is the point at which the total energy of the system becomes negative. In the compressed gas the total

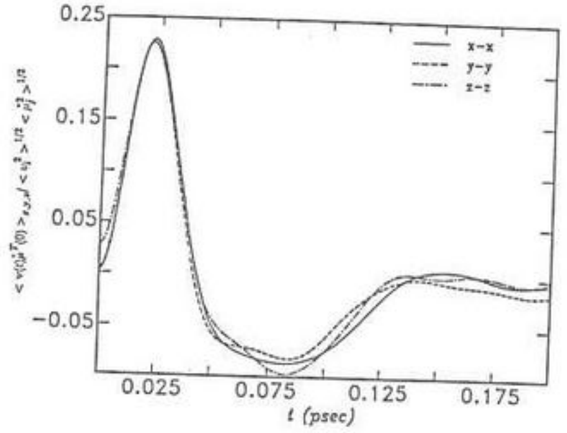

(c)

Figure 45. Ccf between linear and rotational velocity in hydrogen selenide in frame (X, Y, Z) as a function of molar volume at 296 K: (*a*) 180 cm^3/mole, compressed gas; (*b*) 40 cm^3/mole; (*c*) 20 cm^3/mole.

energy is positive, and in the liquid, negative until about 20 cm^3/mole is reached, when it once more becomes positive due to the high external pressures (up to 250 kbar) needed to sustain the sample at 20.0 cm^3/mole at 243 K. In this state a further phase change has occurred from liquid to amorphous solid. Cross correlation between the linear and rotational velocity is therefore sensitive to molar volume, and to the mean intermolecular separation. At the phase change between the compressed gas and liquid there is a discontinuity in the height of the first peak as a function of molar volume which coincides with the point at which the total energy becomes positive from negative.

The overall pattern is similar for the ccf between orientation (the dipole vector) and linear velocity. The intensity once more increases as a function of pressure.

In the frame (x, y, z) the simple ccf $\langle \mathbf{v}(t)\boldsymbol{\omega}(0)\rangle$ has two nonvanishing elements whose amplitude depends on the molar volume. The fundamen-

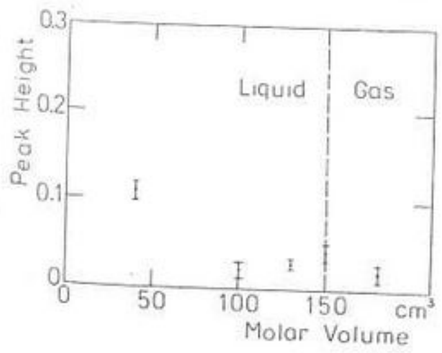

Figure 46. Amplitude of the first peak of the ccf in Fig. 45 as a function of molar volume.

tal molecular dynamics of hydrogen selenide are heavily influenced by cross correlation, which becomes stronger with decreasing molar volume.

The lack of hydrogen bonding in hydrogen selenide is revealed most clearly by higher-order ccf's in frame (x, y, z), whose diagonal elements are anisotropic because the diffusional characteristics are primarily determined by the mass distribution within the molecule itself, and not from intermolecular hydrogen bonding as in water. An extreme example of such anisotropy is methanol,[272] where one diagonal ccf is a thousand times greater in amplitude than the other two.

R. Some Consequences for Quantum Mechanics

For matrix-isolated small molecules such as HD, the rotational spectra generated from the Schrodinger equation are perturbed by mixing with quantized translational lines which appear from the periodicity imposed by the solvent cage. Quantized rotation–translation features occur in the final spectrum. There are shifts in rotational levels, broadening, and disturbance of the rotational selection rules. The existence of the set of classical ccf's in frames (X, Y, Z) and (x, y, z) implies new types of fine and hyperfine structure in the electromagnetic absorption, dispersion, and scattering spectra of liquids and gases, or lattices such as HD in solvents such as argon. These new features could lead to specific and observable information on the nature of rotation to translation to vibration coupling in the liquid state of matter.

The set of nonvanishing ccf's also exists in the compressed and dilute gas states. As dilution proceeds the classical broad-band features typical of a moderately compressed gas give way to quantum absorptions. Under certain conditions, solutions of dipolar molecules in rare gas matrices at low temperatures, the infrared and Raman spectra are quantized. The existence of classical ccf's means that in the dilute gas the translational and rotational wave functions will be mutually perturbed and split the energy levels. Usually, the eigenvalues of linear momentum from Schrodinger's equation form a continuous spectrum from minus infinity to infinity, but in rare gas lattices translational energy levels may become observable at intervals of about $100\,\mathrm{cm}^{-1}$. The levels have been reproduced using a particle in the box model due to Friedmann et al.[273] and the rotational diffusion is linked to the translational. This means that the corresponding wave functions and inner products must also exist in frames (X, Y, Z) and (x, y, z). Usually this kind of perturbation in a compressed gas is thought to result merely in broadening, but under favorable circumstances translational energy levels may be observed.

S. Analogies between Quantum and Classical Mechanics

Consider a linearly independent set $\{A_j(t)\}$, $j = 1, \ldots, n$ of real-time dependent variables of a given n particle system. The set of all possible dynamical variables is a Hilbert space. The ensemble thermodynamic average in this space, $\langle\ \rangle$, is an inner product, so that

$$(A, B) = \langle A(0)B(t)\rangle \tag{288}$$

where A and B are separate dynamical variables. The equilibrium canonical distribution function is

$$f(\mathbf{\Gamma}_0) = \frac{\exp(-H(\mathbf{\Gamma}_0)/kT)}{\int \exp(-H/kT)\, d\mathbf{\Gamma}_0} \tag{289}$$

where $\mathbf{\Gamma}_0$ is the phase space variable and H is the Hamiltonian. With this definition the inner product becomes

$$(A^\times, B) = \int d\mathbf{\Gamma} f(\mathbf{\Gamma}) B(\mathbf{\Gamma}) A^\times(\mathbf{\Gamma}) \tag{290}$$

The state variable A obeys the Liouville equation

$$\dot{A} = i\hat{L}A \tag{291}$$

which has a formal solution

$$A(\mathbf{\Gamma}, t) = \exp(i\hat{L}t)A(\mathbf{\Gamma}, 0) \tag{292}$$

providing a definition of the time acf

$$C(t) = (e^{iLt}A, A^\times) \tag{293}$$

The scalar product used in quantum mechanics and the time-correlation functions are formally equivalent. More generally, two variables A and B can be used to construct the time ccf

$$C(t) = \int d\mathbf{\Gamma} f(\mathbf{\Gamma}) A^\times(\mathbf{\Gamma}) e^{iLt} B(\mathbf{\Gamma}) \tag{294}$$

In analogy with quantum mechanics the two variables A and B are ortho-

gonal if $(A^{\times}, B) = 0$. The propagator $e^{\mathcal{L}t}$ is an orthogonal operator, and by analogy

$$f^{1/2} \equiv \psi_A(\Gamma) \tag{295}$$

is a wavefunction. The time correlation function $C(t)$ is the expectation value of the propagator in the state defined by the wavefunction. The set of nonvanishing ccf's in classical mechanics implies the existence of wave functions in quantum mechanics.[274]

Friedmann and Kimel[273] have considered the far infrared spectrum of HD in an argon lattice, and have accounted for the quantum mechanical mixing of rotational and translational wave functions in great detail. The effect of the correlation between wave functions is to give zero-point translational energy to the rotational quantum states and to raise the rotational energy levels. The cross correlation doubles the rotational band widths of HD with respect to those of pure hydrogen or deuterium in argon lattices, where the spectrum is Raman active. The rotational selection rules are changed considerably as a result of perturbation from the translational motion. Similar effects are also observed in other small molecules such as water trapped in clathrate cages.

There are quantum mechanical equivalents of the noninertial linear velocities and accelerations, and the resulting spectral effects should be observable directly under the right conditions. In analogy with the well-known Stark and Zeeman effects this fine structure would be split into substructure, signalling the appearance of new wave functions due to loss of isotropy in frame $(X\ Y, Z)$. Extra information would also be available for chiral molecules.

T. Rod-like Molecules and Liquid Crystals

Liquid crystals can be made anisotropic[1] by the application of relatively weak external electric and magnetic fields, and these effects are always accompanied by the induction of a new set of nonvanishing ccf's. Several long-rod diffusion theories are available,[275,276] which have recently been tested against new simulation data for the long rod methyl hexa tri yne[277] using 6000 configurations and a site–site pair potential. The Doi–Edwards theory[275] is relevant for dilute gas long rod ensembles, and was tested against a simulation[277] in the gas phase at 150 cm^3/mole. The computed pressure in this condition was 100 ± 200 bar. The usual range of acf's and ccf's was supplemented by the type

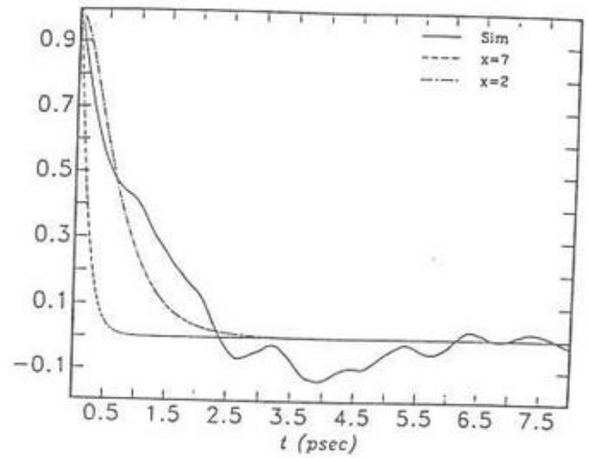

(a)

Figure 47. (*a*).

$$C_{\text{rod}} = \frac{\langle \mathbf{v}(t) \cdot \mathbf{e}_1(0) \mathbf{v}(0) \cdot \mathbf{e}_1(0) \rangle}{\langle (\mathbf{v}(0) \cdot \mathbf{e}_1(0))^2 \rangle} \tag{296}$$

used by Frenkel and Maguire[276] in their theory of hard-rod diffusion. Here $\mathbf{e}_1$ is the initial orientation vector of each molecule in axis I of the dipole moment. A closed solution for this acf is available for direct comparison with simulation.

A second state point was used in the liquid at 50 K and 130 cm^3/mole. Some alignment was observed in the liquid which appears to foreshadow the development of a nematogen. With a small sample of 108 molecules, however, it is not meaningful to see the alignment as characteristic of the nematic phase because swarms in the latter are greater by far than the box size used in the simulation. These swarms define the director axis, which is aligned by an external electric or magnetic field.

Figure 47 is a comparison of C_{rod} from the simulation and the equivalent from the Frenkel–Maguire theory for different x in

$$C_{\text{rod}} = 1/\cosh(xt) \tag{297}$$

The theory fails to reproduce the major features of the simulation, for example, the long negative tail and superimposed oscillations. The root cause of this seems to be that the approach seems to rely on approximation at far too early a stage in the hierarchy of memory functions.

The Doi–Edwards theory is basically a conventional Debye type rotational diffusion approach with the inertial term missing. It is unable to

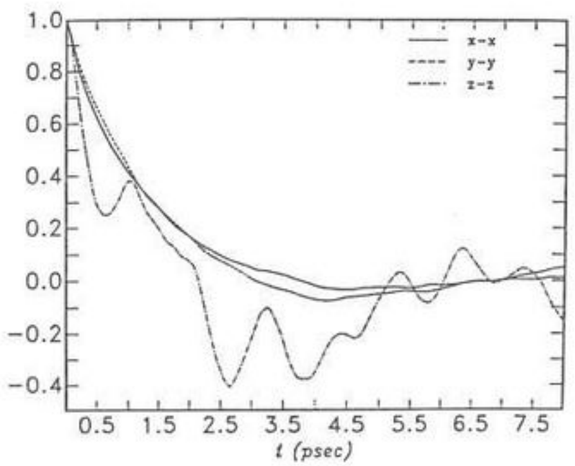

(*b*)

Figure 47. (*a*) Comparison of $\mathbf{C}_{rod}$ from the computer simulation with two results from the Frenkel Maguire theory of hard rod diffusion for different x (see text). Compressed gas. (*b*) Individual computer simulations of elements of $\mathbf{C}_{rod}$ in frame (X, Y, Z). Compressed gas.

describe the set of nonvanishing ccf's in frames (x, y, z) and (X, Y, Z) and has no means of giving even a qualitative description of the statistical correlation between rotation and translation.

U. Survey of Results and Future Progress

Progress away from the empirical and descriptive approach to the phenomenon of molecular diffusion can be made with an appreciation of the set of nonvanishing ccf's. We have attempted to show in the first six sections of this chapter that the traditional approach is limited in comparison with simulation and data now available. In developing the theory further, symmetry is a fundamental consideration, and the principles of group theoretical statistical mechanics are developed and applied in the next two sections.

VII. GROUP THEORY AND STATISTICAL MECHANICS

At the end of the 19th century, Neumann,[278] in a treatise on the luminiferous ether, recognized that there is a link between the symmetry of properties on the the macroscopic scale and the fundamental. The latter was not accepted universally at that time to be molecular in nature. This link is sometimes known[279] as Neumann's Principle, but more often as Curie's Principle.[280] These principles were recognized well before the emergence of Einstein's molecular explanation for Brownian motion, and preceded

the development of correlation functions by more than thirty years. In this section they are extended and applied to molecular dynamics.

We have seen that computer simulation produces a pattern of statistical cross-correlation which is outside the scope of the customary theoretical approach of Section I. Simulation has produced results that the analytical theory had not been able to anticipate. A simple static electric field, for example, induces a statistical cross correlation between the linear and angular velocities of a diffusing molecule. Does the *symmetry* of the electric field vector in the laboratory frame (X, Y, Z) tell us anything about why this particular ccf should appear out of the infinite number possible? We have introduced the frame (x, y, z) fixed in the diffusing molecule, and have seen that the pattern of statistical crosscorrelation is different from that in frame (X, Y, Z). What use can be made of molecular point group theory in this context? What form does the Neumann–Curie Principle take in frame (x, y, z)? Can we devise a form of the principle as a guide to the effect of external force fields in both frames?

Given affirmative answers to these questions we would have constructed guidelines to the symmetry properties[281–290] of molecular diffusion in ensembles, guidelines which can lead to unprecedented experimental insight, new ways of explaining well-established observation, and new experimental techniques.

A. Point-Group Theory in Frame (X, Y, Z)

In the majority of circumstances use is made of point-group theory[291–295] because the ensemble lacks translational symmetry. (In the molecular crystalline condition we would have to deal with space groups because unit cells repeat themselves periodically.) Molecular liquids at field-free, reversible, thermodynamic equilibrium can be considered as spatially isotropic, properties measured in each axis of frame (X, Y, Z) turn out to be the same. There is no translational symmetry in an isotropic atomic or molecular ensemble, whose symmetry is therefore that of a point group, the three-dimensional rotation–reflection group $R_h(3)$. This realization is the key to the well-developed mathematical theory of point groups and their irreducible symmetry representations.[291–295] In this language, the Neumann–Curie Principle can be written as follows, and becomes the first principle[296–299] of group theoretical statistical mechanics (gtsm).

B. The First Principle (Neumann–Curie Principle)

The thermodynamic ensemble average $\langle \mathbf{ABC} \ldots \rangle$ exists in the laboratory frame (X, Y, Z) if the product of symmetry representations $\mathbf{\Gamma(A)\Gamma(B)\Gamma(C)} \ldots$ of the molecular quantities $\mathbf{A}, \mathbf{B}, \mathbf{C}, \ldots$ contains at least once the totally symmetric irreducible representation $D_g^{(0)}$ of $R_h(3)$.

Note that this statement links implicitly concepts on the macroscopic scale, characterized by the thermodynamic average $\langle\ \rangle$, with equivalents on the fundamental atomic or molecular level, characterized by the irreducible representations Γ. Both Neumann and Curie achieved this without the help of point-group theory, but for the same reason their ideas could not be built upon very easily in terms of D representations (Section V).

C. D Representation in Frame (X, Y, Z)

The point group $R_h(3)$ is the symmetry group of isotropic three-dimensional space. Its irreducible representations are $D_g^{(0)}, \ldots, D_g^{(n)}$ and $D_u^{(0)}, \ldots, D_u^{(n)}$, respectively. These are even (g) and odd (u) to the parity reversal $(X, Y, Z) \rightarrow (-X, -Y, -Z)$. A scalar in this notation has symmetry $D_g^{(0)}$, a pseudo-scalar is $D_u^{(0)}$, a polar vector such as $\mathbf{v}$, the center-of-mass velocity, is $D_u^{(1)}$ and an axial vector such as angular velocity ($\boldsymbol{\omega}$) is $D_g^{(1)}$. The Neumann–Curie Principle implies that in isotropic environments such as those of atomic or molecular ensembles, the symmetry of the ensemble average $\langle\mathbf{A}\rangle$ over the physical property $\mathbf{A}$ will be that of $\mathbf{A}$ itself, either in the laboratory or molecule fixed frames. The symmetry of the ensemble average $\langle\mathbf{AB}\rangle$ is given by the product of representations $\boldsymbol{\Gamma}(\mathbf{A})\boldsymbol{\Gamma}(\mathbf{B})$, where $\boldsymbol{\Gamma}$ denotes the symmetry representation in the point group of interest. The latter is $R_h(3)$ in frame (X, Y, Z) and the molecular point group in frame (x, y, z). Thus, the average $\langle\mathbf{AB}\rangle$ over the product of molecular physical properties $\mathbf{AB}$ exists in an isotropic molecular ensemble if $\boldsymbol{\Gamma}(\mathbf{A})\boldsymbol{\Gamma}(\mathbf{B})$ contains the totally symmetric representation (tsr) at least once.

In $R_h(3)$ the tsr is $D_g^{(0)}$, and ensemble averages over scalars of this symmetry exist in field-free isotropic equilibrium. Ensemble averages over pseudo-scalars exist in chiral media, and have opposite sign for each enantiomorph. Ensemble averages over both polar and axial vectors vanish at isotropic equilibrium because the symmetry representations of these quantities do not contain the tsr. These considerations can be extended to higher-order tensors and also to products, such as time-correlation functions. Thus, the generic autocorrelation function $\langle\mathbf{A}(0)\cdot\mathbf{A}(t)\rangle$ exists in frame (X, Y, Z) because the product of representations

$$\boldsymbol{\Gamma}(\mathbf{A})\boldsymbol{\Gamma}(\mathbf{A}) = D_g^{(0)} + D_g^{(1)} + D_g^{(2)} \tag{298}$$

contains the tsr once, representing the trace of the matrix product $\langle\mathbf{A}(0)\mathbf{A}(t)\rangle$. In Eq. (298) we have used the Clebsch–Gordan theorem

$$D^{(n)}D^{(m)} = D^{(n+m)} + \cdots + D^{|(n-m)|} \tag{299}$$

to expand the product of symmetry representations on the left-hand side. The expansion on the right-hand side of this equation contains three terms, the scalar, vector, and tensor products, respectively, $D_g^{(0)}, D_g^{(1)}$, and $D_g^{(2)}$. The vector product of two vectors is another vector, and can be denoted

$$\textit{Vector product part of } \langle\mathbf{A}(t)\mathbf{A}(0)\rangle = \langle\mathbf{A}(t)\times\mathbf{A}(0)\rangle$$

$$= \left\langle \begin{vmatrix} \mathbf{i} & \mathbf{j} & \mathbf{k} \\ A_X(t) & A_Y(t) & A_Z(t) \\ A_X(0) & A_Y(0) & A_Z(0) \end{vmatrix} \right\rangle \tag{300}$$

The overall symmetry of this vector is $D_g^{(1)}$. Here $\mathbf{i}$, $\mathbf{j}$, and $\mathbf{k}$ are unit vectors in the axes X, Y, and Z, respectively. If we examine an individual component of the determinant on the right-hand side of Eq. (300), for example the $\mathbf{j}$-component, we find

$$\{\langle\mathbf{A}(t)\times\mathbf{A}(0)\rangle\}_{\mathbf{j}} = \{\langle A_Z(t)A_X(0)\rangle - \langle A_X(t)A_Z(0)\rangle\}\mathbf{j} \tag{301}$$

with similar results for the other components.

The overall symmetry is however $D_g^{(1)}$, and does not contain the tsr. According to principle 1 these averages all vanish, therefore, at field-free (isotropic) equilibrium, but by principle 3, developed later, may exist in frame (X, Y, Z) in the presence of an external field of the correct symmetry.

Similarly, the tensor product of two vectors is a tensor, a 3×3 matrix, the dyadic product

$$\textit{Tensor part of } \langle\mathbf{A}(t)\mathbf{A}(0)\rangle$$

$$= \left\langle \begin{bmatrix} A_X(t)A_X(0)\mathbf{i}\mathbf{i}^T & A_X(t)A_Y(0)\mathbf{i}\mathbf{j}^T & A_X(t)A_Z(0)\mathbf{k}\mathbf{i}^T \\ A_Y(t)A_X(0)\mathbf{j}\mathbf{i}^T & A_Y(t)A_Y(0)\mathbf{j}\mathbf{j}^T & A_Y(t)A_Z(0)\mathbf{k}\mathbf{j}^T \\ A_Z(t)A_X(0)\mathbf{k}\mathbf{i}^T & A_Z(t)A_y(0)\mathbf{k}\mathbf{j}^T & A_Z(t)A_Z(0)\mathbf{k}\mathbf{k}^T \end{bmatrix} \right\rangle \tag{302}$$

where

$$\mathbf{i}\mathbf{j}^T = \begin{matrix} 0 \text{ if } \mathbf{i} = \mathbf{j}; \\ 1 \text{ if } i \neq j \end{matrix} \tag{303}$$

and so on. The overall symmetry in Eq. (302) is the symmetric second

rank $D_g^{(2)}$ and does not contain the tsr, so that these ensemble averages all vanish at field-free equilibrium. The matrix is symmetric (D rank 2) so that there is index symmetry in the off-diagonal elements.

D. Point-Group Theory in Frame (x, y, z)

In this frame the *molecular* point group is the starting point for the symmetry analysis. Principle 1 can be adapted for use in frame (x, y, z) and becomes the second principle of gtsm.

1. *Principle* 2

The thermodynamic ensemble average $\langle \mathbf{ABC} \ldots \rangle$ exists in frame (x, y, z) of the molecular point group if the product of symmetry representations $\Gamma(\mathbf{A})\Gamma(\mathbf{B})\Gamma(\mathbf{C}) \ldots$ in this point group contains at least once the totally symmetric irreducible representation of the molecular point group itself.

The second principle links quantities on a macroscopic scale to those on the fundamental, but unlike principle 1, the averaging is carried out over properties projected onto frame (x, y, z). In order to use molecular point group theory, the D representations of frame (X, Y, Z) are mapped[291–295] from $R_n(3)$ on to the molecular point group. For each D representation there is an equivalent in the molecular point group. For example, the totally symmetric irreducible representation $D_g^{(0)}$ maps on to the representation of a scalar quantity in frame (x, y, z). A collection of such representations is given in Table II for scalars, pseudoscalars, and axial vectors, and for products of vector representations. This table is further explained later in this chapter.

E. The Effect of Fields—Principle 3

The symmetry effect of external fields may be embodied in the third principle, which is as follows.

1. *Principle* 3

If an external field of force is applied to an atomic or molecule ensemble which subsequently reaches a steady state in the presence of that field, new ensemble averages may be created whose symmetry is that of an applied field.

An applied field of force has its own symmetry signature in a given point group, and in frame (X, Y, Z) this is a D representation. By principle 3 ensemble averages with the same D representation may appear in the N-particle ensemble at the field-on steady state. An electric field, $\mathbf{E}$, for example, is a polar vector of $D_u^{(1)}$ symmetry; a magnetic field $\mathbf{B}$ is an axial vector of $D_g^{(1)}$ symmetry, and a shearing rate of the type $\partial v_X/\partial Z$ has the symmetry[300–303] $D_g^{(0)} + D_g^{(1)} + D_g^{(2)}$.

TABLE II
Symmetry Mapping on Selected Molecular Point Groups

	Scalar		Vector						
Point Group	$D_g^{(0)}$	$D_u^{(0)}$	$D_g^{(1)}$	$D_u^{(1)}$	$D_g^{(1)}D_g^{(1)} = D_u^{(1)}D_u^{(1)} = D_g^{(0)} + D_g^{(1)} + D_g^{(2)}$	$D_u^{(1)}D_g^{(1)} = D_u^{(0)} + D_u^{(1)} + D_u^{(2)}$	No.	No.	Local Symmetry
$C_1(1)$	A	A	$3A$	$3A$	$9A$	$9A$	9	9	Triclinic
$C_i(S_2)$ $(\bar{1})$	A_g	A_u	$3A_g$	$3A_u$	$9A_g$	$9A_u$	9	0	Triclinic
C_2 (2)	A	A	$A + 2B$	$A + 2B$	$5A + 5B$	$5A + 4B$	5	5	Monoclinic
C_{1h} (m)	A^{I}	A^{II}	$A^{\mathrm{I}} + 2A^{\mathrm{II}}$	$2A^{\mathrm{I}} + A^{\mathrm{II}}$	$5A^{\mathrm{I}} + 4A^{\mathrm{II}}$	$4A^{\mathrm{I}} + 5A^{\mathrm{II}}$	5	4	Monoclinic
C_{2h} $(2/m)$	A_g	A_u	$A_g + 2B_g$	$A_u + 2B_u$	$5A_g + 4B_g$	$5A_u + 4B_u$	5	0	Monoclinic
C_{2v} $(2mm)$	A_1	A_2	$A_2 + B_1 + B_2$	$A_1 + B_1 + B_2$	$3A_1 + 2B_1 + 2B_2 + 2A_2$	$2A_1 + 3A_2 + 2B_1 + 2B_2$	3	2	Orthorhombic
D_2 (232)	A_1	A_1	$B_1 + B_2 + B_3$	$B_1 + B_2 + B_3$	$3A_1 + 2B_1 + 2B_2 + 2B_3$	$3A_1 + 2B_1 + 2B_2 + 2B_3$	3	3	Orthorhombic
D_{2h} (mmm)	A_{1g}	A_{1u}	$B_{1g} + B_{2g} + B_{3g}$	$B_{1u} + B_{2u} + B_{3u}$	$3A_{1g} + 2B_{1g} + 2B_{2g} + 2B_{3g}$	$3A_{1u} + 2B_{1u} + 2B_{2u} + 2B_{3u}$	3	0	Orthorhombic
C_3 (3)	A	A	$A + E$	$A + E$	$3A + 3E$	$3A + 3E$	2	2	Trigonal
C_{3v} $(3m)$	A_1	A_2	$A_2 + E$	$A_1 + E$	$2A_1 + A_2 + 3E$	$A_1 + 2A_2 + 3E$	2	1	Trigonal
D_3 (32)	A_1	A_1	$A_2 + E$	$A_2 + E$	$2A_1 + A_2 + 3E$	$2A_1 + A_2 + 3E$	2	2	Trigonal
D_{3d} $(\bar{3}m)$	A_{1g}	A_{1u}	$A_{2g} + E_g$	$A_{2u} + E_u$	$2A_{1g} + A_{2g} + 3E_g$	$2A_{1u} + A_{2u} + 3E_u$	2	0	Trigonal
$S_6(\bar{3})$	A_g	A_u	$A_g + E_g$	$A_u + E_u$	$3A_g + 3E_g$	$3A_u + 3E_u$	3	0	Trigonal
C_4 (4)	A	A	$A + E$	$A + E$	$3A + 2B + 2E$	$3A + 2B + 2E$	3	3	Tetragonal
C_{4v} $(4mm)$	A_1	A_2	$A_2 + E$	$A_1 + E$	$2A_1 + A_2 + B_1 + B_2 + 2E$	$A_1 + 2A_2 + B_1 + B_2 + 2E$	2	1	Tetragonal
C_{4h} $(4/m)$	A_g	A_u	$A_g + E_g$	$A_u + E_u$	$3A_g + 2B_g + 2E_g$	$3A_u + 2B_u + 2E_u$	2	0	Tetragonal
D_4 (422)	A_1	A_1	$A_2 + E$	$A_2 + E$	$2A_1 + A_2 + B_1 + B_2 + 2E$	$2A_1 + A_2 + B_1 + B_2 + 2E$	2	2	Tetragonal
D_{4h} $(4/mmm)$	A_{1g}	A_{1u}	$A_{2g} + E_g$	$A_{2u} + E_u$	$2A_{1g} + A_{2g} + B_{1g} + B_{2g} + 2E_g$	$2A_{1u} + A_{2u} + B_{1u} + B_{2u} + 2E_u$	2	0	Tetragonal
D_{2d} $(\bar{4}2m)$	A_1	B_1	$A_2 + E$	$B_2 + E$	$2A_1 + A_2 + B_1 + B_2 + 2E$	$A_1 + A_2 + 2B_1 + B_2 + 2E$	2	1	Tetragonal
S_4 $(\bar{4})$	A	B	$A + E$	$B + E$	$3A + 2B + 2E$	$2A + 3B + 2E$	3	2	Tetragonal
C_6 (6)	A	A	$A + E_1$	$A + E_1$	$3A + 2E_1 + E_2$	$3A + 2E_1 + E_2$	3	3	Hexagonal
C_{6v} $(6mm)$	A_1	A_2	$A_2 + E_1$	$A_1 + E_1$	$2A_1 + A_2 + 2E_1 + E_2$	$A_1 + 2A_2 + 2E_1 + E_2$	2	1	Hexagonal
C_{3h} $(\bar{6})$	A^{I}	A^{II}	$A^{\mathrm{I}} + E^{\mathrm{II}}$	$A^{\mathrm{II}} + E^{\mathrm{I}}$	$3A^{\mathrm{I}} + 2E^{\mathrm{II}} + E^{\mathrm{I}}$	$3A^{\mathrm{II}} + 3E^{\mathrm{II}}$	3	0	Hexagonal
C_{6h} $(6/m)$	A_g	A_u	$A_g + E_{1g}$	$A_u + E_{1u}$	$3A_g + 2E_{1g} + E_{2g}$	$3A_u + 2E_{1u} + E_{2u}$	3	0	Hexagonal
D_6 (622)	A_1	A_1	$A_2 + E_1$	$A_2 + E_1$	$2A_1 + A_2 + E_2 + 2E_1$	$2A_1 + A_2 + E_2 + 2E_1$	2	2	Hexagonal
D_{3h} $(6m2)$	A_1^{I}	A_1^{II}	$A_2^{\mathrm{I}} + E^{\mathrm{II}}$	$A_2^{\mathrm{II}} + E^{\mathrm{I}}$	$2A_1^{\mathrm{I}} + A_2^{\mathrm{I}} + E^{\mathrm{I}} + 2E^{\mathrm{II}}$	$2A_1^{\mathrm{II}} + A_2^{\mathrm{II}} + 2E^{\mathrm{I}} + E^{\mathrm{II}}$	2	0	Hexagonal
D_{6h} $(6/mmm)$	A_{1g}	A_{1u}	$A_{2g} + E_{1g}$	$A_{2u} + E_{1u}$	$2A_{1g} + A_{2g} + 2E_{1g} + E_{2g}$	$2A_{1u} + A_{2u} + 2E_{1u} + E_{2u}$	2	0	Hexagonal
T_d $(\bar{4}3m)$	A_1	A_2	T_1	T_2	$A_1 + T_1 + E + T_2$	$A_2 + T_2 + E + T_1$	1	0	Cubic
O_h $(m3m)$	A_{1g}	A_{1u}	T_{1g}	T_{1u}	$A_{1g} + T_{1g} + E_g + T_{2g}$	$A_{1u} + T_{1u} + E_u + T_{2u}$	1	0	Cubic
T (23)	A	A	T	T	$A + E + 2T$	$A + E + 2T$	1	1	Cubic
T_h $(m3)$	A_g	A_u	T_g	T_u	$A_g + E_g + 2T_g$	$A_u + E_u + 2T_u$	1	0	Cubic
O (434)	A_1	A_1	T_1	T_1	$A_1 + E + T_1 + T_2$	$A_1 + E + T_1 + T_2$	1	1	Cubic
$C_{\infty v}$	Σ^+	Σ^-	$\Sigma^- + \Pi$	$\Sigma^+ + \Pi$	$2\Sigma^+ + \Sigma^- + 2\Pi + \Delta$	$2\Sigma^- + \Sigma^+ + 2\Pi + \Delta$	2	1	Linear dipolar
C_∞	Σ	Σ	$\Sigma + \Pi$	$\Sigma + \Pi$	$3\Sigma + 2\Pi + \Delta$	$3\Sigma + 2\Pi + \Delta$	3	3	Linear dipolar chiral
$C_{\infty h}$	Σ_g^+	Σ_u^-	$\Sigma_g^- + \Pi_g$	$\Sigma_u^+ + \Pi_u$	$2\Sigma_g^+ + \Sigma_g^- + 2\Pi_g + \Delta_g$	$2\Sigma_u^- + \Sigma_u^+ + 2\Pi_u + \Delta_u$	2	0	Linear nondipolar
D_∞	Σ^+	Σ^+	$\Sigma^- + \Pi$	$\Sigma^- + \Pi$	$2\Sigma^+ + \Sigma^- + 2\Pi + \Delta$	$2\Sigma^- + \Sigma^+ + 2\Pi + \Delta$	2	2	Linear nondipolar chiral

In addition to the ensemble averages that may exist at field-free equilibrium, applied fields set up new ensemble averages in frame (X, Y, Z) whose symmetry, by principle 3, is that of the field. For example, an electric field sets up averages of the type $\langle \boldsymbol{\omega}(t) \times \mathbf{v}(0) \rangle$ similar to those of Eq. (300), but whose symmetry is $D_u^{(1)}$. These have been detected by computer simulation in the form of component ensemble averages which have the property

$$E_Y \text{ induces } \langle \omega_X(t) v_Z(0) \rangle = -\langle \omega_Z(t) v_X(0) \rangle \tag{304}$$

and similarly for the X and Z components of the applied field. These are antisymmetric time ccf's which vanish at field free equilibrium, and have overall symmetry $D_u^{(1)}$. They were found by computer simulation and are not considered in the conventional theory of diffusion.

Similarly, the response of an ensemble of atoms to shear is described by a combination of $D_g^{(1)}$ (vector) symmetry and a tensor symmetry $D_g^{(2)}$. For a strain rate $\partial v_X / \partial Z$, which is traceless (i.e., in which the $D_g^{(0)}$ component is zero) the induced ensemble average is a weighted combination.

F. Symmetries in Frame (x, y, z)

The D symmetry of any quantity in the laboratory frame (X, Y, Z) may be expressed in the molecule fixed frame (x, y, z) by mapping irreducible representations from the $R_h(3)$ point group on to the molecular point group. Table II gives a selection of symmetry mappings on to 36 of the molecular point groups, ranging from lowest symmetry (C_1) to the high-symmetry molecular point groups such as O_h. The significance of such mappings is summarized in principle 2.

Table II describes the symmetry of a scalar, pseudo-scalar, polar, and axial vector, and the product **AA** of two vectors in each molecular point group. The latter may be a product either of two polar or of two axial vectors, and includes the scalar, vector, and tensor components as described in the heading to column six of the table. Column 2 of the table gives the tsr of each point group, and the other columns record the number of times the tsr occurs in the quantity being described in each column. Using principle 2 we can see, for example, that the existence or otherwise of ensemble averages in frame (x, y, z) of each point group is also determined by the number of occurrences of the tsr. Taking the C_{2v} point group of water as an example the table, used with principle 2, shows that the ensemble average $\langle \dot{\mathbf{v}} \rangle_{(x,y,z)}$ may exist in frame (x, y, z) because the molecular linear acceleration is a polar vector whose symmetry representation in the point group C_{2v} is given in column 5. This includes the tsr once, and by principle 2, one scalar component of the ensemble average

of linear acceleration may exist in frame (x, y, z). To find which component, we refer to the character table[291–295] for C_{2v} and find that A_1 refers to the z axis. We conclude that the ensemble average $\langle \dot{v}_z \rangle$ may exist by principle 2 in frame (x, y, z). This finding is overlooked by conventional diffusion theory, and it is important to note that the same average vanishes in frame (X, Y, Z) by principle 1. For a complete picture of statistical processes we need both frames of reference. This can be achieved with combined and systematic use of computer simulation and gtsm.

In other molecular symmetries more than one scalar component of this type may exist in frame (x, y, z), depending on the number of occurrences of the tsr. In the chiral group C_1, for example, there are three occurrences of the tsr both for axial and polar vectors (columns 4 and 5 respectively) and this means that the x, y, and z scalar ensemble averages over both types of vector may exist in frame (x, y, z). In each case each average is independent, and each has a different magnitude. By principle 1 they all vanish, however, in frame (X, Y, Z). In a high-symmetry point group such as T_d, for example that of methane, there are no occurrences of the tsr in columns 4 and 5, and in consequence there can be no surviving scalar components of ensemble averages over vector quantities in frame (x, y, z). In C_{4h} the point group's tsr appears once in column 4, but not in column 5, signifying one component ensemble average over an axial vector such as the angular acceleration in frame (x, y, z). Note that in the chiral point groups C_n and D_n there are always occurrences of the tsr in both columns 4 and 5.

The number of occurrences of the tsr of column 2 in column 6 signifies the number of independent scalar elements that may exist in frame (x, y, z) of the ensemble average $\langle \mathbf{AA} \rangle_{(x,y,z)}$. In the molecular point group of lowest symmetry, C_1, nine scalar components of this ensemble average may exist in frame (x, y, z). For the correlation function $\langle \mathbf{A}(t)\mathbf{A}(0) \rangle_{(x,y,z)}$ each may have a different time dependence, even at field-free equilibrium. In frame (X, Y, Z) in contrast, principle 1 implies that only the autocorrelation function may exist, with one independent time dependence. There is only one occurrence of the tsr in frame (X, Y, Z), but no less than nine in frame (x, y, z) for the same diffusion process. These are the three diagonal and six off-diagonal elements, all with different time dependencies. All may change sign from one enantiomorph to the other.

In point groups of higher symmetry, such as C_{2v}, there are fewer occurrences of the tsr in column 6, indicating the existence of fewer independent elements of the ensemble average. In C_{2v} there are three occurrences of the group's tsr in column 6, and a little group theory is needed to interpret their meaning. The result in column 6 for this point group, as for all point groups, is obtained using products of irreducible

representations.[291–295] The product of representations for two polar vectors, for example, is

$$(A_1 + B_1 + B_2)(A_1 + B_1 + B_2) = A_1A_1 + A_1B_1 + A_1B_2 + B_1A_1 + B_1B_1 + B_1B_2 + B_2A_1 + B_2B_1 + B_2B_2 \quad (305)$$

from which

$$A_1A_1 = A_1; \qquad B_1B_1 = A_1; \qquad B_2B_2 = A_1 \quad (306)$$

using the rules[291–295] for products of irreducible representations. The character table for C_{2v} finally shows that the products in (306) represent the three ensemble averages

$$\langle A_x(t)A_x(0)\rangle; \qquad \langle A_y(t)A_y(0)\rangle; \qquad \langle A_z(t)A_z(0)\rangle \quad (307)$$

each with a different time dependence in frame (x, y, z). This is verified precisely by computer simulation.[1–4] In the laboratory frame there is only one ensemble average, the autocorrelation function with the symmetry of the tsr $D_g^{(0)}$.

Similarly, we may interpret the significance of the tsr occurrences in the other point groups of Table II as they appear in column 6. In some high-symmetry groups such as T_d there is only one occurrence, signifying the one *independent* element

$$\langle A_x(t)A_x(0)\rangle = \langle A_y(t)A_y(0)\rangle = \langle A_z(t)A_z(0)\rangle \quad (308)$$

In other point groups such as C_{3v} there are two occurrences, signifying

$$\langle A_z(t)A_z(0)\rangle \neq \langle A_y(t)A_y(0)\rangle = \langle A_x(t)A_x(0)\rangle \quad (309)$$

that is, two independent elements. In some of the low-symmetry point groups off-diagonal elements may also exist in addition.

G. External Fields: Symmetry

The effect of external fields on averages such as these is to change their individual time dependencies. The overall symmetry, in contrast to frame (X, Y, Z), remains the same, and is given by Table II. It is essential therefore to investigate the overall N-particle ensemble dynamics in both frames for a complete understanding of the diffusional process.

At field-on equilibrium in the presence of shear, for example, we have

asymmetric averages induced in frame (X, Y, Z) (Section VIII) which are part of the overall ensemble average $\langle \mathbf{vv} \rangle$. The latter's symmetry in frame (x, y, z), however, remains the same, and is given in column 6 of Table 2. For each molecular symmetry, therefore, the signature of shear in frame (x, y, z) is different. In frame (X, Y, Z) its symmetry signature is always the same, and is the sum of D symmetries at the head of column 6. We conclude that there is a rich variety of behavior in molecular liquids subjected to couette flow. As usual, symmetry patterns should be investigated in both frames of reference.

Similar considerations apply in frame (x, y, z) for molecular liquids under the effect of an electric or magnetic field. The external field changes the time dependencies of the individual ensemble averages in frame (x, y, z), but leaves the symmetry patterns of Table II unchanged. In frame (X, Y, Z), however, the fields induce new ensemble averages according to principle 3.

H. The Weissenberg Effect

The Weissenberg effect is observed experimentally[304,305] as the pressure (and therefore flow) imparted to a sheared liquid in an axis perpendicular to that of the applied shear plane. It is important in industrial contexts, because the perpendicular flow is caused by a pressure great enough to cause damage, for example, to rollers in the print industry.

The first explanation for the effect has been reported fully elsewhere[300] and is due to new cross correlation functions between elements of the pressure tensor (or stress tensor) in a sheared N-particle ensemble. These can have asymmetry properties described in Section VIII. The existence of these new elements was anticipated by gtsm and confirmed by simulation.[300] They are apparently unknown to conventional rheology and were first characterised by computer simulation. Their description in conventional terms probably requires new constitutive equations and phenomenological parameters. However, it is clear that the underlying cross-correlation functions can be observed experimentally by using computer simulation to match experimental data on Weissenberg flow.

I. Chirality[279]

In a chiral medium (Section VI), pseudoscalar quantities change sign between enantiomorphs. Barron[279] has recently provided a new definition of a chiral influence, which must be odd to parity inversion and even to time reversal. In magnetochiral dichroism,[306–309] (which we consider in more depth later in this section), the chiral influence is a combination of a static magnetic field $\mathbf{B}$, $D_g^{(1)}$, and the propagation vector $\boldsymbol{\kappa}$ $(D_u^{(1)})$ of

unpolarized or linearly polarized electromagnetic radiation. The symmetry signature of this chiral field is therefore

$$\Gamma(\mathbf{B})\Gamma(\boldsymbol{\kappa}) = D_u^{(0)} + D_u^{(1)} + D_u^{(2)} \tag{310}$$

being again a sum of scalar, vector, and tensor components of the type discussed already. These components are all negative to parity inversion and even to time reversal. If the applied chiral influence is made up of colinear vectors, only the $D_u^{(0)}$ component is expected, otherwise principle 3 implies the appearance of averages of all three types in general in response to a chiral external force field.

J. Nonequilibrium: New Fluctuation–Dissipation Theorems

The three principles imply the existence of new fluctuation–dissipation theorems, an ideal vehicle for the development of which is the recent theory of Morriss and Evans,[310] valid for arbitrary applied field strength. We refer to this as Morriss–Evans theory. It is an important step forward in our understanding of nonequilibrium molecular dynamics and provides many new insights to the way in which molecular and atomic ensembles respond to applied force fields of arbitrary strength.

The three principles are generalized in turn by this theory to nonlinear and transient (nonequilibrium) processes.

The main result of the theory is the relation

$$\langle B(t)\rangle = \langle B(0)\rangle - \frac{F_e}{kT}\int_0^t \langle B(s)J(0)\rangle\, ds \tag{311}$$

where $B(t)$ is an arbitrary time-dependent phase variable of the molecular (or atomic) ensemble, and where F_e and J are, respectively, the applied force field and dissipative flux, defined by

$$\frac{dH_0}{dt} = -JF_e \tag{312}$$

Here H_0 is the Hamiltonian. The integrand on the right-hand side of Eq. (311) is a *transient time-correlation function*, which plays a major role for nonlinear, nonequilibrium statistical mechanics analogous to the partition function in thermodynamics and equilibrium statistical mechanics. Equation (311) generalizes the Green–Kubo relations[311] and links the nonequilibrium value of a phase variable (the left-hand side) to the integral over a time-correlation function between the dissipative flux $J(0)$ in the equilibrium state and B at a time s after the external field F_e has been turned on. One example of the theorem at work (Section VIII) is the relation

$$\eta(t) = -\frac{\langle P_{xy}(t)\rangle}{\dot\gamma} = \frac{V}{kT}\int_0^t \langle P_{xy}(s)\,P_{xy}(0)\rangle\, ds \tag{313}$$

for the viscosity, which reduces to the well-known Green–Kubo relation in the limit $\dot\gamma \to 0$. Here $\dot\gamma$ is the strain rate and P_{xy} is the off-diagonal component of the pressure tensor. Equation (313) involves a time-correlation function between $P_{xy}(0)$ from the equilibrium system and $P_{xy}(s)$ *from the perturbed system*, and is valid for arbitrary strain rate $\dot\gamma$. The Morriss – Evans theorem thus deals indiscriminately and consistently with linear and nonlinear response, thus removing the need for linear response approximation.

K. Application of the Theorem to Dielectric Relaxation and the Dynamic Kerr Effect

We consider a static electric force field E_Z applied to a dipolar molecular ensemble. It is well known that the field interacts with each molecule through the latter's multipole moments, that is, the dipole, quadrupole, octopole, and so on. Without loss of generality we can consider that part of the interaction between field and molecular dipole moment. This is characterized by the torque $-\boldsymbol{\mu}\times\mathbf{E}$, where $\boldsymbol{\mu}$ is the molecular dipole moment. The energy $\boldsymbol{\mu}\cdot\mathbf{E}$ supplements the system Hamiltonian. Thus, Eq. (311) reads

$$\langle B(t)\rangle = \langle B(0)\rangle - \frac{E_Z}{kT}\int_0^t \langle B(s)\,\dot\mu_Z(0)\rangle\, ds \tag{314}$$

where μ_Z is the time derivative of μ_Z, and is known as the "rotational velocity". Equation (311) thus reads, for example,

$$\langle \dot\mu_Z(t)\rangle = -\frac{E_Z}{kT}\int_0^t \langle \dot\mu_Z(s)\dot\mu_Z(0)\rangle\, ds \tag{315}$$

In Eq. (314), $B(t)$ is in general *any* phase variable of the N-molecule ensemble, and this equation allows us to take account of the set of nonvanishing ccf's induced by E_Z of arbitrary strength, $E_Z \neq 0$. The following are examples of the new fluctuation–dissipation theorems governing dielectric relaxation and the dynamic Kerr effect.

Setting $B(t)$ to μ_Z, we recover a generalization of the fluctuation dissip-

ation of linear response theory as customarily applied to dielectric relaxation,

$$\langle \mu_Z(t) \rangle = -\frac{E_Z}{kT} \int_0^t \langle \mu_Z(s) \dot{\mu}_Z(0) \rangle \, ds \tag{316}$$

relating the orientational transient $\langle \mu_Z(t) \rangle$ to the nonequilibrium time-correlation function which is the integrand on the right-hand side. Traditional experimental methods use $\mu E_Z \ll kT$, but Eq. (316) shows clearly that for any applied electric field strength the orientational fall transient is dependent on the field strength. Linear response theory equates the time dependence of the fall transient and the equilibrium orientational autocorrelation function. The traditional approach also has no method of explaining why time ccf's, such as that between linear and angular molecular velocity exist for $\mathbf{E} \neq \mathbf{0}$ and vanish *if and only if* $\mathbf{E} = \mathbf{0}$. However, this is easily accommodated by the new theorem using, for example, $B(t) = \mathbf{v}(t)|\boldsymbol{\omega}(t)$, giving the relations

$$\langle \mathbf{v}(t) \rangle = -\frac{E_Z}{kT} \int_0^t \langle \mathbf{v}(s) \cdot \dot{\boldsymbol{\mu}}(0) \rangle \, ds \tag{317}$$

and

$$\langle \boldsymbol{\omega}(t) \rangle = -\frac{E_Z}{kT} \int_0^t \langle \boldsymbol{\omega}(s) \cdot \dot{\boldsymbol{\mu}}(0) \rangle \, ds \tag{318}$$

The fluctuation–dissipation theorem of type (317) shows the presence of a nonvanishing velocity transient due to the fact that the time ccf $\langle \mathbf{v}(t) \cdot \dot{\boldsymbol{\mu}}(0) \rangle$ exists in frame (X, Y, Z), both for $\mathbf{E} \neq \mathbf{0}$ *and* $\mathbf{E} = \mathbf{0}$ from the first principle of group theoretical statistical mechanics. The fluctuation dissipation theorem of Eq. (318) shows the existence of a nonvanishing angular velocity transient due to the fact that the time ccf $\langle \boldsymbol{\omega}(t) \cdot \dot{\boldsymbol{\mu}}(0) \rangle$ exists in frame (X, Y, Z) for $\mathbf{E} \neq \mathbf{0}$ (third principle of group theoretical statistical mechanics), but vanishes in this frame when $\mathbf{E} = \mathbf{0}$ (first principle). The transient ccf's exist for $0 < s < t$ in both cases. We can obtain a third expression merely by multiplying Eqs. (317) and (318), that is,

$$\langle \mathbf{v}(t) \rangle \langle \boldsymbol{\omega}(t) \rangle = \left(\frac{E_Z}{kT} \right)^2 \int_0^t \langle \mathbf{v}(s) \cdot \dot{\boldsymbol{\mu}}(0) \rangle \, ds \int_0^t \langle \boldsymbol{\omega}(s) \cdot \dot{\boldsymbol{\mu}}(0) \rangle \, ds \tag{319}$$

which involves the product of translational and rotational transients.

L. Experimental Observations

The new fluctuation–dissipation theorems can be investigated by computer simulation for all E_Z, but also provide an opportunity for the experimental observation of transient averages caused by cross-correlation functions. An interesting example is $\langle \mathbf{v}(t) \rangle$. This vanishes both at field-off thermodynamic equilibrium and field-on equilibrium (the steady state) because of time-reversal symmetry. However, it may exist as a transient, and should be observable using conventional apparatus to pulse the molecular ensemble with an applied E_Z. A small net translation should be transiently observable, akin to the well-known phenomenon of dielectrophoresis[4] usually attributed to nonuniformities in the applied electric field, that is, to field gradients. Similarly, Eq. (318) shows the existence of a nonvanishing transient angular velocity, which may be observable by techniques sensitive to molecular angular motion, such as far infrared absorption or nuclear magnetic resonance relaxation. The transient angular velocity is intuitively understandable in terms of a removal of external torque.

M. New Dichroic Effects and Absolute Asymmetric Synthesis

The definition of chirality recently provided by Barron[279] and alluded to already in this section implies that the basic requirement for a combination of two vector force fields to be chiral is that one transform as a polar vector and the other as an axial vector and that both be time even or time odd. Thus, at reversible thermodynamic equilibrium,[312] no combination of a static magnetic and static electric field can be chiral. (Note that such a combination can be chiral if one field is made time-dependent, however.) At thermodynamic equilibrium, no combination of static $\mathbf{B}$ and $\mathbf{E}$ can be effective in absolute asymmetric synthesis,[313,314] the preferential production of an enantiomer from a prochiral reaction mixture in what would otherwise be a racemic product.

True chiral influences cause dichroism, an example being magnetochiral dichroism[279] and spin-chiral dichroism.[315] The former is independent of the direction of polarization of the electromagnetic field vector $\boldsymbol{\kappa}$, but reverses if the latter reverses with respect to $\mathbf{B}$. Principle 3 suggests that there is a molecular dynamical mechanism which always accompanies both effects, and which can be observed conversely by the measurement of shifts in the power-absorption coefficient caused by dichroism, or by the

associated birefrigerence. This has the same D symmetry at the depicted on the right-hand side of Eq. (310), a symmetry which is also generated by the ccf $\langle \mathbf{v}(t)\boldsymbol{\omega}(0)\rangle$. This sum of D representations includes pseudoscalar D_u^0, which is invariant to proper rotation in the space of hte complete sample,[279] but which has no directional properties. The pseudoscalar is negative to parity inversion, however, and is the scalar product of an axial and polar vector. Natural optical rotation[279] is a time-even pseudoscalar. The symmetry in frame (X, Y, Z) of the ccf $\langle \mathbf{v}(t)\boldsymbol{\omega}(0)\rangle$ is the sum of the pseudoscalar, a polar vector, negative to parity inversion, and an ungerade second-rank tensor. By principle 3 of gtsm these are all generated by magnetochiral dichroism, which is therefore accompanied by molecular rotation–translation coupling, and is a means of its experimental measurement in the laboratory frame.

Note that the Faraday effect (optical rotation caused by a static magnetic field), does not induce the ccf between linear and angular molecular velocity because the magnetic field has $D_g^{(1)}$ symmetry and cannot, by principle 3, induce effects with ungerade parity-reversal symmetry.

N. Spin-Chiral and Other Dichroic Effects from Principle 3

A true chiral influence is capable of absolute asymmetric synthesis, and it is interesting in consquence to look for other types of true chirality by examining appropriate products of D representations in frame (X, Y, Z).

One of these is spin-chiral dichroism, caused by a combination of $\boldsymbol{\kappa}$ with angular velocity $\boldsymbol{\Omega}$.[315] The angular velocity may be obtained by spinning an electric field around the direction of the unpolarized laser, for example, with the resulting dichroism detected with a Rayleigh refractometer as suggested by Barron and Vrbancich,[316] the laser beam being sent down the arms of this instrument in opposite directions relative to spinning electric fields in each arm. Another experimental alternative is to send circularly polarized laser radiation in opposite directions in each arm.

By Principle 3, a true chiral influence is accompanied in general by all nine elements of the ccf between linear and angular velocity, the "propeller" function. An estimate of the magnitude of magnetochiral dichroism has been given by Barron and Vrbancich[316] who gave a conservative value of about 10^{-8}. A similar effect is expected for spin-chiral dichroism, and can also be investigated by computer simulation in principle.

O. Symmetry Effects in Liquid Crystals

The principles of group theoretical statistical mechanics can be applied[317] to the molecular dynamics of nematogens and cholesterics with point groups

$$C_{\infty v},\ D_{\infty h},\ C_{\infty},\ \text{and}\ D_{\infty}$$

and the effect of alignment with an external static electric field can be treated in terms of new ensemble averages that take the symmetry of the applied field and make swarm averages directly visible in the laboratory frame (X, Y, Z). The symmetry arguments lead to experimentally observable effects and to characteristic ensemble averages of swarm dynamics which should be reproducible numerically by computer simulation.

In a shearing field (Section VIII) which causes a shear strain of the type $\partial v_X/\partial Z$, for example, where v_X is the strain velocity, new time asymmetric cross-correlation functions are observed[300] with the (traceless) D symmetry

$$D_g^{(1)} + D_g^{(2)}$$

The shearing field makes visible directly in the laboratory frame (X, Y, Z) time antisymmetric ensemble averages of $D_g^{(1)}$ symmetry and time-symmetric ensemble averages of $D_g^{(2)}$ symmetry. Examples are the velocity cross-correlation functions

$$\begin{aligned} \langle v_X(0)v_Z(t)\rangle &= -\langle v_X(t)v_Z(0)\rangle \quad (D_g^{(1)}) \\ \langle v_X(0)v_Z(t)\rangle &= \langle v_X(t)v_Z(0)\rangle \quad (D_g^{(2)}) \end{aligned} \tag{320a}$$

The new cross-correlation function between orthogonal atomic velocity components seen in the computer simulation[300] of an atomic ensemble subjected to this type of shear is a weighted sum of the equations above, giving the new and unexpected result

$$\langle v_X(0)v_Z(t)\rangle \neq \langle v_X(t)v_Z(0)\rangle \tag{320b}$$

The effect of this type of shear stress on nematogens and cholesterics is of widespread interest and is explored in this section, which is intended to extend the application of gtsm to the molecular dynamics in liquid crystals. In the unaligned nematogenic phase, for example, the director axis[318–321] forms a frame of reference (x_D, y_D, z_D) with two axes of the frame, say x_D, and y_D, mutually perpendicular to the director axis z_D. The swarm axes form a right-handed frame for consistency of definition when dealing with chiral molecules. The extra time cross correlations set up by the presence of molecular alignment along the director vector are calculated with symmetry arguments, both for electrically dipolar and nondipolar liquid crystal molecules. Both in dipolar and nondipolar nema-

togens, the number of extra cross correlations help to synchronize the molecular dynamics. In the presence of an aligning field, such as **E** or E^2, the director frame becomes virtually coincidental with the laboratory frame (X, Y, Z) and the complete aligned liquid crystal specimen ceases to have the isotropic three-dimensional symmetry $R_h(3)$, taking on $C_{\infty v}$ symmetry, for example, for dipolar molecules in a field **E**. The extra correlation functions and pair-distribution functions that previously existed only in frame (x_D, y_D, z_D), but vanished in the overall isotropic, unaligned, nematogenic sample, now survive ensemble averaging, and accompany the appearance of macroscopic birefringence.

Similar considerations are developed for cholesterics, where the relevant point groups are chiral. They isolate the set of nonvanishing time cross-correlation functions and radial distribution functions which occur exclusively in cholesterics.

A shearing field makes possible the existence in the laboratory frame of new time asymmetric ensemble averages. Shearing would tend to align the director, as with electric fields, but this time would also allow averages of types $D_g^{(1)}$ (antisymmetric in the indices X and Z, and related to shear-induced vorticity) and $D_g^{(2)}$ (symmetric in the indices X and Z, and related to shear-induced deformation) to exist in frame (X, Y, Z). Here we make the simple ansatz that averages equivalent to these D symmetries in the field-free liquid crystal that exist in the absence of the field only in frame (x_D, y_D, z_D) become visible in frame (X, Y, Z) when the liquid crystal is sheared.

P. Basic Symmetry Arguments in Nematogens and Cholesterics

In the unaligned nematogen, or cholesteric phase,[1] group theoretical arguments can be used in the three frames (X, Y, Z), (x_D, y_D, z_D), and (x, y, z), respectively the laboratory, director, and molecule fixed frames of reference. In the frame of reference (X, Y, Z) of the unaligned sample, the relevant point group is $R_h(3)$ of isotropic three-dimensional space. The irreducible representations are $D_g^{(0)}$ (scalar); $D_g^{(0)}$ (pseudoscalar); $D_u^{(1)}$ (polar vector), and $D_g^{(1)}$ (pseudo or axial vector). Higher-order tensors are designated $D_u^{(2)}$, $D_g^{(2)}$, and so on. The point group of the director frame is $C_{\infty v}$ for a dipolar nematogen and $D_{\infty h}$ for a nondipolar nematogen. The irreducible representations are those of these point groups, whichever is appropriate. The director slowly meanders through the laboratory frame but has these point-group symmetries over a well-defined region of three-dimensional space which is large[1] in comparison with molecular dimensions but small in comparison with the volume occupied by the macroscopic sample. In theory, the director point group may have any symmetry, but in nematogens there is alignment in one axis only (z_D). This feature

is absent in isotropic molecular liquids such as water, and in nematogens vanishes at the nematic–isotropic transition temperature. Thus, a nematic phase is distinguished by extra ensemble averages (e.g., dynamic time-correlation functions and static, radial pair-distribution functions) in the director frame of reference. Finally, in the molecule fixed frame (x, y, z) of the point group character tables, the relevant point group and irreducible representations are those of the molecular symmetry itself.

The molecular structure and dynamics of the unaligned nematogen are determined by principle 1 in combination with computer simulation and the theory of diffusion.

The director defines a region of three-dimensional space which is described by the point groups $C_{\infty v}$ and $D_{\infty h}$, respectively, depending on whether the individual molecules are dipolar or nondipolar. This region is referred to conveniently as the "swarm." Thermodynamic ensemble averages may be constructed inside the swarm, bringing principle 2 into operation, but in frame (x_D, y_D, z_D).

1. *The $C_{\infty v}$ Swarm*

This applies to electrically dipolar nematogen molecules, the vast majority. Mapping[291–295] the irreducible representations of a scalar, vector, and so on from $R_h(3)$ to $C_{\infty v}$ gives

$$\begin{aligned} &D_g^{(0)} \rightarrow \Sigma^+; \qquad D_u^{(0)} \rightarrow \Sigma^- \\ &D_g^{(1)} \rightarrow \Sigma^- + \Pi; \qquad D_u^{(1)} \rightarrow \Sigma^+ + \Pi \\ &D_g^{(2)} \rightarrow \Sigma^+ + \Pi + \Delta; \qquad D_u^{(2)} \rightarrow \Sigma^- + \Pi + \Delta \\ &D_g^{(3)} \rightarrow \Sigma^- + \Pi + \Delta + \Phi; \qquad D_u^{(3)} \rightarrow \Sigma^+ + \Pi + \Delta + \Phi \end{aligned} \tag{321}$$

The totally symmetric irreducible representation in the $C_{\infty v}$ swarm is Σ^+. Using principle 2 it can be shown that extra cross-correlation functions exist inside the swarm that vanish in (X, Y, Z). For example, one independent element of $\langle \mathbf{v}(t)\boldsymbol{\omega}(0)\rangle$ exists because the product of representations inside the $C_{\infty v}$ point group

$$\Gamma(\mathbf{v})\Gamma(\boldsymbol{\omega}) = (\Sigma^+ + \Pi)(\Sigma^- + \Pi) = \Sigma^+ + 2\Sigma^- + 2\Pi + \Delta \tag{322}$$

contains the tsr Σ^+ once. Using this point group's character table[291–295] shows that this is

$$\langle v_{x_D}(t)\omega_{y_D}(0)\rangle = -\langle v_{y_D}(t)\omega_{x_D}(0)\rangle \tag{323}$$

This type of ccf vanishes in frame (X, Y, Z). This is one member of the set of nonvanishing ccf's inside the swarm whose members all vanish in (X, Y, Z). Thus any attempt to describe molecular dynamics inside a swarm with computer simulation must produce the result shown in Eq. (323). The swarm volume is bigger than the molecular dynamics "cube" itself, and spontaneous swarm formation under the right conditions can be measured through the spontaneous appearance of the result.[323] This ccf element will vanish for all t if the swarm disappears for some reason, for example, at the nematic (or cholesteric) to isotropic phase change. This gives a simple test for the occurrence of a liquid crystal in computer simulation.

There are many other differences between swarm dynamics and those in (X, Y, Z). For example, time-autocorrelation functions (acf's) become anisotropic

$$\langle \mu_{z_D}(t)\mu_{z_D}(0)\rangle \neq \langle \mu_{x_D}(t)\mu_{x_D}(0)\rangle = \langle \mu_{y_D}(t)\mu_{y_D}(0)\rangle \tag{324}$$

$$\langle \omega_{z_D}(t)\omega_{z_D}(0)\rangle \neq \langle \omega_{x_D}(t)\omega_{x_D}(0)\rangle = \langle \omega_{y_D}(t)\omega_{y_D}(0)\rangle \tag{325}$$

Under some circumstances, thermodynamic averages may exist in the swarm over polar vectors such as $\dot{\mathbf{v}}$ or $\ddot{\boldsymbol{\mu}}$ which have positive time-reversal symmetry. This again can be picked up by computer simulation, and signifies that the swarm can have a net linear acceleration inside the macroscopic unaligned nematogen, measured with respect to the frame (x_D, y_D, z_D). These net accelerations vanish in frame (X, Y, Z).

2. *The $D_{\infty h}$ Swarm*

This refers to electrically nondipolar molecules which form a nematic phase. An example is hexaphenyl (linear end-to-end arrangement of phenyl groups). In this case the irreducible representations of $R_h(3)$ map on to $D_{\infty h}$ as follows:

$$D_g^{(0)} \to \Sigma_g^+; \qquad D_u^{(0)} \to \Sigma_u^-$$

$$D_g^{(1)} \to \Sigma_g^- + \Pi_g; \qquad D_u^{(1)} \to \Sigma_u^+ + \Pi_u$$

$$D_g^{(2)} \to \Sigma_g^+ + \Pi_g + \Delta_g; \qquad D_u^{(2)} \to \Sigma_u^- + \Pi_u + \Delta_u$$

$$D_g^{(3)} \to \Sigma_g^- + \Pi_g + \Delta_g + \Phi_g; \qquad D_u^{(3)} \to \Sigma_u^+ + \Pi_u + \Delta_u + \Phi_u$$

There are fewer new ensemble averages specific to the $D_{\infty h}$ swarm. For example, there can be no ccf's between $\mathbf{v}$ and $\boldsymbol{\omega}$ because the product of symmetry representations

$$\Gamma(\mathbf{v})\Gamma(\boldsymbol{\omega}) = (\Sigma_g^- + \Pi_g)(\Sigma_u^+ + \Pi_u) = \Sigma_u^+ + 2\Sigma_u^- + 2\Pi_u + \Delta_u \tag{326}$$

does not contain the group's tsr Σ_g^+. It is more difficult therefore for the molecular dynamics to be synchronised in a $D_{\infty h}$ swarm, which helps to explain why there are far fewer observed to date. However, the results of Eqs. (324) and (325) are retained in this type of swarm, the relevant products of representations containing in each case two occurrences of the tsr. Computer simulation must be able to pick up this result when attempting to describe the molecular dynamics within a nondipolar swarm, for example, one made up of long rods. In the $D_{\infty h}$ swarm the mean molecular angular acceleration vanishes, but the mean molecular linear center-of-mass acceleration exists. In general, the set of nonvanishing ensemble averages in frame (x_D, y_D, z_D) of this swarm contains fewer members than in the $C_{\infty v}$ swarm.

3. *The $C_{\infty v}$ Swarm*

This is found in an unaligned cholesteric phase[1] made up of chiral dipolar molecules. The D representations map onto the following in the point group C_∞

$$D_g^{(0)} \text{ and } D_u^{(0)} \to \Sigma$$

$$D_g^{(1)} \text{ and } D_u^{(1)} \to \Sigma + \Pi$$

$$D_g^{(2)} \text{ and } D_u^{(2)} \to \Sigma + \Pi + \Delta$$

$$D_g^{(3)} \text{ and } D_u^{(3)} \to \Sigma + \Pi + \Delta + \Phi$$

These mappings show that the cholesteric C_∞ swarm has more intrinsic nonvanishing ensemble averages in the frame (x_D, y_D, z_D) than the nematic $C_{\infty v}$ swarm. For example, the product of representations

$$\Gamma(\mathbf{v})\Gamma(\boldsymbol{\omega}) = (\Sigma + \Pi)(\Sigma + \Pi) = 3\Sigma + 2\Pi + \Delta \tag{327}$$

shows that there are three independent elements in the swarm frame of a ccf such as $\langle \mathbf{v}(t)\boldsymbol{\omega}(0)\rangle$. Reference to the C_∞ point group character table shows these to be

$$\langle \nu_{z_D}(0)\,\omega_{z_D}(t)\rangle \neq \langle \nu_{y_D}(0)\,\omega_{x_D}(t)\rangle = \langle \nu_{x_D}(0)\omega_{x_D}(t)\rangle \tag{328}$$

$$\langle \nu_{x_D}(0)\,\omega_{y_D}(t)\rangle = -\langle \nu_{y_D}(0)\,\omega_{x_D}(t)\rangle$$

This cholesteric swarm also allows the existence of off-diagonal elements

of time acf's, the overall symmetry being the same pattern as Eq. (328), two independent diagonal elements and one independent off-diagonal. All ccf elements change sign from one enantiomorph to the other. A computer simulation of a cholesteric swarm would be expected to reproduce these results. At the cholesteric to isotropic phase transition, the set of ccf elements of Eq. (328) all disappear with the director and the swarm frame, and this is another test for computer simulation.

4. *The D_∞ Swarm*

This is a cholesteric swarm with overall nondipolar symmetry. The relevant mappings are as follows:

$$D_g^{(0)} \text{ and } D_u^{(0)} \rightarrow \Sigma^+$$

$$D_g^{(1)} \text{ and } D_u^{(1)} \rightarrow \Sigma^- + \Pi$$

$$D_g^{(2)} \text{ and } D_u^{(2)} \rightarrow \Sigma^+ + \Pi + \Delta$$

$$D_g^{(3)} \text{ and } D_u^{(3)} \rightarrow \Sigma^- + \Pi + \Delta + \Phi$$

again providing the opportunity for several new time ccf patterns to develop in the swarm.

Extra time cross correlations are set up in frame (x, y, z) which are governed by principle 2 and the point-group symmetry of the molecule itself. The molecules making up nematogens and cholesterics are often of quite low symmetry, thus allowing many more thermodynamic ensemble averages to become visible at the molecular level which are different from those at the intermediate swarm level and which vanish at the macroscopic level. A computer simulation must be able to produce numerical results which reproduce self-consistently all the symmetry-predicted thermodynamic averages in all three frames. Thermodynamically and statistically therefore, the existence of unaligned nematogens and cholesterics is accompanied by the appearance of extra time cross correlations at the swarm and molecular level. Properties specific to such liquid crystals can be traced to these cross correlations, which can therefore be related to these observable properties with computer simulation.

5. *The Electrically Aligned Nematogen*

In the aligned nematogen, the director axis no longer meanders in three dimensions, but is locked in one axis, say Z, of the laboratory frame (X, Y, Z) by the torque generated between the molecular dipole moment μ and the electric field E_z. On the basis of principle 3, the first-order

applied electric field of symmetry $D_u^{(1)}$ sets up new ensemble averages of the same symmetry at field-on equilibrium. One example is the time ccf

$$\langle v_X(t)\,\omega_Y(0)\rangle = -\langle v_Y(t)\,\omega_X(0)\rangle \tag{329}$$

which becomes directly visible in the laboratory. This was first demonstrated, as we have seen in earlier chapters, for molecular liquids using computer simulation, but has yet to be explored in aligned nematogens and other liquid crystals. The ccf (Eq. 329) represents the $D_u^{(1)}$ part of the tensor $\langle \mathbf{v}(t)\,\omega(0)\rangle$ which has

$$D_u^{(0)} + D_u^{(1)} + D_u^{(2)}$$

symmetry. The $D_u^{(1)}$ is the vector part $\langle \mathbf{v}(t) \times \omega(0)\rangle$.

The effect of the static electric field E_z on a nematogen made up of molecules each with the electric dipole moment μ is to make the frames (x_D, y_D, z_D) and (X, Y, Z) indistinguishable as reference frames for molecular dynamics. This is because the director axis z_D is the laboratory axis Z. The extra ensemble averages that have been shown to exist in, for example, a $C_{\infty v}$ swarm now exist in (X, Y, Z) itself. If the nematogen is only partially aligned, the ensemble averages lose some amplitude but are still visible in (X, Y, Z). Similar conclusions are valid for a second-order field E^2, but in this case the field interacts with the polarizability tensor of the molecule, producing orientation, but not alignment. This means that half the aligned molecules have dipoles in one direction, on average, and half in the other. This is described in D language as a sum of $D_g^{(0)}$- and $D_g^{(2)}$-type ensemble averages in frame (X, Y, Z). Mappings of both these D representations on to the $C_{\infty v}$ point group contain the latter's tsr, as is also the case for the other swarm point groups. Thus a field E^2 makes $D_g^{(2)}$ averages of the swarms directly observable in frame (X, Y, Z). (The $D_g^{(0)}$ represents scalars which are frame invariant, i.e., their thermodynamic averages exist in any frame of reference.) In the aligned or oriented state we denote, for convenience, "$C_{\infty v}$ nematogens," constructed from swarms of the same symmetry, and so on.

6. *The $C_{\infty v}$ Nematogen*

The mappings given already for this swarm can be utilized directly to find the nonvanishing ensemble averages in frame (X, Y, Z) in the $C_{\infty v}$ nematic. For example, whenever a D representation of group $R_h(3)$ maps onto a $C_{\infty v}$ representation of the aligned nematic that contains the latter group's tsr, extra ensemble averages will appear in frame (X, Y, Z) itself.

Thus for example, the averages previously confined to the swarm and described earlier now exist directly in (X, Y, Z):

$$\langle \nu_X(t)\, \omega_Y(0)\rangle = -\langle \nu_Y(t)\, \omega_X(0)\rangle \tag{330}$$

$$\langle \mu_Z(t)\, \mu_Z(0)\rangle \neq \langle \mu_X(t)\, \mu_X(0)\rangle = \langle \mu_Y(t)\, \mu_Y(0)\rangle \tag{331}$$

$$\langle \omega_Z(t)\, \omega_Z(0)\rangle \neq \langle \omega_X(t)\, \omega_X(0)\rangle = \langle \omega_Y(t)\, \omega_Y(0)\rangle \tag{332}$$

Equation (330) signals the existence of direct rotation translation coupling in the aligned nematic which has a considerable effect on the molecular dynamics because of the large degree of alignment possible experimentally, even with a weak electric field, of equivalent energy μE_Z much smaller than the thermal energy kT. So far in computer simulations, alignment has been achieved, and ccf's such as Eq. (330) observed, but only through the use of field energies μE_Z about the same as kT. This is because the simulations dealt with isotropic molecular liquids such as water. No complete computer simulation of an aligned nematogen is yet available.

Equations (331) and (332) show that the sample is anisotropic in the laboratory frame under the influence of an aligning first-order electric field E_z. It is therefore birefringent. Our symmetry arguments have therefore consistently reproduced a well-known feature of nemotogenic behavior, especially noticeable in dielectric loss and dispersion. The dielectric complex permittivity is essentially[1] the Fourier transform of Eq. (331) and is by symmetry and gtsm measurably different in Z, being identical in X and Y. The complex permittivity is the square of the complex refractive index, implying birefringence as observed experimentally. We have shown that this is describable in terms of the point group $C_{\infty v}$ and its irreducible representation.

One interesting implication of symmetry is that the ensemble averages over time-even polar vectors, such as $\langle \dot{\mathbf{v}}\rangle$ or $\langle \ddot{\boldsymbol{\mu}}\rangle$ include the tsr of $C_{\infty v}$ and must have the possibility of existence in the aligned nematogen of this symmetry. In this case the $D_u^{(1)}$ representation implies a nonvanishing Σ^+, that is, a nonvanishing linear acceleration or force in the Z axis of the aligned nematogen. The applied E_Z cannot generate the mean acceleration directly, but only through a torque $-\boldsymbol{\mu} \times E_Z$ on each dipolar molecule. The net linear acceleration must come from correlation between molecular rotation and translation, and is an experimental measure of this phenomenon. The net linear acceleration of the aligned sample would result in such effects as a meniscus at the surface of the nematogen as the sample is forced against the electric-field-generating apparatus, normally an electrode. This meniscus should be measurable with a microscope.

Similarly, gtsm predicts the possibility of nonvanishing rotational acceleration, the second time derivative of the dipole moment, implying

$$\langle \ddot{\mu}_Z(t)\, \ddot{\mu}_Z(0)\rangle \to \langle \ddot{\mu}_Z\rangle^2; \qquad t \to \infty \tag{333}$$

$$\langle \mu_Z(t)\, \mu_Z(0)\rangle \to \langle \mu_Z\rangle^2; \qquad t \to \infty \tag{334}$$

Equation (334) implies the existence of a zero-frequency (infinite time) component of the dielectric spectrum, as observed[1] experimentally in the Z axis of the aligned nematogen. This is the static permittivity component in axis Z, which becomes different from those in X and Y. A similar effect is expected on the fourth spectral moment,[1] which is the Fourier transform, essentially speaking, of Eq. (333).

7. *The $D_{\infty h}$ Nematogen*

In this case the molecules of the swarm are nondipolar, but if they are polarizable new thermodynamic averages of total symmetry $\Gamma(E^2)$ appear in frame (X, Y, Z) by principle 3. The sample is oriented along the axis of the applied field, for example the Z axis. In D language,

$$\Gamma(E^2) = D_g^{(0)} + D_g^{(2)} \tag{335}$$

More generally

$$\Gamma(\mathbf{EE}) = D_g^{(0)} + D_g^{(1)} + D_g^{(2)} \tag{336}$$

but the notation E^2 implies $\mathbf{E}$ parallel to itself, so that $\mathbf{E} \times \mathbf{E}$ vanishes and by principle 3 no $D_g^{(1)}$ averages appear in (X, Y, Z). This leaves the other two D terms on the right-hand side of Eq. (336), representing averages of the second Legendre polynomial type

$$\tfrac{1}{2}\langle 3(\mathbf{A}(t) \cdot \mathbf{B}(0))^2\rangle - 1 \tag{337}$$

and even-order Langevin functions.[1] In Eq. (336) $\mathbf{A}$ and $\mathbf{B}$ must have the same parity-reversal symmetry.

Averages of this kind that had previously been visible only in the swarm frame become visible under the effect of the field in the laboratory frame. In this case they must all be even to parity reversal symmetry. This time there is no net linear acceleration, therefore, and no net dipole $\langle \mu_Z\rangle$.

Note that the sum (Eq. 335) maps on to

$$2\Sigma_g^+ + \Pi_g + \Delta_g$$

of $D_{\infty h}$. This implies two independent occurrences of this point group's tsr, and two independent types of thermodynamic average in the sample oriented by E^2. This means that the time dependence of the ZZ component of averages such as Eq. (337) is different from those of the YY and XX components, which are the same. In other words, the sample is anisotropic and birefringent, and supports even-order Langevin functions.

8. *The C_∞ Cholesteric*

In this cholesteric symmetry, alignment with a first-order electric field produces a unidirectional spiral symmetry along the axis of the applied field, say Z. Ensemble averages that map on to symmetry representations in the C_∞ point group that contain the group's tsr at least once now survive in the frame (X, Y, Z). In this point group the tsr appears in the symmetry representations both of polar and axial vectors. If a vector quantity is also even to time-reversal symmetry, its thermodynamic ensemble average might not vanish. The average switches sign from one enantiomer to the other, and must vanish by symmetry only in the racemic mixture. This produces the possibility of observing in the electrically aligned cholesteric net molecular linear acceleration, molecular angular acceleration, and a net molecular rotational acceleration which vanish in the racemic mixture.

9. *The D_∞ Cholesteric*

In this case similar considerations apply to orientation by an E^2 field, as in the case of $D_{\infty h}$. The second-order field induces averages of type in Eq. (337), but this time the vectors **A** and **B** can have different parity-reversal symmetry.

Q. The Effect of a Shearing Field

The symmetry of a shearing field (Section VIII) consists of a vector component $D_g^{(1)}$ and a tensor component $D_g^{(2)}$. A shear of the type $\partial v_X/\partial Z$ produces by computer simulation[300] velocity ccf's between orthogonal molecular cartesian components X and Z.

These D symmetries of the laboratory frame map differently on to the four swarm point groups considered in this Chapter

$$D_g^{(1)} + D_g^{(2)} \rightarrow \begin{matrix} \Sigma^+ + \Sigma^- + 2\Pi + \Delta\,(C_{\infty v}) \\ \Sigma_g^+ + \Sigma_g^- + 2\Pi_g + \Delta_g\,(D_{\infty h}) \\ 2\Sigma + 2\Pi + \Delta\,(C_\infty) \\ \Sigma^+ + \Sigma^- + 2\Pi + \Delta\,(D_\infty) \end{matrix}$$

and there are two independent occurrences in the C_∞ group, one in each

of the others. This distinguishes the symmetry effect of shear on a dipolar cholesteric from the other types considered here. Only in the dipolar cholesteric is the shear-induced vorticity transferred to the point group of the swarm. In the other point groups the tsr does not occur in the relevant representation of $D_g^{(1)}$. This will help decide whether shearing an isotropic phase of a liquid crystal induces a phase transition into the nematic or cholesteric phase.

R. Computer Simulation—A Specific Application

One specific application of the symmetry theory is to test for the appearance of predicted averages in a computer simulation of long rods, or ellipsoids, of $D_{\infty h}$ symmetry or $C_{\infty v}$ symmetry. The predicted averages will be immediately useful in deciding whether a transition from an isotropic to a liquid crystal phase has indeed occurred. Long rods are $D_{\infty h}$ symmetry but the addition of a dipolar term in the potential, with charges and asymmetric mass distribution, produces $C_{\infty v}$ symmetry. Liquid crystals and long-rod polymers are known to be highly non-Newtonian in response to shear and work is in progress to simulate linear molecules with applied shearing fields with SLLOD and PUT[300] (Section VIII) and arbitrary applied field strength. This will be a stringent test of the symmetry expectations.

S. Symmetry in Smectic Liquid Crystals

Group theoretical statistical mechanics can be applied to determine the number of nonvanishing ensemble averages in the point groups of the smectic liquid crystals, modelled on the 32 possible crystallographic point groups supplemented by the four linear symmetries (Table II). Assuming that the thermodynamic average exists according to the number of irreducible representations in each point group that are totally symmetric, it is possible to conclude whether or not that average exists at thermodynamic equilibrium. The conclusion is valid within the point-group symmetry of the smectic liquid crystal. The number of ensemble averages supported by the smectic point group, exemplified by the time-correlation functions, decreases from triclinic to monoclinic to orthorhombic to trigonal to tetragonal to hexagonal to cubic. Within each of these major classifications the pattern of nonvanishing correlation functions and other ensemble averages has its own distinctive signature, based on point-group theory. By choosing the correlation functions that are known Fourier transforms of spectra, this type of analysis leads to a convenient method of determining how spectra are affected by the type of smectic point-group symmetry. The analysis leads to an appreciation of the differences in allowed ensemble averages between the various smectic point groups and molecular and

other types of liquid. The treatment can be extended straightforwardly to consider the effects of external fields.

1. *Local Smectic Point Groups*

In the smectic liquid crystals, the relevant point-group symmetries are similar to those of the 32 point groups of solid molecular crystals, described by the following seven major classifications: triclinic, monoclinic, orthorhombic, trigonal, tetragonal, hexagonal, and cubic. Each of these major classifications supports a number of point-group symmetries which cover all known crystal symmetries. Molecules crystalize within these point groups, forming an underlying structure classified by 230 space groups. However, the external symmetry and physical appearance of a molecular crystal falls into one of the point groups. Similarly, the physical properties of a smectic liquid crystal may be explored with a point-group description of the local structure which distinguishes it from an isotropic molecular liquid. In principle the point-group symmetry within the smectic phase may be any symmetry, but in order to construct a systematic approach to the problem of smectic local ordering, it is assumed that the smectic symmetry can be described by the 32 crystallographic point groups supplemented by the four point groups of the nematic and cholesteric liquid crystals. We therefore provide symmetry data for the 36 point groups of Table II, any one of which may provide a framework for the application of gtsm and the determination of nonvanishing ensemble averages of the molecular dynamics within the local smectic point-group symmetry. Many such averages exist at the local level, but disappear if the smectic sample is isotropic on the macroscopic scale of a laboratory sample. If the smectic liquid crystal maintains the point-group anisotropy at this level, and is anisotropic overall, then the ensemble averages survive averaging in the laboratory frame (X, Y, Z) as well as in the local frame of the point group, which we denote (x_D, y_D, z_D) as for the nematics and cholesterics.

The differences between solid molecular crystals and liquid crystals with three-dimensional anisotropy is not easy to define. De Vries[322] has pointed out that the most significant difference is that in the solid crystal any alkyl chains at the ends of the molecule have very little disorder, or none at all, whereas in a liquid crystal, which has three-dimensional anisotropy, these chains are slightly disordered. The difference in local point-group symmetry seems to be minimal. For example, the smectic H phase of BBEA (4-*n*-butyloxybenzal-4-ethylaniline) is a liquid and not a solid molecular crystal because there is no transmission of phonon modes through the smectic liquid crystal, which is capable of flow. Translational coupling is much weaker than rotational coupling. When the two compete, as in structures with optically active molecules, the translational correlation is destroyed so as to achieve a more favorable rotational arrangement. A molecular crystal structure of an optically active compound has a single three-dimensional lattice, but that of a three-dimensional smectic phase becomes twisted if the molecules are optically active, similar to a cholesteric phase.[1] Three-dimensional anisotropic liquid crystals may be mixed in all proportions, in contrast to molecular crystals. If translational order disappears, there is no three-dimensional order at all.

Smectic liquid crystals and solid molecular crystals therefore differ essentially in translational order. In the smectic liquid crystals there is still a residual point-group symmetry, however, although translational space-group symmetry may have been partially or completely destroyed.

The difference between a smectic liquid crystal and an isotropic molecular liquid can be expressed in terms of extra ensemble averages supported by the former within definable local point-group symmetries. In the isotropic molecular liquid these are absent, its point group in three dimensions is $R_h(3)$.

2. *Mapping from $R_h(3)$ to the Smectic Point Groups*

Table II may be used to summarize these mappings. Thus, for cubic (O_h) symmetry, the principles of gtsm state that thermodynamic averages exist in frame (x_D, y_D, z_D), governed by this local cubic symmetry, provided that the symmetry representations of the ensemble averages contain at least once the tsr of this cubic point group. This is the A_{1g} irreducible representation. This result is independent of the molecular symmetry within the point group. [Analogously, gtsm states that the ensemble averages in an isotropic environment exist if their symmetry representations contain the tsr $D_g^{(0)}$ of the point group $R_h(3)$, irrespective of the molecular symmetry.]

In general we must define the irreducible representation of the quantity being averaged in the $R_h(3)$ point group and then in the relevant local smectic point group. If, for example, the latter is the tetragonal D_{2d} (or $\bar{4}$ 2**m** in the Hermann–Mauguin international notation), the relevant tsr is the irreducible representation A_1. However, gtsm implies the powerful result that any thermodynamic ensemble average within the local smectic point group D_{2d} of the frame (x_D, y_D, z_D) may exist in this frame if its irreducible representation contains A_1. This is a powerful result because it is wholly independent of any residual space group structure in the smectic liquid crystal. Proceeding on these grounds, it is possible to link the symmetry of ensemble averages in the liquid and smectic liquid crystal by mapping the irreducible representation of the quantities being averaged from the point group $R_h(3)$ to D_{2d}. For ease of development it is convenient as usual to divide quantities into scalars, pseudoscalars, polar and

axial vectors, and higher-order tensors. A scalar is characterised by the tsr in any point group. The irreducible representation of the pseudoscalar in $R_h(3)$ is, as we have seen in other contexts, $D_u^{(0)}$, which is odd to parity reversal, but still a zeroth order quantity with no directional property. This representation maps on to B_1 of the point group D_{2d}. In chiral point groups: C_n, D_n, T, O the irreducible representations of both the scalar and pseudoscalar map on to the tsr of the point group, so that ensemble averages over both scalars and pseudoscalars can exist in chiral point groups at the local level in smectic liquid crystals. There are two distinct liquid crystal enantiomorphs.

The polar vector (e.g., velocity) is represented in $R_h(3)$ *by* $D_u^{(1)}$, meaning that it is odd to parity reversal and has first-order directional properties. The axial vector, on the other hand, is $D_g^{(1)}$, which is even to parity reversal. An example of a polar vector is molecular linear velocity, $\mathbf{v}$. Molecular angular velocity is an axial vector. The irreducible representations $D_u^{(1)}$ and $D_g^{(1)}$, respectively, map on to $B_2 + E$ and $A_2 + E$ of the point group D_{2d}. These do not contain the point group's tsr, and in consequence no ensemble average over a polar or axial vector can exist in the frame (x_D, y_D, z_D) of the local smectic point group D_{2d}.

In local smectic point groups where the tsr appears as part of the irreducible representation in the point group of a polar or axial vector quantity, the thermodynamic average in the local frame of reference (x_D, y_D, z_D) may exist, provided that it is positive to time-reversal symmetry. Examples are listed in Table II.

Second rank tensor quantities are characterized in $R_h(3)$ by $D_g^{(2)}$ or $D_u^{(2)}$ and are second-order directional quantities which are even or odd to parity reversal.

Relations between D products are given as usual by the Clebsch–Gordan theorem, which is also applicable in the point groups of the smectic liquid crystals because the sum of D representations maps on to the same sum in the smectic point group. Thus, if we extend our consideration of ensemble averages to time-correlation functions which are averages over products of vectors, we have, for example,

$$\Gamma(\mathbf{v})\Gamma(\boldsymbol{\omega}) = D_u^{(1)} D_g^{(1)} = D_u^{(0)} + D_u^{(1)} + D_u^{(2)} \quad (R_h(3)) \tag{338}$$

$$= (B_2 + E)(A_2 + E) = A_1 + A_2 + 2B_1 + B_2 + 2E \quad (D_{2d}) \tag{339}$$

This shows that the D representations of the time-correlation tensor generated by the tensor product of molecular linear and angular velocity is a sum of three ungerade D representations in the molecular liquid point group $R_h(3)$. The time-correlation function vanishes for all t in the isotropic liquid because its complete D representation does not include $D_g^{(0)}$. In the D_{2d} smectic point group, however, this is not the case, because the irreducible representation of the ccf $\langle \mathbf{v}(t)\boldsymbol{\omega}(0)\rangle$ is the sum $A_1 + A_2 + 2B_1 + B_2 + 2E$, which includes the tsr A_1 once. Therefore, gtsm implies that one element of $\langle \mathbf{v}(t)\boldsymbol{\omega}(0)\rangle$ may exist in the D_{2d} local point group of the smectic liquid crystal. This result may be checked in principle with molecular dynamics computer simulation.

T. Time-Reversal Symmetry

Time-reversal symmetry is defined as in other contexts as the operation $(\mathbf{q}, \mathbf{p}) \rightarrow (\mathbf{q}, -\mathbf{p})$, which leaves positions unchanged but reverses momenta. Parity reversal is the operation $(\mathbf{q}, \mathbf{p}) \rightarrow (-\mathbf{q}, -\mathbf{p})$. When dealing with scalars and pseudoscalars, the ensemble average over these quantities must be unchanged (i.e., positive) to time reversal. When dealing with vectors, however, some are positive to time reversal, like the electric field $(\mathbf{E})$, the position vector $(\mathbf{r})$, the linear acceleration, $(\dot{\mathbf{v}})$, the angular acceleration, $(\dot{\boldsymbol{\omega}})$, and the acceleration due to gravity, $(\mathbf{g})$. Others are negative to time reversal, such as the magnetic field, $(\mathbf{B})$, the linear velocity $(\mathbf{v})$, the angular velocity, $(\boldsymbol{\omega})$, and the electromagnetic field propagation vector $(\boldsymbol{\kappa})$. A thermodynamic ensemble average over a vector which is negative to time reversal vanishes, but one which is positive may exist if the vector is also positive to parity reversal in the isotropic liquid point group $R_h(3)$. In the local smectic phase point groups, however, the latter requirement is not necessary, and the thermodynamic ensemble average exists, provided it is carried out over a vector which is positive to time reversal and provided the irreducible representation of that vector includes the tsr of the point group. Thus, the average $\langle \mathbf{r} \rangle$, for example, may exist in the point group C_{3v} of the trigonal class, because the vector's irreducible representation in the point group is $A_1 + E$. The latter includes the tsr, A_1 once. From gtsm one independent ensemble average exists over a polar vector with positive time-reversal symmetry. An example is $\langle \mathbf{r} \rangle$. Other examples in this local smectic point group are $\langle \dot{\mathbf{v}} \rangle$ and $\langle \dot{\boldsymbol{\omega}} \rangle$. This may again be investigated with computer simulation. In the tetragonal local smectic point group D_{2d}, however, all these ensemble averages should vanish by gtsm.

When dealing with time-correlation functions, the time-reversal arguments must be applied with care to each individual case. The pitfalls of the procedure may be illustrated, as in other contexts, with reference to the simple time ccf of the type $\langle \mathbf{A}(t)\dot{\mathbf{A}}(0)\rangle$. If $\mathbf{A}$ represents linear velocity, v, for example, the product within the averaging brackets $\langle\ \rangle$, is overall negative to time reversal. However, this type of time-correlation function clearly does not vanish for all t because it is simply the time derivative of

$\langle \mathbf{A}(t)\mathbf{A}(0)\rangle$. It exists according to the elementary theory of correlation functions in reversible thermodynamic equilibrium. It is itself a function which is a time derivative, and is intrinsically negative to time reversal. More generally, the class of time correlation functions which are time derivatives of other correlation functions have an existence for $0 < t < \infty$ despite the fact that the product of the two quantities inside the averaging brackets may in itself appear negative to time reversal.

Bearing in mind these considerations of time reversal, mappings of some D representations from the point group $R_h(3)$ are given in Table II for 36 local smectic point groups. Column 1 of the table contains the name of the point group in Schonflies and Hermann–Mauguin notation (the latter in brackets). Column 2 is the representation of the scalar in the point group, (i.e. the tsr), column 3 contains the symmetry representation of the pseudoscalar, column 4 that of the axial vector, column 5 that of the polar vector. Columns 6 and 7 map products of D representations on to each point group. Columns 8 and 9 give the number of independent ensemble averages expected in the local smectic point group for representative time-correlation functions, column 8 for the rotational velocity correlation tensor, and column 9 for the angular linear velocity cross-correlation tensor. Both tensors are defined in frame (x_D, y_D, z_D) of the local smectic point group. Finally, column 10 records the crystal class of the point group if it were being used to describe solid molecular crystals.

Note that in the isotropic molecular liquid environment only one independent ensemble average (the trace) is expected in column 8, and none in column 9, thus evidencing by gtsm a considerable difference between the local molecular dynamics, of smectic liquid crystals and isotropic molecular liquids.

Some examples of the symmetry of the correlation functions in columns 8 and 9 are given as follows:

EXAMPLE 1: MONOCLINIC $C_{1h}(\mathbf{m})$

1. Rotational Velocity Correlation Tensor

The irreducible representation of this tensor in the point group C_{1h} is

$$\Gamma(\dot{\boldsymbol{\mu}}(t)\Gamma(\dot{\boldsymbol{\mu}}(0)) = (2A^1 + A^{11})(2A^1 + A^{11})$$
$$= 4A^1A^1 + 2A^1A^{11} + 2A^{11}A^1 + A^{11}A^{11} = 5A^1 + 4A^{11} \quad (340)$$

showing five occurrences of the tsr in the product of representations of the correlation tensor. Thus five independent ensemble averages may

exist in the local smectic frame of reference (x_D, y_D, z_D). The individual products that give A^1 in Eq. (340) are (1) $4A^1A^1$ and (2) $A^{11}A^{11}$. The others give A^{11}. Referring to the point group character table for C_{1h} we find that A^1 represents the cartesian components x_D and y_D of the local smectic frame of reference. The A^{11} entry represents z_D. The product $4A^1A^1$ therefore represents four independent components of the rotational velocity correlation tensor:

$$\langle \dot{\mu}_{x_D}(t)\,\dot{\mu}_{x_D}(0)\rangle; \quad \langle \dot{\mu}_{y_D}(t)\,\dot{\mu}_{y_D}(0)\rangle; \quad \langle \dot{\mu}_{x_D}(t)\,\dot{\mu}_{y_D}(0)\rangle; \quad \langle \dot{\mu}_{y_D}(t)\,\dot{\mu}_{x_D}(0)\rangle$$

The fifth component $\langle \dot{\mu}_{z_D}\dot{\mu}_{z_D}(0)\rangle$ comes from $A^{11}A^{11}$. The complete symmetry of the correlation tensor in the local smectic frame of reference is therefore

$$\langle \dot{\boldsymbol{\mu}}(t)\,\dot{\boldsymbol{\mu}}(0)\rangle = \begin{bmatrix} a & d & 0 \\ e & b & 0 \\ 0 & 0 & c \end{bmatrix}, \qquad C_{1h}(m)$$

and the five independent elements are recorded in the table.

Similar arguments applied to the generic acf $\langle \mathbf{A}(t)\mathbf{A}(0)\rangle$ show these five independent elements, with the same symmetry pattern. In a molecular crystal this result is related to the number of lattice modes, but in the smectic liquid crystal there are no phonon modes.

2. The Cross Correlation Function $\langle \boldsymbol{v}(t)\boldsymbol{\omega}(0)\rangle$

The irreducible representation is now

$$\Gamma(\mathbf{v})\Gamma(\boldsymbol{\omega}) = (2A^1 + A^{11})(A^1 + 2A^{11})$$
$$= 2A^1A^1 + A^{11}A^1 + 4A^1A^{11} + 2A^{11}A^{11} = 4A^1 + 5A^{11} \quad (341)$$

showing four occurrences of A^1. Thus, the crystal class supports four independent ensemble averages which are scalar elements of $\langle \mathbf{v}(t)\omega(0)\rangle$. Bearing in mind that the linear velocity $\mathbf{v}$ is referred to by the cartesian components X, Y, and Z of the C_{1h} point-group character table, and the angular velocity component ω by R_X, R_Y, and R_Z, we arrive at the symmetry

$$\langle \mathbf{v}(t)\,\boldsymbol{\omega}(0)\rangle = \begin{bmatrix} 0 & 0 & a_1 \\ 0 & 0 & b_1 \\ C_1 & d_1 & 0 \end{bmatrix} \tag{342}$$

Thus four independent elements exist which all vanish in the equivalent molecular liquid.

EXAMPLE 2: ORTHORHOMBIC D_2 (232)

1. Rotational Velocity acf

The relevant irreducible representation of the time acf is

$$\Gamma(\dot{\boldsymbol{\mu}})\Gamma(\dot{\boldsymbol{\mu}}) = (B_1 + B_2 + B_3)\,(B_1 + B_2 + B_3) = 3A_1 + 2B_1 + 2B_2 + 2B_3 \tag{343}$$

which contains the totally symmetric component three times. From the axioms of gtsm we can expect three independent ensembles in the local smectic point group D_2 (232), a chiral class. From the point group character table for D_2, and using the rules for forming the products of irreducible representations, we have the symmetry

$$\langle \dot{\boldsymbol{\mu}}(t)\,\dot{\boldsymbol{\mu}}(0)\rangle = \begin{bmatrix} a & 0 & 0 \\ 0 & b & 0 \\ 0 & 0 & c \end{bmatrix} \quad (D_2)$$

In this case all the off-diagonal elements vanish, leaving three independent diagonal elements. The far infra-red spectrum in the local smectic frame is different for each element.

2. The ccf $\langle \mathbf{v}(t)\boldsymbol{\omega}(0)\rangle$

The irreducible representation is

$$\Gamma(\mathbf{v})\Gamma(\boldsymbol{\omega}) = (B_1 + B_2 + B_3)(B_1 + B_2 + B_3) = 3A_1 + 2B_1 + 2B_2 + 2B_3 \tag{344}$$

which again contains A_1, three times and is the same as Eq. (343). This is because the D_2 point group is chiral, and $D_g^{(1)}$ and $D_u^{(1)}$ of $R_h(3)$ map

on to the same representation in D_2, (i.e., $B_1 + B_2 + B_3$). Using Eq. (344) and the cartesian and R representations in the point-group character table for D_2 leads to the symmetry

$$\langle \mathbf{v}(t)\,\boldsymbol{\omega}(t)\rangle = \pm \begin{bmatrix} a_1 & 0 & 0 \\ 0 & b_1 & 0 \\ 0 & 0 & c_1 \end{bmatrix}$$

Thus, the three diagonal elements of $\langle \mathbf{v}(t)\boldsymbol{\omega}(0)\rangle$ exist in the class D_2 (232). These elements change sign in the opposite enantiomer.

EXAMPLE 3: ORTHORHOMBIC C_{2v} (2 mm)

1. Rotational Velocity a.c.f.

In this achiral orthorhombic crystal class the irreducible representation is

$$\Gamma(\dot{\boldsymbol{\mu}})\Gamma(\dot{\boldsymbol{\mu}}) = (\mathrm{A_1} + \mathrm{B_1} + \mathrm{B_2})(\mathrm{A_1} + \mathrm{B_1} + \mathrm{B_2}) = 3\mathrm{A_1} + 2\mathrm{A_2} + 2\mathrm{B_1} + 2\mathrm{B_2} \tag{345}$$

leading to the symmetry recorded in Table II. Three independent diagonal elements exist as in the orthorhombic D_2.

2. The ccf $\langle \mathbf{v}(\mathrm{t})\,\boldsymbol{\omega}(0)\rangle$

Here the irreducible representation is

$$\Gamma(\mathbf{v})\Gamma(\boldsymbol{\omega}) = (A_1 + B_1 + B_2)(A_2 + B_1 + B_2) = 2A_1 + 3A_2 + 2B_1 + 2B_2 \tag{346}$$

which contains A_1 twice. Reference to the point-group character tables reveals that the two independent elements are off-diagonals, so that the complete matrix symmetry is

$$\langle \mathbf{v}(t)\,\boldsymbol{\omega}(0)\rangle = \begin{bmatrix} 0 & a_1 & 0 \\ b_1 & 0 & 0 \\ 0 & 0 & 0 \end{bmatrix} \; C_{2v} \tag{347}$$

This contrasts with the orthorhombic $\mathrm{D_2}$ (232) crystal class where only the diagonals of the ccf are visible.

EXAMPLE 4: TRIGONAL C_{3v} (3m)

1. Rotational Velocity

The irreducible representation in this case is

$$\Gamma(\dot{\boldsymbol{\mu}})\Gamma(\dot{\boldsymbol{\mu}}) = (A_1 + E)(A_1 + E) = 2A_1 + A_2 + 3E \tag{348}$$

which contains the tsr twice. One comes from the product A_1A_1 and the other from EE, which signifies the product $(x_D, y_D)(x_D, y_D)$ in the Cartesian representation of the point group character table. It is well known that this notation implies the equivalence of x_D and y_D. The product implies four rotational velocity-correlation function elements according to gtsm. These four elements are not independent, and are grouped together, being equivalent to one A_1, generated by the product rule

$$EE = A_1 + A_2 + E \tag{349}$$

However, from the elementary theory of time correlation functions, we know that

$$\langle \dot{\mu}_{x_D}(t)\, \dot{\mu}_{x_D}(0)\rangle \neq \langle \dot{\mu}_{x_D}(t)\, \dot{\mu}_{y_D}(0)\rangle \tag{350}$$

because one is an autocorrelation function, with finite value at $t = 0$, and the other a ccf, which vanishes at $t = 0$. This, together with the independent appearance of $\langle \dot{\mu}_{z_D}(t)\, \dot{\mu}_{z_D}(0)\rangle$ from A_1A_1, leads to the final symmetry

$$\langle \dot{\mu}_{x_D}(t)\, \dot{\mu}_{x_D}(0)\rangle = \langle \dot{\mu}_{y_D}(t)\, \dot{\mu}_{y_D}(0)\rangle \neq \langle \mu_{z_D}(t)\, \dot{\mu}_{z_D}(0)\rangle \tag{351}$$

The two independent nonvanishing elements are thus

$$\langle \dot{\mu}_{x_D}(t)\, \dot{\mu}_{x_D}(0)\rangle = \langle \dot{\mu}_{y_D}(t)\, \dot{\mu}_{y_D}(0)\rangle \tag{352}$$

and $\langle \dot{\mu}_{z_D}(t)\, \dot{\mu}_{z_D}(0)$. The further result

$$\langle \dot{\mu}_{x_D}(t)\, \dot{\mu}_{y_D}(0)\rangle \neq \langle \dot{\mu}_{y_D}(t)\, \dot{\mu}_{x_D}(0)\rangle \tag{353}$$

follows from the fact that the irreducible representation (Eq. 348) allows two and only two independent nonvanishing elements. The symmetry of the complete acf matrix is thus

$$\langle \dot{\boldsymbol{\mu}}(t)\, \dot{\boldsymbol{\mu}}(0)\rangle = \begin{bmatrix} a & 0 & 0 \\ 0 & a & 0 \\ 0 & 0 & b \end{bmatrix}; \qquad C_{3v}(3m) \tag{354}$$

and is recorded in the table.

2. The ccf $\langle \mathbf{v}(t)\, \boldsymbol{\omega}(0)\rangle$

The relevant irreducible representation is

$$\Gamma(\mathbf{v})\Gamma(\boldsymbol{\omega}) = (A_1 + E)(A_2 + E) = A_1 + 2A_2 + 3E \tag{355}$$

allowing one occurrence of A_1, and by gtsm, one independent nonvanishing ccf element. This comes from the product $EE = A_1 + A_2 + E$. The non-vanishing element must therefore be from the four possibilities generated from $(x_D, y_D)(x_D, y_D)$. There is no independent occurrence of the diagonal element $\langle v_{z_D}(t)\, v_{z_D}(0)\rangle$ from (Eq. 355), and therefore the single independent element is

$$\langle v_{x_D}(t)\, \omega_{y_D}(0)\rangle = -\langle v_{y_D}(t)\, \omega_{x_D}(0)\rangle \tag{356}$$

The minus sign comes from the fact that the overall matrix symmetry is odd to parity reversal; the result (Eq. 356) represents the vector cross product symmetry, denoted $D_u^{(1)}$ in the $R_h(3)$ point group. The overall matrix symmetry is thus

$$\langle \mathbf{v}(t)\, \boldsymbol{\omega}(0)\rangle = \begin{bmatrix} 0 & a_1 & 0 \\ -a_1 & 0 & 0 \\ 0 & 0 & 0 \end{bmatrix} C_{3v}(3m) \tag{357}$$

as in Table II.

EXAMPLE 5: THE CUBIC CRYSTAL CLASSES

There are five cubic crystal classes of high symmetry. Two of these (T and O) are chiral. Applying the same methods as in Examples 1–4 results in the classification in Table II, which shows that the diagonal elements are supported for the rotational velocity and other time auto-correlation functions. Cross correlation functions are supported only in the chiral

classes T and O. No more than one independent element appears in each class, that is, no more than one occurrence of the relevant totally symmetric irreducible representation in each local nematic point group. The far infrared spectrum remains the same along the x_D, y_D, and z_D axes of the cubic point group.

Table II provides a classification scheme for nonvanishing thermodynamic ensemble averages in the given point group classification scheme. Each point group may accommodate molecules of independent symmetry, but the overall thermodynamic average is determined by the point group symmetry alone. We have shown only a few representative thermodynamic ensemble averages in Table II, but in general all such averages may be accommodated. For example, if we wish to consider polarizability of a volume element in the isotropic environment, we take the $R_h(3)$ point group and represent the polarizability with the D symmetry $D_g^{(0)} + D_g^{(2)}$, a symmetric second rank tensor even to parity reversal. The overall macroscopic polarizability of a point group representation of local smectic symmetry may then be investigated according to how many occurrences there are of the tsr in the local point group. The latter's character table may then be used to find out in more detail the nature of the polarizability tensor in the local smectic point group, that is, which ensemble averages over the polarizability vanish and which exist. If we are investigating pyroelectric symmetry, on the other hand, we note that pyroelectricity has $D_u^{(1)}$ symmetry in $R_h(3)$ and then we map this on to the smectic point group representing local symmetry in the liquid crystal as in Table 2. This shows that in some local smectic point groups pyroelectric properties are supported in principle while in others they are not, according to whether the totally symmetric representation occurs in the point group. In some cases the pyroelectricity is different along each smectic axis (three occurrences of the tsr). For a given point group symmetry, care must be taken to examine the time reversal symmetry of the quantity being averaged thermodynamically.

Some D symmetries of physical quantities are listed below.

1. The magnetic dipole is an axial (or pseudo) vector of $D_g^{(1)}$ symmetry.
2. Electric polarizability, thermal and electric conductivity, thermoelectricity, thermal expansion, and magnetic susceptibility each have $D_g^{(0)} + D_g^{(2)}$ symmetry in $R_h(3)$.
3. The quadrupole moment has $D_g^{(2)}$ symmetry.
4. The gyration tensor of optical activity has $D_u^{(0)} + D_u^{(2)}$ symmetry.
5. The first hyperpolarizability has $D_u^{(1)} + D_u^{(3)}$ symmetry.

6. Piezoelectricity and the electrooptic Kerr effect have $2D_u^{(1)} + D_u^{(2)} + D_u^{(3)}$ symmetry.
7. Elasticity is a symmetric fourth rank tensor of $2D_g^{(0)} + 2D_g^{(2)} + D_g^{(4)}$ symmetry.

Thermodynamic ensemble averages over all these quantities vanish in the isotropic liquid environment except for polarizability and elasticity, which contain the $D_g^{(0)}$ representation. In the local smectic point groups, however, new thermodynamic averages may exist which vanish in the laboratory frame if the local (crystal-like) smectic symmetry is not maintained to the macroscopic level. (A key difference between a smectic liquid crystal and a molecular solid crystal is that the same (crystal) point group symmetry is maintained in the latter from the local to the macroscopic level.) Local ensemble averages may exist in the smectic liquid crystal depending on the number of occurrences of the appropriate totally symmetric irreducible representation and on the time reversal symmetry of the quantity being averaged. The molecular electric polarizability and quadrupole moment are both positive to time reversal symmetry, and extra ensemble averages over these quantities might appear in some of the local point groups. For example, in the orthorhombic class of C_{2v} point group symmetry the representation $D_g^{(0)} + D_g^{(2)}$ of the electric polarizability maps on to $3A_1 + A_2 + B_1 + B_2$, showing that there are three independent non-vanishing thermodynamic averages over the molecular polarizability in this local point group. These correspond in the cartesian notation of the point group character table to X^2, Y^2, and Z^2, the three diagonal elements of the polarizability tensor average. All three become equal in the isotropic molecular liquid. Again, this result is independent of the individual molecular symmetry within the C_{2v} point group. In the monoclinic, C_{1h} crystal class $D_g^{(0)} + D_g^{(2)}$ maps on to $4A^1 + 2A^{11}$, meaning that four independent thermodynamic averages over polarizability exist in this class. These are denoted X^2,Y^2,Z^2, and XY in the point-group character table opposite to the A^1 entry, signifying the existence of three independent diagonal thermodynamic averages and one off-diagonal symmetric pair, $XY = YX$. In the molecular liquid, only one average exists, the trace of the diagonal averages, which are the same in the three isotropic laboratory axes in the molecular liquid. Group theoretical statistical mechanics provides a unifying picture of the properties of these ensemble averages together with those of the set of non-vanishing time correlation functions for each local point group.

These results provide a coherent system of predicting the existence of ensemble averages in the point groups of the table. The numerical value of these averages and the time dependence of the correlation functions

must be obtained with additional complementary methods, such as band-shape analysis and molecular dynamics computer simulation. Not only would this provide a needed and detailed check on the predictions of gtsm applied to smectic liquid crystals, but it would also be a new era of fruitful investigation of liquid crystal molecular dynamics, extending the range of liquid state computer simulations.

These methods can also be extended to deal with the effect of external fields on smectic liquid crystals, using the third principle. This states that the symmetry of ensemble averages set up in a molecular environment subjected to an externally applied macroscopic force field is the symmetry of the applied field itself. In an ensemble of atoms subjected to a strain rate of overall symmetry $D_g^{(0)} + D_g^{(1)} + D_g^{(2)}$, recent computer simulation[300] has indeed revealed the existence of new types of ensemble average set up by the field and taking its overall symmetry. These ccf's explain the fundamental origin of the well known Weissenberg effect of rheology (Section VIII). Similarly, an electric field of symmetry $D_u^{(1)}$ sets up ensemble averages of this symmetry in the $R_h(3)$ point group, and thus also in the local smectic point groups. The symmetry of the electric-field-induced ensemble average in a given point group is $D_u^{(1)}$, mapped on to its equivalent irreducible representation in the local point group. Similar predictions can be made for other applied macroscopic fields, such as a magnetic field, an electromagnetic field, and strain rate, applied to the smectic liquid crystal in the laboratory axes X, Y, and Z. These methods, used with computer simulation and experimental spectroscopy, for example, will reveal a great deal about fundamental and unknown areas of chemical physics. They can also be extended to deal with n-time correlation functions[323] and higher order angularly resolved pair distribution functions.[324]

VIII. SIMULATION AND SYMMETRY IN NON-NEWTONIAN FLUID DYNAMICS

The past few years have seen the rapid evolution of nonequilibrium molecular dynamics computer simulation[325,326] for the numerical investigation of fluid dynamics, including couette flow, shear, extrusion, turbulence, and the phenomena of non-Newtonian rheology. It is now possible to investigate directly the linear relation between stress and strain, first proposed by Newton, in terms of his fundamental equations of motion. This allows an understanding of the rheology of "simple" liquids with computer simulation, and thereby a better understanding of the flow engineering of colloidal dispersions, flocs, gells, suspensions, polymer shearing and

extrusion, new materials such as polymer liquid crystals, the transportation of residue suspensions, and other practical problems.

In general, sheared liquids are "non-Newtonian" in that the linear relation between stress and strain does not hold in general. The subject of non-Newtonian rheology tackles such phenomena as the thinning and thickening of a liquid in response to shear, and the onset of turbulence. Nonequilibrium molecular dynamics (nemd) computer simulation has advanced to the point where these phenomena can be described numerically. It has been shown that shear thinning and thickening (dilatency), viscoelasticity, and related phenomena can all be reproduced in simple ("atomic") liquids, using sufficiently scaled shear rates to correspond with the picosecond time capability of most contemporary computers. Heyes has shown[326] that sedimentation during storage, the levelling of liquids, lubrication, gell stability, and processability are all areas in which non-Newtonian effects are important but largely intractable to conventional rheology. There are several phases[326] in the development of non-Newtonian response which Heyes has classified with the Deborah Number

$$D = \tau_r \dot{\gamma} \tag{358}$$

where τ_r is the structural relaxation time and $\dot{\gamma}$ the shear rate. Newtonian behavior occurs when D is low and the viscosity is a constant. However, if the stress exceeds a critical value, the strain rises more quickly than the linear relation proposed by Newton allows. Viscoelastic effects appear when D is about 1. The material typically exhibits an increasing time dependent stress, which fails to approach a constant value, so that viscosity is not uniquely defined. A further increase in the strain rate results in shear thinning, followed by shear thickening, or dilatency. At this point relaxation effects take place too slowly to be observable, unless high pressures are used. The basics of all these phenomena have now been observed by computer simulation,[325,326] using new concepts and new equations of motion such as those devised by D. J. Evans and co-workers.[325] These have been developed by Heyes and co-workers[326] for many purposes, including couette, laminar, elongational, and sheet flows in atomic ensembles. For laminar flow, for example, the SLLOD equations of motion[326] are

$$\dot{\mathbf{r}} = \mathbf{p}/m + \dot{\gamma} r_Y \hat{X} \tag{359}$$

$$\mathbf{p} = \mathbf{F} - \dot{\gamma} P_Y \hat{X} - \alpha \dot{P} \tag{360}$$

where X is a unit vector in the X direction, $\mathbf{F}$ is the force on the particle,

r is the position, **p** the momentum, $\dot{\gamma}$ the strain rate, **P** the applied pressure, and α a constant. These are Newton's equations supplemented by extra terms due to laminar shear. They were first devised by D. J. Evans and co-workers[325] and use thermostatting procedures which may be Gaussian isokinetic or profile unbiased.[326] The former has the disadvantage of rigidly fixing the total kinetic energy.

A. *D* Representation of Simple Couette Flow

In couette flow in an incompressible ensemble[300] a shear is applied with a given stress and strain rate. Newton's relation between the two is

$$\Pi_{XZ} = \eta \frac{\partial v_X}{\partial Z} \tag{361}$$

where η is the viscosity, a scalar quantity with $D_g^{(0)}$ symmetry. The Newton relation applies in the limit of vanishing strain rate. Otherwise η becomes a function of the strain rate itself

$$\mathbf{\Pi} = 2\eta(\dot{\gamma})\dot{\gamma} \tag{362}$$

In both equations, gtsm (Section VII) applies in the shear-on steady state, through principle 3.

In general, the complete tensor symmetry of the shear may be found by considering that of the strain rate tensor, which is

$$\Gamma(\dot{\gamma}) = \Gamma(\mathbf{v}\mathbf{r}^{-1}) = D_u^{(1)} D_u^{(1)} = D_g^{(0)} + D_g^{(1)} + D_g^{(2)} \tag{363}$$

The shear stress tensor and pressure tensor have the same D symmetry ($\mathbf{P} = -\mathbf{\Pi}$), which is made up of scalar, vector, and tensor components positive to parity inversion. In simple couette flow there is no diagonal part to the strain rate, and the scalar part of the D representation vanishes. This leaves an antisymmetric component (Section VII) of $D_g^{(1)}$ symmetry and a symmetric traceless component with D symmetry $D_g^{(2)}$. This symmetry signature applies whatever the complexity of the mathematical treatment, and irrespective of the molecular symmetry in the ensemble, and simplifies the rheological approach to structured fluids, where there are five conservation and eight constitutive equations.[327]

According to principle 3 of Section VII, extra ensemble averages may appear in frame (X, Y, Z) with the symmetry $D_g^{(1)} + D_g^{(2)}$. This D symmetry is a combination of the vector and tensor parts of the generic time correlation function $\langle \mathbf{A}(t)\mathbf{A}(0)\rangle$, which may therefore appear under shear

in frame (X, Y, Z). When there is only one component of the strain rate, that is, $\partial v_X/\partial Z$, then only one off-diagonal element of the correlation function is expected to be observable, and is the microscopic characteristic of the macroscopic stress.

In the special case of couette flow in an atomic ensemble[300] a fundamentally new type of ccf is anticipated to exist by gtsm which is a weighted combination of antisymmetric (vector), and symmetric (tensor) components, and which has been described by Eqs. (320a) of Section VII. The weighted combination, Eq. (320b), is in general dissymmetric in time, and this is precisely as observed by nemd computer simulation,[300,301] using both Gaussian isokinetic and profile unbiased thermostatting.

B. Consequences for Langevin Theory

We can attempt to analyze this observation by computer simulation of shear-induced dissymmetric cross correlation functions with linked Langevin equations in the linear, Markovian approximation of Section I. The difference between the analytical results and computer simulation are interpreted in terms of the fact that the simulated cross-correlation functions are nonlinear and non-Markovian, and also seem to be nonstationary, that is, dissymmetric to time displacement or index reversal. In this condition, the Onsager reciprocal relations,[328] which pertain to equilibrium, reversible, linear, and stationary processes, no longer hold, and the simple Langevin equation is no longer able to describe the results of computer simulation with any accuracy.

In order to obtain a qualitative Langevin description, use has to be made of cross friction coefficients which are either symmetric or antisymmetric in the indices X and Z of the laboratory frame (X, Y, Z). However, this produces results which are distinctly different from the simulations[300,301] in the sense that the simulated ccf's are finite at $t = 0$, but the analytical counterparts vanish at $t = 0$.

C. Derivation and Solution of the Langevin Equations

The starting point of the derivation of the Langevin equations is Eq. (3.48) of Ref. (325), the Dolls tensor adaptation of Newton's equation of motion

$$m\dot{\mathbf{v}} = \mathbf{F} - \nabla\mathbf{u} \cdot m\mathbf{v} \tag{364}$$

where **F** is the force and **v** is the velocity of a particle externally subjected to shear. The latter is represented by the tensor $\nabla\mathbf{u}$ with nine components in general. It is assumed that the shear causes a strain rate response in

the N-particle ensemble consisting of $D_g^{(1)}$-type vorticity and $D_g^{(2)}$-type deformation. The former is represented from Eq. (364) as

$$F_X = m\dot{\nu}_X + m\frac{\partial u_X}{\partial Z}\nu_Z \tag{365a}$$

$$F_Z = m\dot{\nu}_Z - m\frac{\partial u_Z}{\partial X}\nu_X \tag{365b}$$

and the latter by the same equations but with a positive sign on the right hand side of Eq. (365b). We assume that these equations can be written with

$$\dot{\gamma}_{XZ} = \frac{\partial u_X}{\partial Z}; \qquad \dot{\gamma}_{ZX} = \frac{\partial u_Z}{\partial X}$$

The deterministic equations (Eq. 365) are developed now into Langevin equations which are solved in the linear Markovian approximation for the dissymmetric cross correlation function, whose components are symmetric and antisymmetric. The Langevin equations corresponding to (Eq. 365) are

$$F_{X\,\text{stochastic}} = m\dot{\nu}_X + m\beta\nu_X + m\beta_{XZ}\nu_Z \tag{366a}$$

$$F_{Z\,\text{stochastic}} = m\dot{\nu}_Z + m\beta\nu_Z - m\beta_{ZX}\nu_X \tag{366b}$$

These equations have been written for $D_g^{(1)}$-type vorticity. For $D_g^{(2)}$-type deformation the minus sign on the right-hand side of Eq. (366b) is replaced by a plus sign. In Eq. (366) the beta's are friction coefficients in the linear, Markovian approximation. It has been assumed that

$$\beta_{XZ} = \frac{\partial u_X}{\partial Z}; \qquad \beta_{ZX} = \frac{\partial u_Z}{\partial X} \tag{367}$$

that is, that the components of the strain rate response can be identified with cross-friction coefficients in the linear, Markovian approximation. More generally, the friction coefficients are non-Markovian memory functions, as we have seen in earlier sections and the Langevin equation is nonlinear.[3] However, in the linear, Markovian approximation (366) the Langevin equations may be solved for the cross-correlation functions of interest:

$$\langle \nu_X(t)\nu_Z(0)\rangle = \frac{\langle \nu_X(0)\nu_X(0)\rangle}{(c-b^2)^{1/2}}\beta_{XZ}e^{-bt}\sin\{(c-b^2)^{1/2}t\}; \qquad c > b^2 \tag{368a}$$

$$\langle \nu_X(t)\nu_Z(0)\rangle = \frac{\langle \nu_X(0)\nu_X(0)\rangle}{(b^2-c)^{1/2}}\beta_{XZ}e^{-bt}\sinh\{(b^2-c)^{1/2}t\}; \qquad b^2 > c \tag{368b}$$

where

$$b = 4\beta; \qquad c = \beta^2 - \beta_{XZ}\beta_{ZX}$$

with a similar expression for $\langle \nu_Z(t)\nu_X(0)\rangle$ with β_{XZ} replaced by β_{ZX}. For shear-induced vorticity

$$\beta_{XZ} = -\beta_{ZX} \tag{369a}$$

and for shear-induced deformation

$$\beta_{XZ} = \beta_{ZX} \tag{369b}$$

The final dissymmetric cross-correlation function assumed to be a *weighted* sum of both types

$$\langle \nu_X(t)\nu_Z(0)\rangle = A\langle \nu_X(t)\nu_Z(0)\rangle_{\text{vorticity}} + B\langle \nu_X(t)\nu_Z(0)\rangle_{\text{deformation}} \tag{370a}$$

and

$$\langle \nu_Z(t)\nu_X(0)\rangle = -A\langle \nu_Z(t)\nu_X(0)\rangle_{\text{vorticity}} + B\langle \nu_Z(t)\nu_X(0)\rangle_{\text{deformation}} \tag{370b}$$

where A and B are weighting constants. If $A \ll B$, for example, the cross-correlation functions from Eq. (370) will be slightly dissymmetric, and the same for $A \gg B$. There will be intermediate cases of varying dissymmetry. However, despite being able to explain quantitively the major feature of the simulation, that is, that the cross-correlation functions are dissymmetric, Eq. (370) is not able to show why the simulated ccf's[300,301] remain finite at $t = 0$. Equation (370) produces ccf's which vanish at $t = 0$.

The simple linear, Markovian approach thus fails qualitatively at short times.

The failure of the Langevin equations (Eq. 366) to describe the results from computer simulation is an important indication of the fact that non-Newtonian sheared N- particle ensembles have several features which are fundamentally different from their equilibrium counterparts:

1. The sheared ensemble supports cross correlation functions which are dissymmetric in time displacement and in the indices X, Z of the shear plane. These ccf's have the property[300,301]

$$\langle \nu_X(0)\, \nu_Z(0) \rangle \neq 0 \tag{371}$$

which is not reproduced by the linear Markovian approximation represented in Eq. (366). This is unlikely to be remedied by developing the friction coefficients into memory functions, thus making the system non-Markovian, and we are led to consider

2. that the system is nonlinear. In one sense it is nonlinear because the stress and the strain rate are not linearly related, as in Newton's law of sheared fluids. In this sense the system is nonlinear because it is non-Newtonian. If we are to attempt an approach to the new ccf's with Langevin equations, we are led to the conclusion that the friction coefficients are no longer simple linear multiples of velocity, as in Eq. (366), because this approach fails qualitatively at $t \rightarrow 0$ both for Markovian and non-Markovian approximations to the rigorous Eq. (365). More generally, the Langevin equation can be nonlinear, containing friction coefficients that multiply powers of velocity on the right-hand side. In general the equation would contain a sum of such terms, with interesting analytical implications.

3. The new cross correlation functions are observed by numerical simulation to be dissymmetric in time displacement. They are not therefore stationary[1–4] in the conventional sense, because they are neither symmetric in time displacement nor antisymmetric.

4. This leads directly to the conclusion that in the presence of shear, the N-particle ensemble no longer obeys the Onsager reciprocal relations, which are laws applicable to N-particle ensembles at thermodynamic equilibrium, where the system is reversible.

5. The ccf's are therefore indicative of a dynamical process under shear which is irreversible, in the sense that they are not governed by Onsager's reciprocal relation.

An N particle ensemble in the steady state under shear which is non-Newtonian produces dissymmetric time cross-correlation functions which indicate a statistical process which is non-linear, irreversible, non-Markovian and dissymmetric in time displacement, being in this sense nonstationary. In consequence, a simple linear Markovian description fails qualitatively as $t \rightarrow 0$. This leads to an entirely new appreciation of non-Newtonian N-particle dynamics.

D. Shear Induced Structural Effects and GTSM

Angular resolution[326] of the pair-radial distribution function in computer simulations of shear induced thickening in atomic (Lennard–Jones) liquids has revealed the presence of anisotropic local structure, which can be explained on the basis of group theoretical statistical mechanics using principle 3, that the symmetry of allowed ensemble averages in the steady state in the presence of shear is the same as that of the applied strain rate. The computer simulation results[329] can be reproduced from group theory by assuming that the crystal-like lattice arrangement of atoms which appear in the simulations under shear can be described by some of the 32 crystallographic point groups in Table II, hexagonal, trigonal, and triclinic. The hexagonal lattice symmetries C_{3h} and C_{6h}, the trigonal symmetry S_6, and the triclinic symmetry $C_i(S_2)$ are found to support the crystal-like structures necessary to explain the observed[329] angular resolution of the pair-radial distribution function.

The nemd computer simulations of Heyes and co-workers[326] have revealed a number of significant new phenomena of non-Newtonian rheology in atomic liquids using a battery of new numerical techniques. Among the most interesting of these is in the context of shear thinning and thickening. Simulations have shown[329] that as the shear rate is increased the atoms of the liquid ensemble form structurally arrested states with crystal-like symmetries. The point group of the ensemble is therefore changed from $R_h(3)$ to that of the shear induced lattice. Gtsm can be used to to explain the observed symmetry of angularly resolved pair radial distribution functions (rdf's) in non-equilibrium simulations of these atomic ensembles. Only a small number of lattice symmetries support the observed anisotropy under shear, and gtsm is used to explain why shear is able to produce this anisotropy.

We have seen that principle 3 is a statement of how externally applied force fields of given symmetry set up extra ensemble averages at field-applied equilibrium. It is also valid in transient, nonequilibrium regimes. In both cases the overall symmetry of the new ensemble averages is that of the applied field. The complete D symmetry of the strain rate tensor is $D_g^{(0)} + D_g^{(1)} + D_g^{(2)}$, which by principle 3 sets up new ensemble averages, such as pair distribution functions or time correlation functions in frame (X, Y, Z) at the field on steady state. State of the art nonequilibrium computer simulation[300,301] shows the presence of new time ccf's with the overall symmetry of the strain rate. Principle 3 produces similar entirely

novel results[300] for the time ccf's of pressure tensor components, revealing the fundamental origin of the Weissenberg effect of macroscopic non-Newtonian rheology, and explaining through ccf's the pressure set up in a sheared liquid in a direction perpendicular to the plane of shear. The new ccf's are also sensitive to the typical macroscopic phenomena of non-Newtonian rheology, including the appearance of shear induced thickening and thinning,[326] the appearance of string phases,[330] and structurally arrested states. These all involve time ccf's in frame (X, Y, Z) for an atomic liquid, and also in frame (x, y, z) for a molecular liquid. Conventional methods of macroscopic rheology have failed to recognize this, in the same way that conventional diffusion theory has failed to recognize the role of ccf's at equilibrium. In both cases they are governed by principle 3.

E. Crystal-Like Arrested States at High Shear Rates—An Excess of Symmetry

Principle 3 may be applied to angularly resolved pair distribution functions, defined[329] by

$$f_{\alpha\beta}(r) = \left(\sum_{i \neq j}^{N} \sum^{N} \langle R_{\alpha ij} R_{\beta ij} / R_{ij}^2 \rangle \right) \Big/ N \tag{372}$$

$$g_{\alpha\beta}(r) = 15 V f_{\alpha\beta}(r) / (V(r) N) \tag{373}$$

The angular component $f_{\alpha\beta}$ measures the anisotropic dispositions of molecules or atoms, and involves the ensemble average $\langle R_{\alpha ij} R_{\beta ij} \rangle$. Peaks in $g_{\alpha\beta}$ supply information on shear-induced structurally arrested states. In Eq. (373), V is the volume of the shell bounded by $r \pm \delta r/2$

$$V(r) = 4\pi r^2 \delta r \tag{374}$$

for a shear resulting in a strain-rate response of type $\partial v_X / \partial Z$. Principle 3 predicts the existence of the ensemble average $\langle R_{Xij} R_{Zij} \rangle$, but no other off-diagonal elements such as $\langle R_{Xij} R_{Yij} \rangle$ or $\langle R_{Yij} R_{Zij} \rangle$. This is simulated by Heyes[331] and is in satisfactory agreement with numerically derived data for low shear rates, but as the latter increase, off-diagonal elements of the angularly resolved pair rdf appear which are disallowed by principle 3 in $R_h(3)$. Heyes has explained this in terms of slow structural relaxation, outside the time window of the simulation. The applied shear has clearly led to lower symmetry in frame (X, Y, Z), a crystal-like environment has been generated from a shear-induced phase change, taking the ensemble from $R_h(3)$ to some other crystal-like point group of lower symmetry. The

problem is how to apply group theoretical methods within this new group to explain the results actually observed by Heyes (Figs. 7 and 8 of Ref. 331).

In order to explain Fig. 8 of Ref. 331 it is necessary to assume that the overall point group of at least some part of the ensemble is no longer $R_h(3)$ of the isotropic liquid, distorted by shear, but is that of a shear-induced crystal-like structure. From the "snapshots" of the simulation provided by Heyes,[331] this appears to be hexagonal, trigonal, or triclinic, an overall triangular lattice which produces

$$f_{XX} \neq f_{YY} \neq f_{ZZ} \neq f_{XZ} \neq f_{XY} \neq f_{YZ} \neq 0 \tag{375}$$

To find the symmetry of the applied shear within each of these crystal-like point groups it is necessary to map $D_g^{(0)} + D_g^{(1)} + D_g^{(2)}$ onto the appropriate irreducible representation within that crystal-like point group. These representations appear in Table II. The following are examples of this procedure for shear-induced crystal-like point groups.

F. Hexagonal C_{3h} (Hermann Mauguin $\bar{6}$)

In this crystal point group, one of the hexagonal crystal symmetries, the symmetry of shear is

$$D_g^{(0)} + D_g^{(1)} + D_g^{(2)} = A^{11}A^{11} + E^1A^{11} + A^{11}E^1 + E^1E^1 \tag{376}$$

which allows ensemble averages of the type

$$\langle R_{Xij} R_{Xij} \rangle \neq \langle R_{Yij} R_{Yij} \rangle \neq \langle R_{Zij} R_{Zij} \rangle; \tag{377a}$$

$$\langle R_{Xij} R_{Yij} \rangle \neq \langle R_{Xij} R_{Zij} \rangle \neq \langle R_{Yij} R_{Zij} \rangle \tag{377b}$$

using principle 3 with the C_{3h} point group rather than the $R_h(3)$ point group. Equation (377) predicts angularly resolved pair-distribution functions with the property Eq. (375). Thus both the diagonal and off-diagonal elements have a different r dependence if the structurally arrested state has the crystal symmetry C_{3h} or $\bar{6}$. Comparison of this result with available computer simulations by Heyes can be made by examining the numerical data in Figs. 7 and 8 of Ref. (331). These show that at strain rates $\dot{\eta} = 110$ and $\dot{\gamma} = 30$ in normalized units the diagonal elements g_{YY} and g_{ZZ} are almost equal but discernably different, the third, g_{XX}, being distinctly different from the other two. In Fig. 8 of Ref. 331 the amplitudes of the off-diagonal elements g_{XY} and g_{YZ} are greater than the third element g_{XZ}, all three being distinctly different.

Our calculations, based on principle 3 applied to the various point groups, show that the hexagonal point group $C_{6h}(6/m)$ also gives this result, along with the trigonal S_6 and the triclinic S_2. Other hexagonal or in general triangular-type lattices are either disqualified on the basis of being chiral, or produce degeneracies, in the sense that one or more angularly resolved pair rdf elements are equal.

We are able to conclude that shear thickening is accompanied by the appearance of structurally arrested states in which the crystal-like symmetry supports six different angularly resolved radial pair distribution functions. These are rationalized with group theoretical statistical mechanics.

G. Shear-Induced Depolarized Light Scattering

The existence by gtsm and nemd computer simulation[300,301] of new dissymmetric ccf's implies that there exists theoretically a hitherto unmeasured depolarized component of light scattered from a sheared N-particle ensemble. In atomic ensembles, and in ensembles of molecules of symmetry higher than T_d, this is the only component, neglecting weak collision-induced effects.

The third principle of gtsm allows the existence of the new current correlation function[332–334]

$$C_{XZ} = \langle \nu_X(0)\nu_Z(t)\exp(i\mathbf{q}\cdot(\mathbf{r}(0)) - \mathbf{r}(t))\rangle \tag{378}$$

in an N particle ensemble subjected to the shear strain $\partial\nu_X/\partial Z$. This has the same dissymmetry properties as the velocity and pressure tensor ccf's.[300,301] Here $\mathbf{q}$ is the scattering vector and

$$\mathbf{r}(t) - \mathbf{r}(0) = \Delta\mathbf{r}(t) = \int_0^t \mathbf{v}(t)dt \tag{379}$$

where $\mathbf{v}$ is the center-of-mass velocity of the diffusing particle (atom or molecule). We have

$$\langle \Delta r^2(\tau)\rangle = \int_0^\tau \int_0^\tau \langle \nu_X(t_1)\nu_Z(t_2)\rangle dt_2 dt_1 \tag{380a}$$

$$= 2\int_0^\tau (t-\tau)\langle \nu_X(0)\nu_Z(t)\rangle dt \tag{380b}$$

The current ccf (Eq. 378) is related to a self-dynamic structure factor[332–334] by

$$F_{XZ}^{(s)}(\mathbf{q}, t) = \langle \exp(i\mathbf{q}\cdot(\mathbf{r}(0) - \mathbf{r}(t)))\rangle \tag{381}$$

which upon double differentiation provides

$$\frac{d^2}{d\tau^2}F_{XZ}^{(s)}(\mathbf{q}, \tau) = -q^2 C_{XZ}(\tau) \tag{382}$$

Equation (382) gives the result

$$J_{XZ}^{(s)}(\mathbf{q}, \omega) = \frac{\omega^2}{q^2}S_{XZ}^{(s)}(\mathbf{q}, \omega) \tag{383}$$

where J is the temporal Fourier transform of C_{XZ}, and S that of Eq. (381). The latter is the intermediate scattering function in the ideal self-dynamic limit for the sheared N-particle ensemble. Equations (383) shows that this is related to the new current ccf defined by Eq. (378).

H. Light-Scattering Geometry

Integrating Eq. (382) gives the result

$$\lim_{q\to 0}\left(\frac{d}{dt}F_{XZ}^{(s)}(\mathbf{q}, t)_{\tau>\tau_l}\right) = -q^2\int_0^\infty \langle \nu_X(0)\nu_Z(t)\rangle dt \tag{384}$$

where τ_l is the correlation time. This shows that the intermediate scattering function S is related to the new dissymmetric cross correlation functions generated by shear.[300,301] The function S is observable by light scattering where the initial polarization vector is in the X axis of the laboratory frame (X, Y, Z) and where the scattered polarization vector is in the Z axis of this frame. The plane XZ is that of the shear strain $\partial\nu_X/\partial Z$.

The existence of shear induced ccf's means that there will be depolarized light scattered from a sheared N-particle ensemble with intensity S. This spectrum is related to the temporal Fourier transform of Eq. (378) *by Eq.* (383).

In atomic ensembles, or in ensembles of molecules of symmetry greater than T_d, this will be the sole contribution to the new type shear-induced light scattering apart from small contributions[332–334] from collision induced polarization anisotropies. At equilibrium in the absence of shear, this spectrum will disappear, because the shear-induced dissymmetric ccf's disappear.

In order to observe the spectrum experimentally, the incident laser

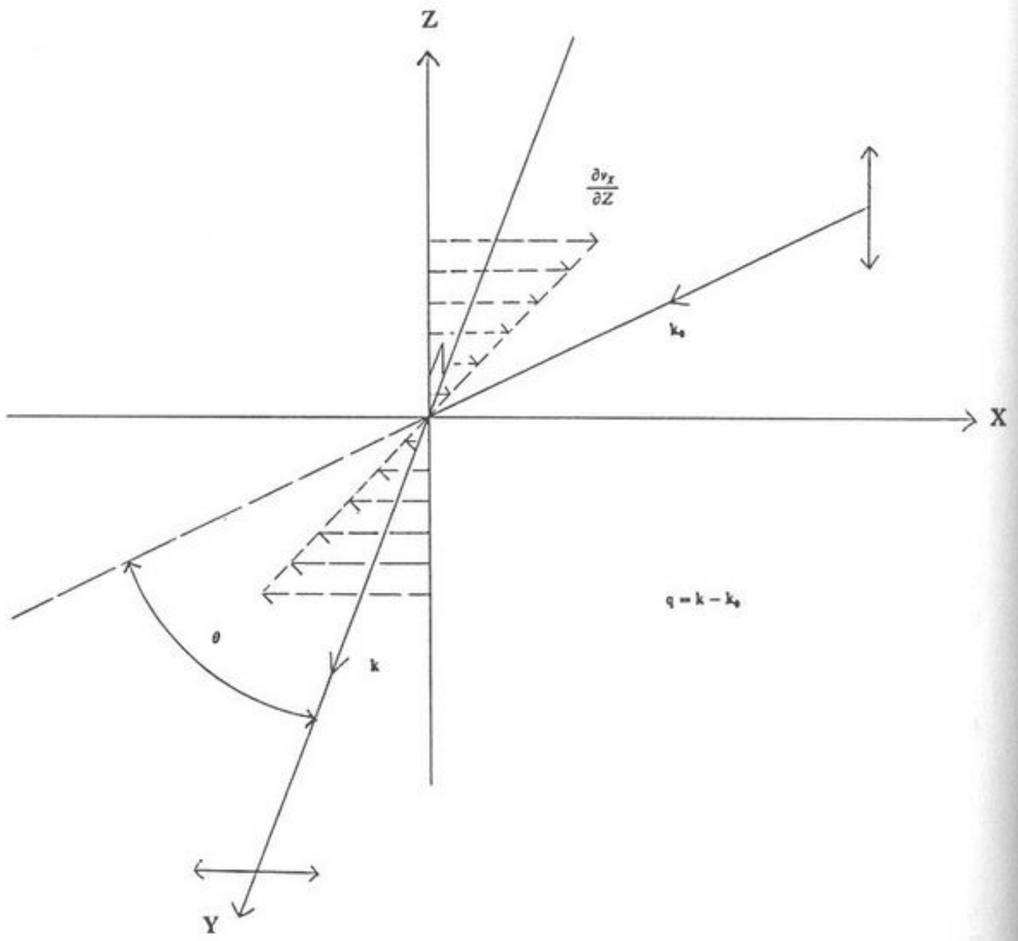

Figure 48. Shear-induced depolarized light-scattering geometry.

beam, polarized in the X axis, is scattered conveniently from an arrangement of coaxial cylinders, and scattered radiation is observed polarized in the axis Z for a given scattering angle, angular frequency and scattering vector. This is the spectrum S which gives J by Eq. (383), and thus the temporal Fourier transform of Eq. (378). The inner cylinder (a stirring rod) rotates rapidly and the outer cylinder is the wall of a round light-scattering cuvette. This arrangement creates a shear on a liquid held between the cylinders. The geometry is illustrated in Fig. 48.

The high frequency wing of the spectrum S is amplified by the multiplication by the square of the angular frequency in Eq. (383) to give the second spectral moment J. The latter is related directly to the new ccf (Eq. 378) and this ccf is in turn a direct measure of non-Newtonian effects in a sheared fluid.

The new depolarized spectrum J *is therefore a direct measure of the non-Newtonian nature of sheared* N *particle ensembles.*

Depolarized scattering depends solely on the optical anisotropy of the scattering center, and this may be thought of as a scattering element of polarizability tensor $\boldsymbol{\alpha}$. The scattered electric field vector of the electromagnetic radiation is then

$$E_X = \sum_j \alpha^j_{XZ} \exp(i\mathbf{q} \cdot \mathbf{r}_j(t)) \tag{385}$$

where α^j_{XZ} the XZ component of the polarizability tensor $\boldsymbol{\alpha}$ of the jth scattering element, and $\mathbf{q}$ the scattering vector. Let us situate the center of mass on an atom of our sheared ensemble. On average, we have, for atomic ensembles

$$\alpha^j_{XZ} = \alpha_0 \frac{\langle R_X R_Z \rangle}{R^2} \tag{386}$$

where the vector $\mathbf{R}$ is defined with respect to the center of mass of the polarizability element in frame (X, Y, Z), and where the averaged quantity on the rhs of Eq. (386) is proportional to the angularly resolved radial distribution function introduced by Heyes and Szczepanski.[335] The latter, denoted by ρ_{XZ}, is dependent on the positions of nearest neighbours, next nearest neighbors, and so on, around the center of mass atom, and is assumed here to be approximately the time independent equilibrium average. Therefore, we have

$$\alpha^j_{XZ} = \alpha_0 \rho_{XZ}(\mathbf{R}) \tag{387}$$

where "R" is the argument of the angularly resolved pair-radial distribution function. Without loss of generality, we can assume that

$$\rho_{XZ}(\mathbf{R}) = \rho_{XZ}(\mathbf{R}_0) \tag{388}$$

where $\mathbf{R}_0$ is the position of the first peak of the pair-radial distribution function. Finally, we have

$$\alpha^{j}_{XZ}(t) = \alpha^{j}_{XZ}(0) = \alpha_0 \rho_{XZ}(\mathbf{R}_0) \tag{389}$$

so that the depolarized light scattering spectrum is given by

$$S_{VH}(\mathbf{q}, \mathrm{t}) \propto \rho^2_{XZ}(\mathbf{R}_0) S^{(s)}_{XZ}(\mathbf{q}, t) \tag{390}$$

In order to provide an idea of the frequency and scattering vector dependence of the spectrum J this can be computed for an ensemble of atoms subjected to shear strain by PUT computer simulation.[300,301] The new current correlation function of type in Eq. (378) is computed directly and its temporal Fourier transform gives J.

I. Polarimetry

The plane of polarization of electromagnetic radiation is expected to be changed a little by shearing on the basis of the argument given above, and this could be detected with a simple polarimeter, providing a direct method of observing the effect of shear on polarized electromagnetic radiation.

J. Shear Induced Dipole Relaxation

In a dipolar molecular ensemble the existence of shear induced dissymmetric ccf's[300,301] implies that of shear-induced polarizability and polarization and direct dissymetric cross correlation between orthogonal components of the permanent molecular dipole moment whose Fourier transform[1–4] is a complex frequency-dependent permittivity. The relaxation of the shear induced permittivity provides a direct method of investigating non-Newtonian phenomena such as shear thinning, thickening, and turbulence in dipolar media. At far infrared frequencies[1] the direct shear-induced cross correlation between orthogonal components of the molecular rotational velocity can be isolated and observed experimentally in principle as a power absorption spectrum with crossed wire grid polarizers.

The shear-induced permittivity spectrum can cover the frequency regions of experimentally obtainable strain rates (up to MHz) and may be used to investigate non-Newtonian effects experimentally. The high-frequency adjunct of this shear induced frequency process, a far infrared power absorption[1–4] likewise has a sheared induced component which is the Fourier transform of the shear induced dissymmetric ccf of the molecular rotational velocity

$$\langle \dot{\mu}_Z(t) \dot{\mu}_X(0) \rangle \neq \langle \dot{\mu}_X(t) \dot{\mu}_Z(0) \rangle \tag{391}$$

It is argued that this can be isolated and observed experimentally and directly with crossed wire grid polarizers, providing another direct probe of non-Newtonian rheology.

K. Shear Symmetry in the Dielectric and Far Infrared

Using the language of irreducible D representations the symmetry of strain rate of type (1) is again assumed to be

$$\Gamma(\dot{\gamma}) = D^{(1)}_g + D^{(2)}_g \tag{392}$$

a traceless, purely off-diagonal, symmetry with a vector part $D^{(1)}_g$ and a tensor part $D^{(2)}_g$. The third principle imparts this symmetry to ensemble averages at the shear-applied steady state, giving rise to dissymmetric ccf's at the atomic (or molecular) level. Conventional rheology does not postulate the existence of atoms and molecules, and in consequence is unable to explain this fundamental result.

In atomic ensembles, the dissymmetric ccf's are exemplified by velocity ccf's (Section VII) and also by related types with the same symmetry, such as the mixed velocity–position ccf's[300,301]

$$\langle v_Z(t) r_X(0) \rangle \neq \langle v_X(t) r_Z(0) \rangle \tag{393}$$

and the position–position ccf's

$$\langle r_Z(t) r_X(0) \rangle \neq \langle r_X(t) r_Z(0) \rangle \tag{394}$$

In ensembles of dipolar molecules, the permanent molecular dipole moment $\boldsymbol{\mu}_0$ is always expressible as the vector sum of the position vectors of the atoms of the molecule in frame (X, Y, Z). This immediately implies the existence of the shear induced dissymmetric ccf's of $\boldsymbol{\mu}_0$, and of its time derivative,[1] the rotational velocity $\dot{\boldsymbol{\mu}}_0$. We have the results

$$\langle \mu_{0Z}(t) \mu_{0X}(0) \rangle \neq \langle \mu_{0X}(t) \mu_{0Z}(0) \rangle \tag{395}$$

and

$$\langle \dot{\mu}_{0Z}(t) \dot{\mu}_{0X}(0) \rangle \neq \langle \dot{\mu}_{0X}(t) \dot{\mu}_{0Z}(0) \rangle \tag{396}$$

The Fourier transform of Eq. (395) is a dissymmetric, shear-induced complex permittivity. That of Eq. (396) is a dissymmetric far infrared power absorption accompanied by a dispersion in the referactive index. Thus, the results of Refs. 300 and 301 immediately give new types of

observable, shear-induced spectra, which are direct probes of non-Newtonian phenomena.

L. Shear-Induced Molecular Polarizability and Polarization

The terms "polarizability" and "polarization" are usually applied to the response of a dielectric to an applied electric field. However, the existence[300,301] of dissymmetric ccf's of the molecular dipole moment implies that of a *shear-induced molecular polarizability* which is given in the shear applied steady state by

$$\langle \alpha_{XZ} \rangle = \frac{\langle \mu_{0Z} \mu_{0X} \rangle}{\Delta E_{\text{shear}}} \tag{397}$$

where ΔE_{shear} has the units of energy (J), and the polarizability has the units of $C^2m^2J^{-1}$. More conventionally, the polarizability is given in units of volume (the "volume definition") by dividing the right-hand side of Eq. (397) by $4\pi\epsilon_0$, where ϵ_0 is the permittivity of free space. The shear induced molecular polarizability then has units of m^3.

The results of Ref. 300 show that at $t = 0$ (the "equilibrium value"),

$$\langle v_Z(0) v_X(0) \rangle = \langle v_X(0) v_Z(0) \rangle \tag{398}$$

so that the shear-on equilibrium value of the polarizability, given by Eq. (397), is not dissymmetric in X and Z. The equilibrium value of the energy in the denominator of Eq. (397) is then the energy of formation of the numerator, the $t = 0$ value of the cross-correlation function of the permanent molecular dipole moment in the shear-on steady.

The existence of the shear induced molecular polarizability implies that the sample is *polarized by shear*. This is formally analogous to the polarization caused by an electric field, which is the basis of dielectric spectroscopy, but is due to the field of force caused by shear, the "shearing field." We refer to this as shear-induced polarization. In the same way that dielectric polarization may be expressed as a power series in the applied electric field, shear induced polarization is a power series in the applied shearing field. The coefficients of the series in electric-field-induced polarization are: the molecular polarizability (multiplied by the electric field); the molecular hyperpolarizability (multiplied by the electric field squared) and so on. Those in shear-induced polarization are the shear-induced molecular polarizability; shear induced molecular hyperpolarizability, and so on.

The shear-induced polarization may be expressed through a total molecular dipole moment with components X and Z. These are sums of the equivalents for the permanent molecular dipole moment and those induced by shear. (This is again formally analogous to the total dipole moment produced by electric polarization, which is a sum of the permanent dipole, that induced by the product of polarizability and the electric field, and so on.) At shear-on equilibrium the total molecular dipole components are

$$\mu_{X,\text{total}} = \mu_{0X} + \mu_{1X} + \mu_{2X} + \cdots \tag{399a}$$

and

$$\mu_{Z,\text{total}} = \mu_{0Z} + \mu_{1Z} + \mu_{2Z} + \cdots \tag{399b}$$

We now express the shear-induced dipole components μ_{1Z} and so on in terms of integrals over dissymmetric ccf's of type in Eq. (395). This is accomplished using the Morriss–Evans theorem described in Section VII.

M. Adaptation of the Morris–Evans Theorem

The Morriss–Evans theorem is a generalisation of the Green–Kubo relations[1–4] and a fusion of linear and nonlinear response theory, providing a new framework for fluctuation–dissipation theorems in general (Section VII).

Taking the first induced term in Eq. (399), we have, by definition

$$\langle \mu_{1X} \rangle = \frac{F_{\text{shear}}}{\Delta E_{\text{shear}}} \langle \mu_{0X}(0) \mu_{0Z}(0) \rangle = \langle \mu_{1Z} \rangle \tag{400}$$

where F_{shear}, is the shearing field. The structure of the Morriss–Evans theorem allows this to be written as

$$\langle \mu_{1Z} \rangle = -\frac{F_{\text{shear}}}{\Delta E_{\text{shear}}} \int_0^\infty \langle \mu_{0X}(t) \dot{\mu}_{0Z}(0) \, dt \tag{401}$$

with a similar expression for $\langle \mu_{1X}(t) \rangle$.

In Eq. (401) we have taken the $t \to \infty$ limit of the Morriss–Evans integral, which implies that the nonequilibrium average $\langle\langle \ \rangle\rangle$ becomes the shear-on steady-state average $\langle \ \rangle$, because the external field is applied for an infinite time, allowing the system to reach a steady state.

We note finally that the factor before the integral in Eq. (401) can be expressed in the form

$$\frac{F_{\text{shear}}}{\Delta E_{\text{shear}}} = \frac{\text{Constant}}{\langle \mu_{0X} \rangle} \frac{\partial v_X}{\partial Z} \tag{402}$$

where the "constant" is the shear-induced polarization constant.

N. Shear Induced Dipole Relaxation and Far Infrared Power Absorption

These are three of the many areas of observation affected by the phenomenon implied by Ref. 300, and specifically by the existence of dissymmetric ccf's of the permanent molecular dipole moment and its time derivative in frame (X, Y, Z).

Shear-induced dipole relaxation, a relatively low-frequency process which can cover several frequency decades, is expressed in spectral terms through the Fourier transformation of the shear-induced dipole ccf. In the shear-on steady state it causes polarization, which is the result of statistical correlation between orthogonal X and Z components of the permanent molecular dipole moment. The polarization may be isolated and detected experimentally by a special arrangement of electrodes, one in the XY plane and the other in the ZY plane, one electrode being perpendicular to the other and both being perpendicular to the plane of shear, XZ. In the Hz to kHz frequency region, the relaxation of the shear-induced polarization may be detected with a Wayne–Kerr bridge, and with other types of bridge technique and sweep frequency apparatus up to the MHz range. Direct measurements with orthogonal electrodes of shear induced polarization seem never to have been made, but would isolate the cross-correlation between the X and Z components of the permanent molecular dipole moment.

Analogously, the high-frequency adjunct of the shear induced dipole relaxation process is a far infrared power absorption and accompanying refractive index dispersion. The power absorption spectrum in the far infrared can be isolated in principle by the use of wire grid polarizers. One polarizer is oriented in the Z axis between the exit port of a far infrared interferometer and the sheared sample, the spectrum taken, and the experiment repeated with a polarizer in the X direction between the sample and the detector. The polarizers selectively block out radiation in the presence and absence of shear.

Careful choice of sample and conditions, with accessible laboratory strain rates, leads to this far infrared spectrum, which is a direct measurement of the non-Newtonian molecular rotational velocity ccf. The fundamental reason for this is that the far infrared power absorption is always the high frequency adjunct of a dipole relaxation process which occurs at much lower frequencies, and the high- and low-frequency parts of the

overall dynamical process are never independent. This has been demonstrated experimentally by Evans and Reid[1–4] using supercooled liquids and glasses, work which isolated the far infrared gamma process as the high frequency, ever present, adjunct of much lower frequency alpha and beta processes in supercooled liquids and glasses. The gamma process may be separated from the other two by a dozen frequency decades, but is always observable. Similarly, the accessible laboratory strain rate may be only a few kHz at most, but the molecular response extends from Hz to THz frequencies in general. This is simply due to the fact that a molecular diffusion process evolves temporally from the picosecond scale onwards.

In contrast to the absorption processes above, light scattering involves an induced dipole moment, equivalent to our $\boldsymbol{\mu}_1$. Conventionally, this is attributed to the molecular polarizability. However, in the shear applied steady state, the shear induced molecular polarizability can also cause *depolarized* light scattering, as discussed already. Light-scattering apparatus is implemented analogously at high or low frequencies (Rayleigh Brioullin and photon correlation spectroscopy respectively).

O. The D Symmetries of Shear in the Presence of Fields

The important industrial technique of *electrorheology* is based on shear in the presence of an electric field, static or time dependent. The simultaneous application of shear and an electric field, through the use of rotating electrodes for example (Sections IV–VI), leads to the possibility of new ensemble averages whose D symmetries are governed by principle 3. An electric field is a polar vector (Section VII) of $D_u^{(1)}$ symmetry. The combined D symmetry of electrorheology (electric field plus shear) is therefore

$$\Gamma(\mathbf{E})\Gamma(\dot{\gamma}) = D_u^{(1)} D_g^{(1)} D_g^{(1)} = D_u^{(0)} + 3D_u^{(1)} + 2D_u^{(2)} + D_u^{(3)} \tag{403}$$

using the Clebsch–Gordan theorem. The overall parity inversion symmetry is negative (ungerade), so that by principle (3) the ensemble averages specific to electrorheology must also be negative to parity inversion. The overall time reversal symmetry of the D combination depends on whether the electric field is static or alternating. The former is positive to time reversal and the latter is negative. The time-reversal symmetry of shear is a product of that of position and linear velocity, and is therefore negative to time reversal. The time-reversal symmetry of electroshearing is therefore overall negative in a static and overall positive in an alternating electric field.

The various possible field combinations in electroshearing can be expressed as subsets of the general triple vector product $\mathbf{vrE}$ with 27 elements. In couette flow, there are no scalar $\mathbf{v} \cdot \mathbf{r}$ components, so that the

field combinations with **E** all involve $\mathbf{v} \times \mathbf{r}$ or $\mathbf{v}\mathbf{r}^T$. From the signature (Eq. 403) the possible combinations allowed by symmetry are as follows:

1. The symmetry product $D_u^{(1)} D_g^{(1)}$ gives the three possible combinations $\mathbf{E} \cdot \mathbf{v} \times \mathbf{r}$, $\mathbf{E} \times \mathbf{v} \times \mathbf{r}$, and $\mathbf{E} \times \mathbf{v}\mathbf{r}^T$.
2. The product $D_u^{(1)} D_g^{(2)}$ gives the three further possible combinations $\mathbf{E} \times \mathbf{v}\mathbf{r}^T$, $\mathbf{E}(\mathbf{v}\mathbf{r}^T)^T$, and $\mathbf{E}\mathbf{v}\mathbf{r}$.

Thus, depending on the relative geometry of the applied fields, different D symmetries are generated. If electroshearing is carried out with an electric field between rotating electrodes, which also serve as shearing plates, then **E** is parallel to $\mathbf{r} \times \mathbf{v}$, so that only fewer D signatures are possible than in the general Eq. (403).

The application of principle 3 in this context produces the following, for example.

1. The rotation of plane-polarized light is one possible consequence of applying the field combination $\mathbf{E} \cdot \mathbf{v} \times \mathbf{r}$ to the sheared liquid using an alternating electric field. This particular field combination has positive time-reversal symmetry and negative parity-inversion symmetry and includes the pseudoscalar $D_u^{(0)}$. These satisfy the requirements for the field combination to be chiral.[279] There is the possibility, therefore, from principle 3, of a new kind of effect which which resembles the Faraday effect. The magnetic field which induces optical rotation in the latter is *not* however a true chiral influence in the definition given by Barron[279] because the magnetic field is a $D_g^{(1)}$ axial vector. A chiral influence must be negative to parity inversion and also positive to time reversal[279] (Section VII). In the new effect the magnetic field of Faraday's experiment is replaced by a truly chiral combination of time-dependent electric field and shear. In order to observe the expected optical rotation (signature $D_u^{(0)}$) the electric field vector must be parallel to the vector generated by the cross product $\mathbf{v} \times \mathbf{r}$. In a liquid being sheared by rotating plates, the latter is perpendicular to the plane of shear, and thus parallel to an alternating (or otherwise time-dependent) electric field applied using the rotating plates as electrodes. Principle 3 means that the combined influence of shear and electric field introduces in frame (X, Y, Z) new ccf's as well as the ensemble average of signature $D_u^{(0)}$ of optical rotation angle. If the sample also absorbs, the combination of shear and electric field produces dichroism.

As we have seen in Section VII, the chiral nature of the shear and time-dependent electric field combination also induces the appropriate elements of the ccf $\langle \mathbf{v}(t)\boldsymbol{\omega}(0) \rangle$ between the molecular linear and angular velocities. Ccf's of this type ought to be observable in a computer simulation of electroshearing, together with several other effects anticipated by the D signature on the right-hand side of Eq. (403). Another example follows.

2. Electric field and shear can also result in the generation of thermal conductivity, defined as the Green–Kubo integral[336] over the heat flux tensor **J** of Irving and Kirkwood. The tensor **J** has the same D symmetry as the right-hand side of Eq. (403), and in consequence all possible field combinations in electroshearing may contribute in principle to its appearance in the frame (X, Y, Z). This has recently been confirmed by computer simulation.[337] However, in this case it is necessary to use a static electric field, so that the overall time reversal symmetry is negative. Then, principle 3 shows that the application of a static electric field across the shearing plates will result in measurable changes in the sample's thermal conductivity, a property which may be used as an analytical tool for non-Newtonian electrorheology.

3. In electrorheology the electrodes, which are also the shearing plates, may be built into a circuit to measure the dielectric complex permittivity as a function of frequency over a several decade range. The thermodynamic average over the molecular permanent dipole moment, $\langle \boldsymbol{\mu} \rangle$, is positive to time reversal and negative to parity inversion with the D signature $D_u^{(1)}$ of a polar vector. This means that the dielectric frequency spectrum is affected by shear, and can be used to measure its non–Newtonian manifestations, reinforcing the conclusions arrived at earlier in this chapter.

4. If a static electric field is used and the overall time reversal symmetry is in consequence negative, principle 3 means that it is possible to induce ensemble averages over quantities such as molecular linear velocity, creating a drift in the sample. This may be used[279] to separate physically the enantiomers of a racemic mixture by applying the electric field to shearing plates immersed in a sample of the racemic mixture. The drift in linear velocity creates a propeller action[279] which is in a different sense for the two enantiomers which drift apart and which can be concentrated in different ends of the vessel.

5. As we have seen, a combination of shear and an alternating electric field is a true chiral influence negative to parity inversion and positive to time reversal. In this sense, the material being electrosheared is a chiral medium, even though the individual molecules in the liquid may be structurally achiral. A beam of chiral radiation incident upon the chiral medium so defined will be attenuated differently according to whether the beam is left- or right-handed, (e.g., left or right circularly polarized electromagnetic radiation). Examples of such chiral radiation are circularly polarized lasers in the ultraviolet, visible, and infrared, including the far infrared